Universitat Autònoma de Barcelona

Development of Quantum Dot-based tools for *in vitro* and biosensing applications

Helena Montón i Domingo

Thesis to apply for the degree of doctor in Cellular Biology

Departament de Biologia Cel·lular, Fisiologia i Immunologia

Faculty of Biosciences

Universitat Autònoma de Barcelona

Supervisors:

Dr. Arben Merkoçi, Nanobioelectronics and Biosensors Group,

ICREA & Institut Català de Nanociència i Nanotecnologia (ICN2)

Dr. Carme Nogués, Departament de Biologia Cel·lular, Fisiologia i Immunologia, Universitat Autònoma de Barcelona

Bellaterra, setembre de 2015

TABLE OF CONTENTS

Chapter 1. Quantum dots as tools for *in vitro* and biosensing applications

---

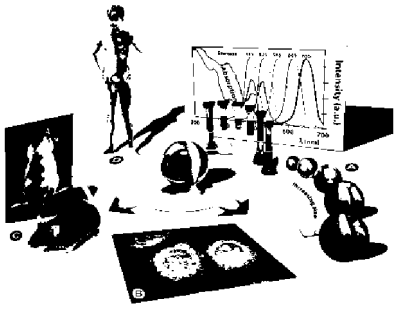

1.1. Introduction

During the last decades, the use of nanotechnology-based tools and methods in biology and medicine has generated a new field of research, generally called nanomedicine. In order to define an object as a nanomaterial, it must possess at least one dimension at the nanoscale. Thanks to their small sizes, nanomaterials have a very high surface to volume ratio, which is the cause of most of the properties observable at the nanoscale. Nanomedicine takes advantage of those properties to achieve the goals of traditional medicine: diagnosing, treating and preventing diseases [1,2].

Nanoparticles (NPs) are probably the most applied nanomaterials in nanomedicine. Their size can be compared to those of proteins and even nucleic acids, making them the ideal tools to interact with biological systems. In the literature, there are thousands of examples of how nanomedicine makes use of different types of nanoparticles, such as gold NPs[3,4], silver NPs[5,6], magnetic NPs[7,8], and Quantum Dots (QDs)[9,10]. QDs are nanoparticles made of one or more semiconductors that can be easily conjugated with diverse biomolecules. The unique optical and electrochemical properties of QDs make them an excellent building block for the development of novel diagnostics biosensors [11ï 13].

The aim of this chapter is to briefly show the state of the art of the use of QDs as tools for in-vitro cell analysis as well as in biosensing applications with a focus on DNA.

1.2. Origin and properties of Quantum Dots

Quantum Dots were first discovered in a glass matrix in early eighties by Alexey Ekimov [14] and then in colloidal solutions by Louis E. Brus [15]; however the term "quantum dot" was used for the first time in a scientific publication by Mark Reed and

collaborators to define ñsemiconductor heterostructures with quantum confinement to zero dimensionsò [16].

Since then, QDs have been extensively studied. Specially two scientists, Dr. Bawendi and Dr. Alivisatos explored QD optical properties and found ways to make them water soluble [17i 23]. This allowed QDs to be exported to other fields apart from physics and chemistry, such as biology where they can be used in a wide range of applications. With the aim to provide QDs commercially available and to keep improving their features for biological applications, a start-up biotechnology company emerged from Dr. Alivisatos group: Qdot Corporation, the most known and one of the first companies to produce and distribute QDs.

1.2.1. Quantum Dot structure

Commercial QDs are clusters of atoms of a semiconductor material (mostly cadmium mixed with selenium or tellurium), which are usually coated with an additional semiconductor shell (zinc sulfide) creating a core/shell crystalline heterostructure with diameters typically between 2 and 10 nm. An additional polymer coating is added to the nanocrystalline particle in order to provide water solubility and functional groups for conjugation with diverse biomolecules (Figure 1) [24].

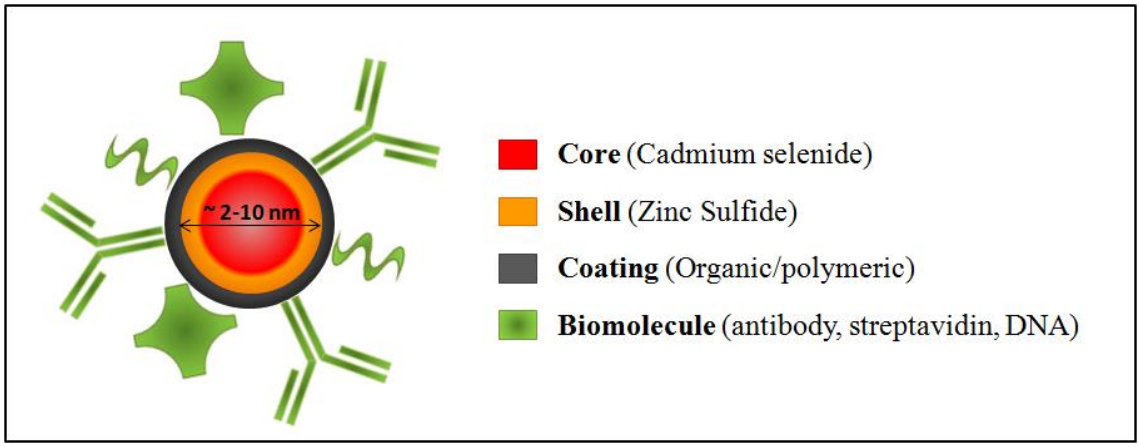

Figure 1. Schematic (not in scale) of the overall structure of typical commercially available QDs for bioapplications. The layers represent the distinct structural elements: core, shell, polymeric coating and conjugated biomolecules.

1.2.2. Quantum Dot properties

QDs have unique optical and electrochemical properties, which depend both on the material they are made of and on their high surface to volume ratio [25].

Fundamentally, QDs are fluorophores: substances that absorb photons of light and then re-emit photons at a different wavelength. The most well-known feature of QDs is that their color, due to their characteristic absorption of light, varies depending on their size, which means that by tuning the size of QDs during their synthesis different colors of exciting/emitting QDs can be obtained (Figure 2A). As mentioned above, most of commercial QDs are made of two different semiconductor materials. The first one, which forms the core of the QDs, determines their color (the excitation and emission wavelengths), whereas the second one, which forms the shell of the QDs, improves their stability and brightness through increasing the quantum yield (the number of photons emitted compared to the number of photons used for excitation) [26]. For example,

CdSe/ZnS QDs exhibit an 80% more quantum yield than QDs made just of CdSe [27]. At the same time, ZnS shell, gives protection against environmental changes and photo-oxidative degradation that would occur in presence of biological media [28]. From now on, unless otherwise stated, we will generally refer to core/shell QDs (usually of CdSe core and ZnS shell composition).

Optical properties of QDs make them a superior fluorescence label compared to organic dyes [29,30]. For the same spectral characteristics (maximum emission peak), QDs possess narrower emission bands, broad absorption spectra (Figure 2B) [29], higher photostability and brightness (between 10 and 100 times higher than organic dyes), besides they are more stable and less affected by photobleaching than organic dye molecules [31,32] (Figure 2C) [30].

Although most of QDs applications take advantage of their optical properties, their electrochemical properties can be very useful not only for sensing purposes, but also for QDs characterization and quantification [25,33]. An important difference between the optical and the electrochemical measurements of QDs is that the former gives information about the whole QDs structure, whereas the latter focus more on the electron-transfer events on the surface. Electrochemical properties of QDs rely on redox potentials of the semiconductor materials, which form the nanocrystals. Thus it is possible to study the purity of the QDs using standard instrumentation and simple experimental condition, in contrast with other techniques such as scanning tunneling spectroscopy and photoelectron spectroscopy, which require much more expensive equipment and sample treatment.

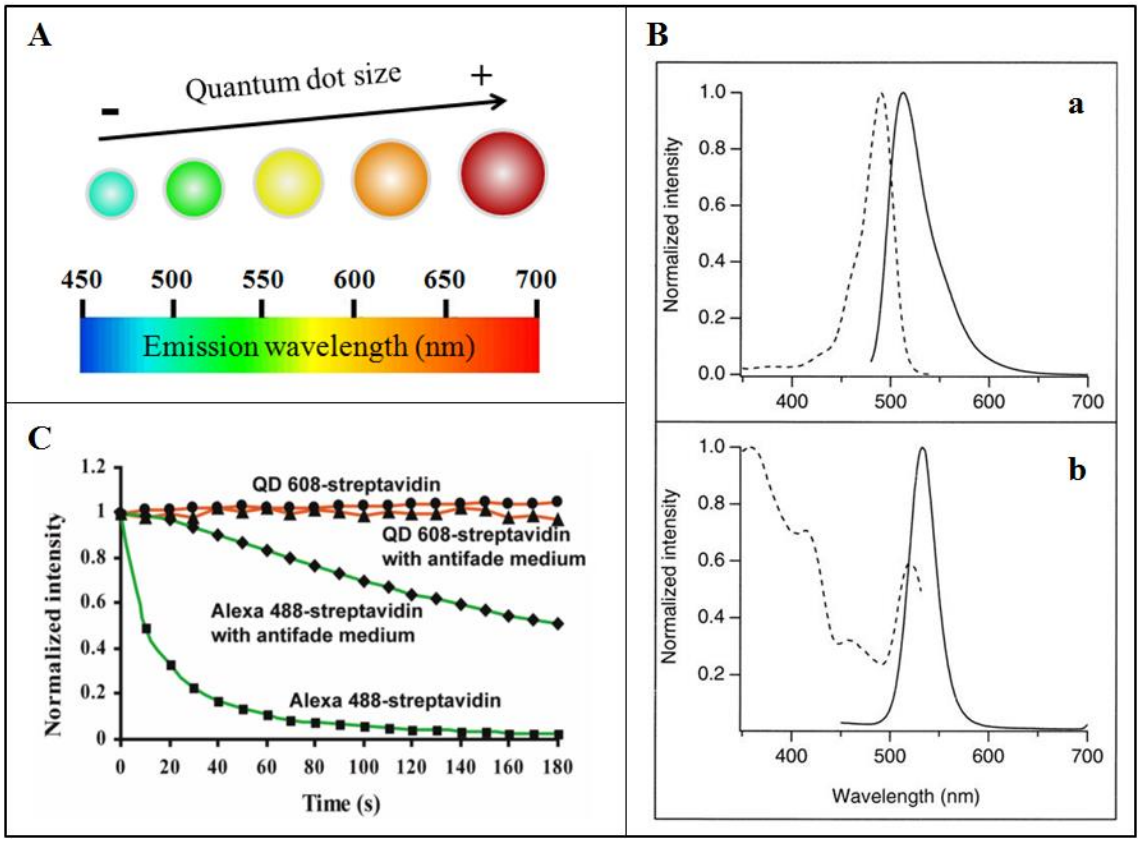

Figure 2. A. Cartoon showing the relation between size and color of QDs. Increasing the size of QDs it increases also the emission wavelength. **B. Comparison between QDs and organic dyes**: (a) absorption spectra and (b) emission spectra of QDs (dashed line) and organic fluorophore (continous line). Adapted from ref. [29] with kind permission of AAAS. **C. Photobleaching of QDs and Alexa dyes**. The fluorescence of QDs is basically unchanged after 3 min, whereas that of Alexa (a common organic dye) decreases significantly. Adapted from ref. [30] with kind permission of Nature Publishing Group.

QDs are generally affected by defects in their surface that can act as redox centres, making difficult to obtain a reproducible electrochemical signal. Such defects are minimized using core/shell QDs [34]. Electrochemical stripping analysis using for example square wave voltammetry (SWV) can also be exploited for QDs characterization and quantification. This technique takes advantage of the metallic ions

of the QDs (i.e. Cd, Pb etc. present onto the QD surface), which can be detected by SWV at certain medium conditions (solvent, pH). Various reports, which have used SWV to characterize and apply QDs, will be discussed in the following sections.

Although optical and electrochemical properties of QDs have been exploited to develop a wide range of applications, they have not been yet explored to be used together. Considering that a single QD has an optical and electrochemical signature, they have huge potential for dual analysis of samples.

For QDs to be used in any biological application, they need to have an organic coating, which is mostly polymeric (typically polyethileneglycol-PEG), that provides water solubility and functional groups for conjugation. For this reason, most of commercial QDs used in biology and medicine have their surface modified with hydrophilic molecules, which have several functions: improving the solubility in water, facilitating the functionalization of QDs with specific biomolecules, protecting QDs from deterioration in biological environment and preventing leak of heavy metals from the core and shell of the QDs (which would lead to cytotoxic effects) [35,36].

The most used and stable method to functionalize QDs with biomolecules is the formation of a covalent bond, such as the amide coupling, between the biomolecule and the functional groups on the surface of the QDs. Generally it is done using 1-ethyl-3-(3-dimethylaminopropyl)carbodiimide (EDC) as cross linker between amine groups on the surface of the biomolecule and the carboxyl group on the surface of the QDs [37,38] (Figure 3A).

Although commercially available QDs are generally designed to carry out posterior covalent binding *via* EDC chemistry with diverse biomolecules (immunoglobulins, streptavidin, biotin, receptor ligands, oligonucleotides, etc.), they can also be supplied

already modified with common molecules used in biological and pre-clinical research [39], such as antibodies, streptavidin or biotin among others (Figure 3B).

A big amount of functional groups are displayed in the surface of QDs (thanks to their high surface to volume ratio), allowing the conjugation of several biomolecules to a single QD [40]. This feature confers to QDs-based labels a high affinity for targets, providing more sensitivity to the detection method.

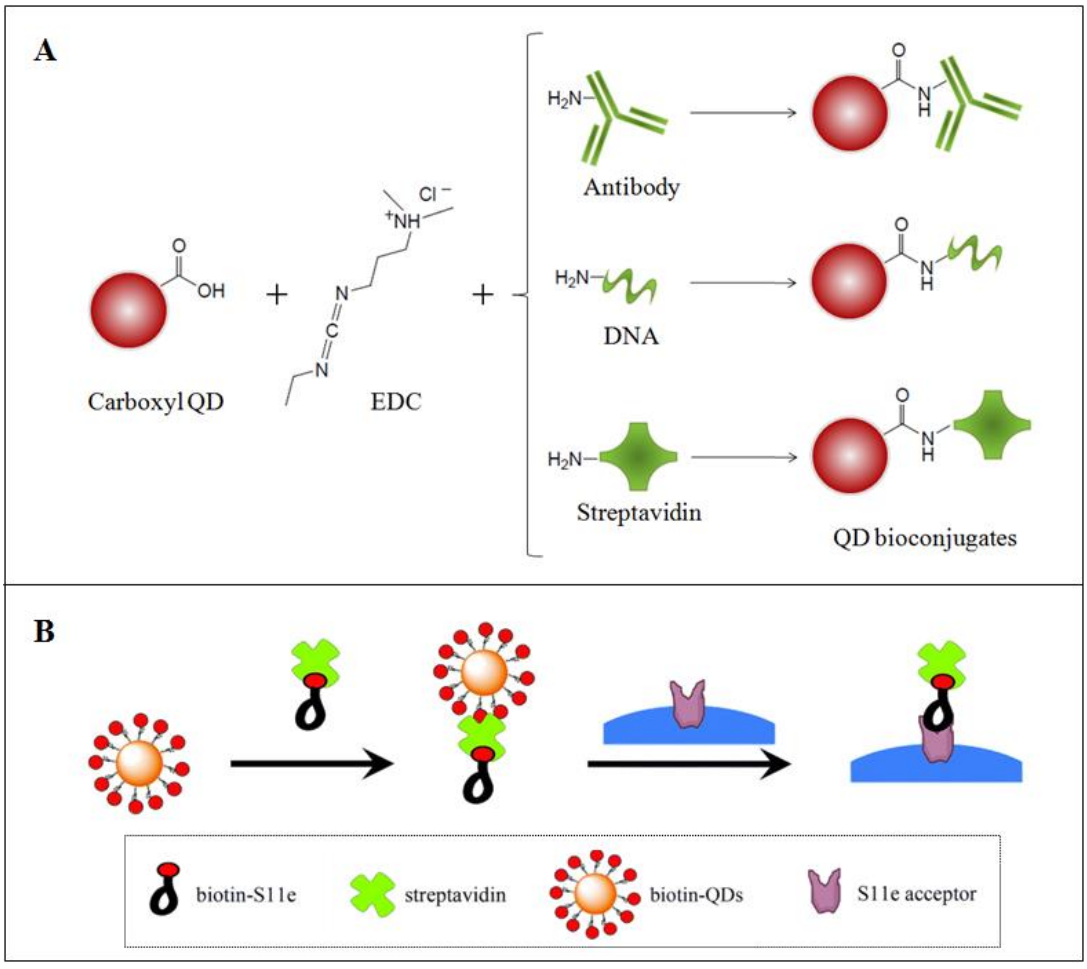

Figure 3. A. Schematic representation of QDs coupled through EDC chemistry to biomolecules. **B.** Schematic representation of a bioconjugated QD coupled to a recognition element for a specific target cell. Adapted from ref [39] with kind permission of The Royal Society of Chemistry.

1.3. Application of Quantum dots in cell detection

Nowadays, bioconjugated QDs are often used as replacements for conventional dyes, when their unique optical/electrochemical characteristics are required to achieve optimal results. Specifically, QDs can be used to efficiently target cancer cell biomarkers due to their high luminescence and stability, which consequently translates to a better stability of the stained sample, providing a robust tool for diagnosis and imaging[41]

1.3.1. Use of QDs in conventional technologies for cell detection

Conventional technologies for specific cell detection are mainly based in fluorescence. Fluorescence-based equipments (such as fluorescence microscopes or flow cytometers) are excellent and widely available tools for the detection of cancer cells through the use of fluorescently labeled targeting biomolecules. The outstanding photostability of bioconjugated QDs provides the researchers to follow longer optimizations and sample analysis procedures.

Bioconjugated QDs have been widely used to determine the expression of cell specific biomarkers related to pathological conditions such as cancer. Wu et al. used QDs linked to immunoglobulin G (IgG) and streptavidin to label the breast cancer marker Her2 (human epidermal growth factor receptor 2) on the surface of fixed and live SKBR3 breast cancer cells [30].

QDs-based detection has also been used to monitor prostate cancer progression by detecting the prostate-specific antigen (PSA) in human prostate cancer cells. The authors used a probe consisting of a secondary antibody conjugated to a QD, obtaining an intense fluorescent signal that was stable for several hours, providing superior sensitivity to the assay (Figure 4A). With this method, the authors were able to detect

low abundance proteins such as PSA, which cannot be clearly discerned using the conventional immunocytochemistry (ICC) methods [42]. Following the same direction, the effectiveness of QD immunostaining and comparisons with current clinical methods were also studied by Chen et al. [43]. They used lung cancer tissue microarrays to detect caveolin-1 and proliferating cell nuclear antigen. The authors reported that QD-based immunostaining methods have higher detection sensitivities in comparison with conventional clinical techniques (Figure 4B).

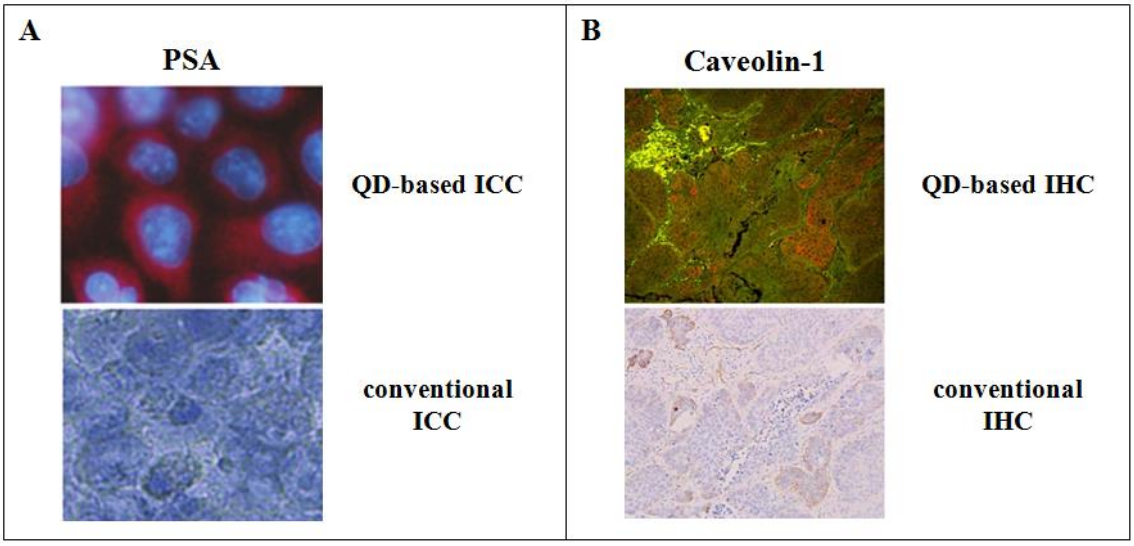

Figure 4. A. Immunocytochemistry of PSA using QDs and organic dyes. The use of QDs allow for a more high definition of the target biomolecule within cells. Adapted from ref [42] with kind permission of PAGEPress. **B. Immunohistochemistry of Caveolin-1.** QDs tissue labeling gives a much better resolution of the distribution of caveolin-1. Adapted from ref [43] with kind permission from Springer Science and Business Media.

So far, there is no doubt that QD immunostaining can provide new capabilities to extend the utility of clinical assays for the detection of specific cell surface biomarkers. Although immunostaining is probably the most employed method in biology to detect

biomarkers on specific cells, another standard technique is flow cytometry. QDs provide flow cytometry users with a new array of stable fluorescent labels, which can be excited with a big range of wavelength light sources and that remain fluorescent under constant illumination. This offers a greater flexibility in designing flow cytometry experiments, when compared with conventional dyes that are limited in the excitation source and undergo photobleaching.

For example, QD-antibody conjugates were used to quantify the levels of protein tyrosin kinase c-abl in K-562 leukemia cells by flow cytometry [44]. The authors prepared water-soluble CdSe QDs and conjugated them with anti-c-abl antibodies. To carry out the assay, a sample of K-562 cells was previously treated with anti-c-abl siRNAs for 6 days and another sample was not (control). Then both samples were fixed and permeabilized to allow QD-anti-c-abl antibody to enter at the cytoplasmic space and detect the c-abl protein, specifically. Flow cytometric analysis successfully showed differences between treated and untreated cells due to the different amount of c-abl protein present in the cytoplasm of K-562 cells (Figure 5).

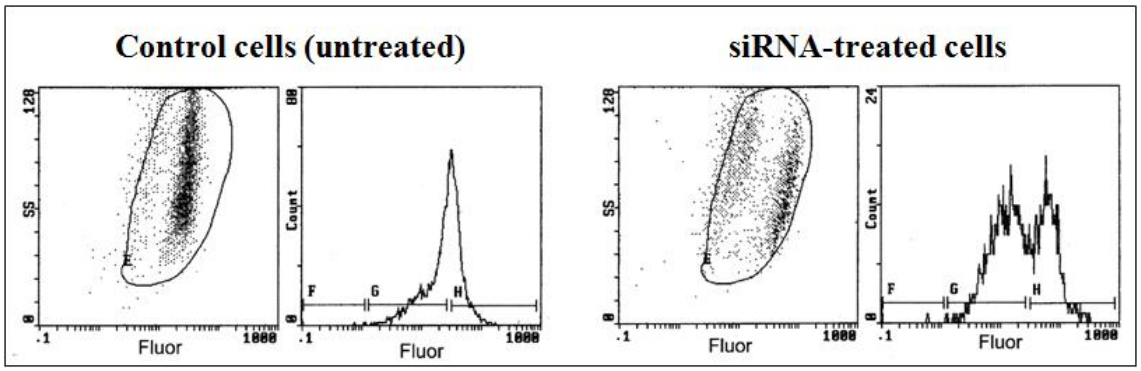

Figure 5. Flow cytometry results using QDs as labels. Different amounts of c-abl protein can be detected using QD-anti-c-abl antibody in control and siRNA-treated cells. Adapted from ref [44] with kind permission from ACS Publications.

Alternatively, Barat et al. used engineered antibody fragments (called cys-diabodies) to modify QDs, for specific detection of Her2 breast cancer biomarker [45]. They developed an oriented coupling of anti-Her2 cys-diabody onto QDs by introducing cysteine residues at the C-termini of the antibody fragments what allowed a thiol-reactive coupling at a site away from the antigen binding site. They tested anti-Her2 cys-diabodies-QD in both Her2 positive and Her2 negative cells. By using flow cytometry the authors confirmed the specific binding activity of cys-diabody QDs: no binding was observed in Her2 negative Jurkat cells, whereas cys-diabody QDs bound efficiently Her2 positive MCF7 (breast carcinoma cells), SK-OV-3 (ovarian carcinoma) and LnCaP/PSCA (prostate carcinoma) cells.

1.3.2. Use of QDs in cell biosensing

One of the main focuses of nanomedicine is the early detection of cancer, which causes millions of deaths every year all over the world [46]. An early diagnosis of cancer often leads to a more efficient treatment that can be the difference between the life and death of the patient. In this context QDs are offering new possibilities to develop efficient sensors for cancer diagnostics. Both optical and electrochemical techniques for QD-biosensing applications have been reported.

Zhang et al [47], detected the presence of overexpressed folate receptor, biomarkers of epithelial-derived tumors, using QDs as fluorescent reporter. They modified the surface of CdS/ZnS QDs by electrostatically absorbing folic acid, the natural ligand of folate receptor. Due to its redox behavior, folic acid turns ñOffò the fluorescence of QDs, when the two are in close proximity. The presence of folate receptor on the surface of cancer cells induces the folic acid to specifically bind it, and thus desorbing from the surface of QDs, turning ñOnò their fluorescence (Figure 6). The authors achieved a

detection limit of 10 ng/mL of folate receptor. This simple turn Off/On mechanism, based on the electrostatic absorption of folic acid, showed how different functionalization strategies of QDs can be used to obtain different applications.

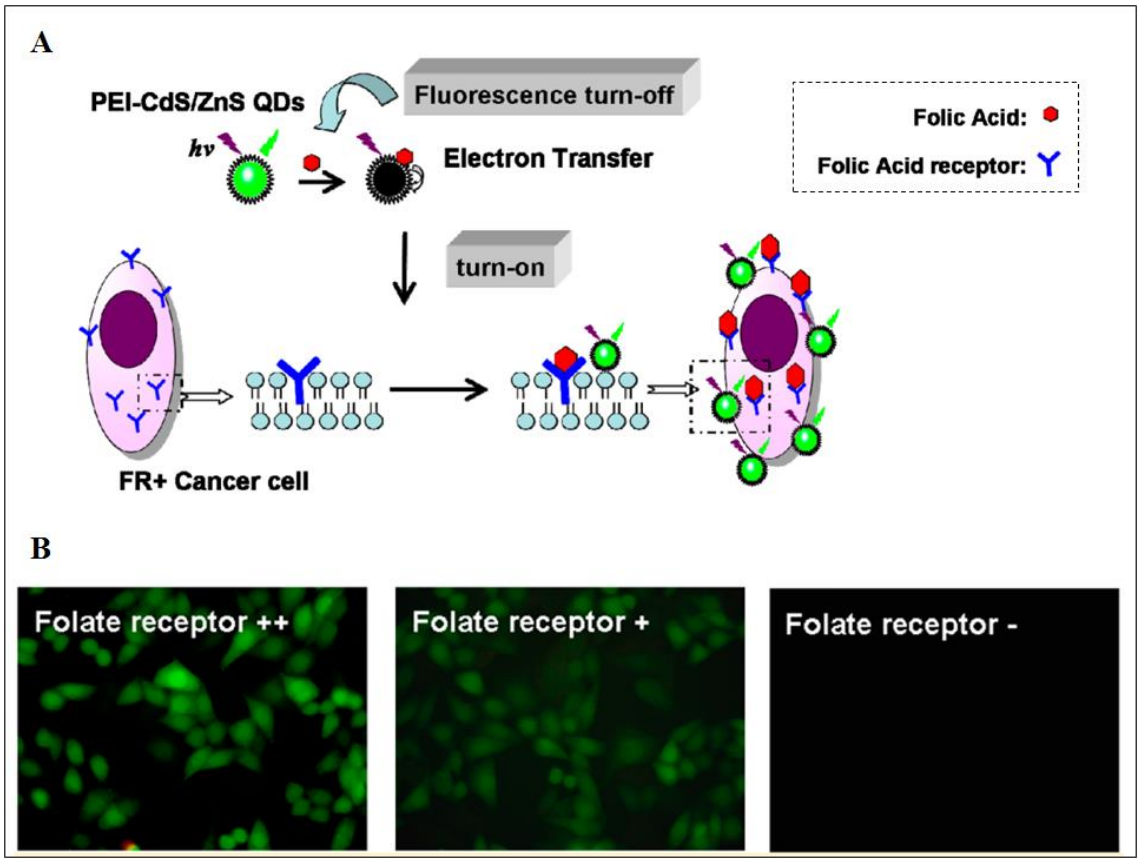

Figure 6. Schematic illustration and results for the optical detection of folate receptor. A. The electrostatic absorption of folic acid on the surface of QDs turns ñOffò their fluorescence. In the presence of folate receptor the folic acid molecules are desorbed from the QDs because they have more affinity for their receptor turning ñOnò the fluorescence of QDs. **B.** Resulting images of folate receptor detection. The more folate receptors within the cells the more desorption of folic acid from QDs and the more turned on fluorescence. Adapted from ref [47] with kind permission from ACS Publications.

Similarly to the previous example, the work proposed by Ma et al, used the possibility to turn Off/On the fluorescence of QDs to early detect Parkinsonôs disease (Figure 7)

[48]. The author modified CdSe/ZnS QDs with ubiquinone-terminated disulphides. The redox state of the ubiquinone affects the fluorescence intensity of QDs, making possible to study the activity of Complex I, an enzyme involved in the electron-transfer chain of mitochondria. Misregulation of Complex I can seriously damage the mitochondria activity, favoring the appearance of Parkinsonôs disease. In the proposed sensor, Complex I can indirectly modify the fluorescence of the QDs by modifying the redox state of ubiquinone. The authors managed to demonstrate the in vitro detection of Complex I level in human neuroblastoma cells.

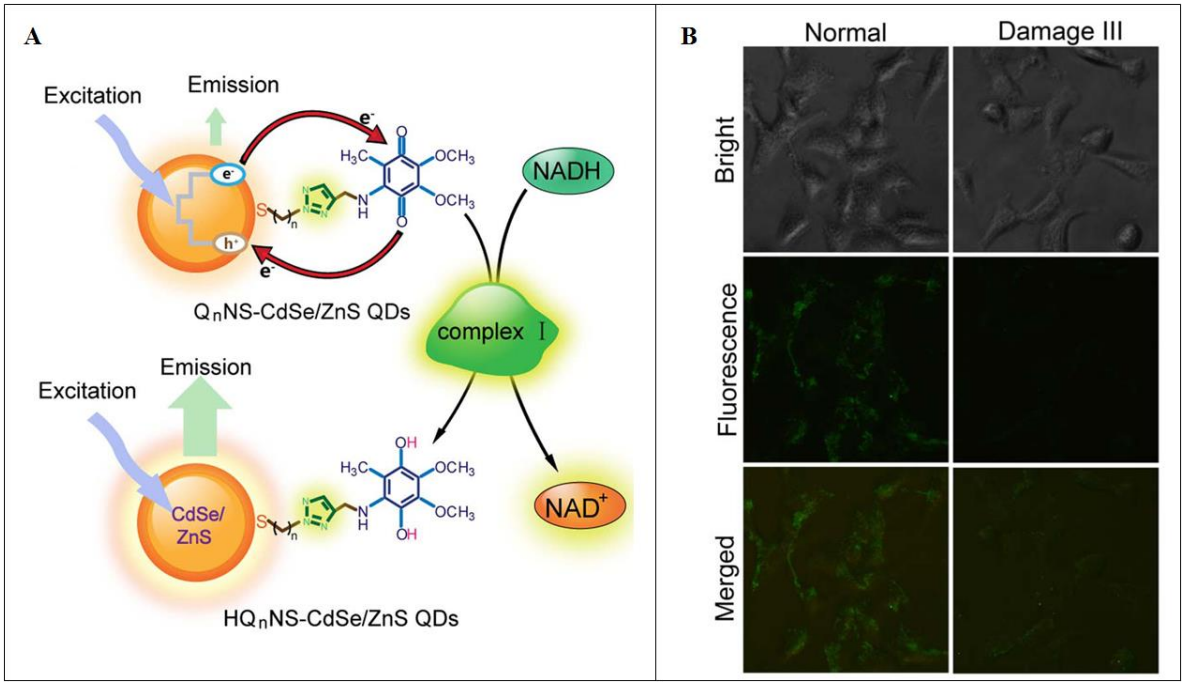

Figure 7. Illustration and results of the use of ubiquinone-modified QDs to study the activity of Complex I. **A.** Ubiquinone can act as quencher of the QDs, but, in the presence of NADH, Complex I changes the redox status of ubiquinone, limiting its quenching effect over the QDs. **B.** Results showing that in normal cells the QDs are highly fluorescent due to Complex I activity, whereas in damaged cells, where Complex I activity is limited, the over fluorescence is very low, indicating the quenching effect of ubiquinone over the QDs. Adapted from ref [48] with kind permission from Nature Publishing Group.

In recent years, scientists have also been exploiting the semiconductor properties of QDs to develop new electrochemical techniques. These new techniques provide the scientific community with sensitive, easy to use and cheap methodologies that can be applied in several sensing applications. Although the electrochemical detection of QDs is used in many protein and nucleic acid sensors, its use for cell sensors is still limited to few and complex devices [49ï 52].

For example, Liu et al. used aptamers-modified QDs for electrochemically detect cancer cells[51]. The authors fabricated an electrode based on a layer-by-layer structure using multiwall carbon nanotubes, gold nanoparticles, and polydopamine to achieve high electrochemical performances. Subsequently, they modified the electrode surface with concanavalin A, a protein that binds strongly to the cell membrane, to force the cells to approach to the surface of the electrode. In order to achieve high levels of sensitivity and specificity, the authors designed an electrochemical label based on the combination of an aptamer, specific for model cancer cells, and DNA-modified QDs that enable the formation of a so called concatamer (Figure 8). In this way, for one aptamer there were several QDs producing an amplified signal. The authors used this strategy for both optical and electrochemical measurements of cancer cells, being able to specifically detect cancer cells over normal cells and achieving a limit of detection of 50 cell/mL.

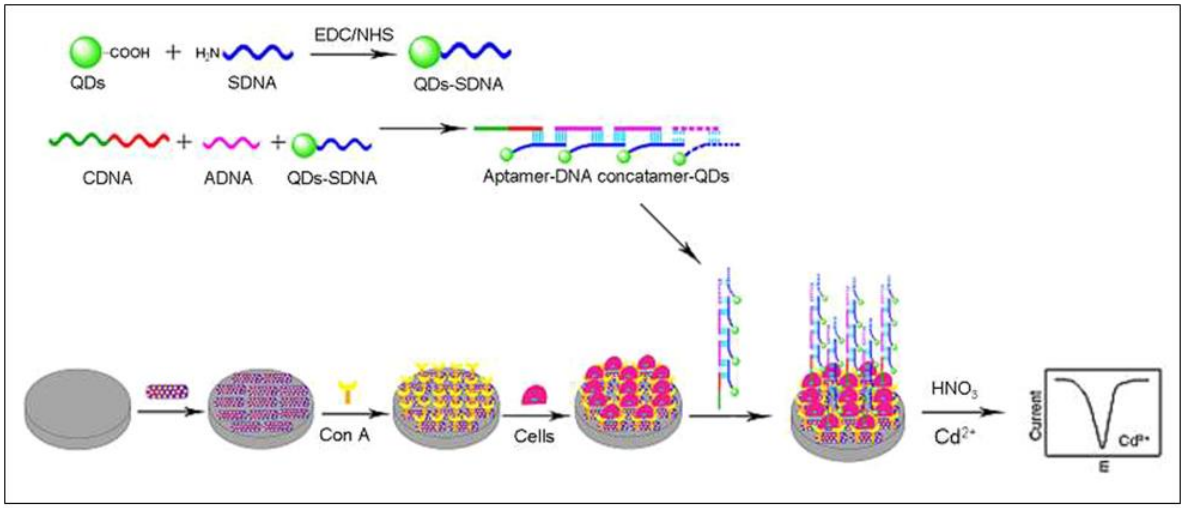

Figure 8. Scheme of the electrochemical cancer cell detection based on QDs-concatamers. Using Concavalin A modified electrodes and aptamer-DNA concatamer QDs, the authors managed to electrochemically detect cancer cells. Adapted from ref. [51] with kind permission from ACS Publications.

Jie and coworkers also managed to detect cancer cells using QDs as electrochemical labels [52]. In this case the authors modified magnetic particles with an aptamer specific for cancer cells. The aptamer also hybridized to a complementary DNA strand used to modify a cluster of QDs, which were assembled on the surface of a dendrimer. In the presence of the target cell, the aptamer dehybridized from the DNA to bind the corresponding cancer cell, and thus releasing the QDs cluster from the magnetic particles. Finally, using magnetic separation, the QDs clusters, which were free in solution, were collected and measured using a mercury film on a glassy carbon electrode (Figure 9). The authors achieved a limit of detection of 89 cells/mL.

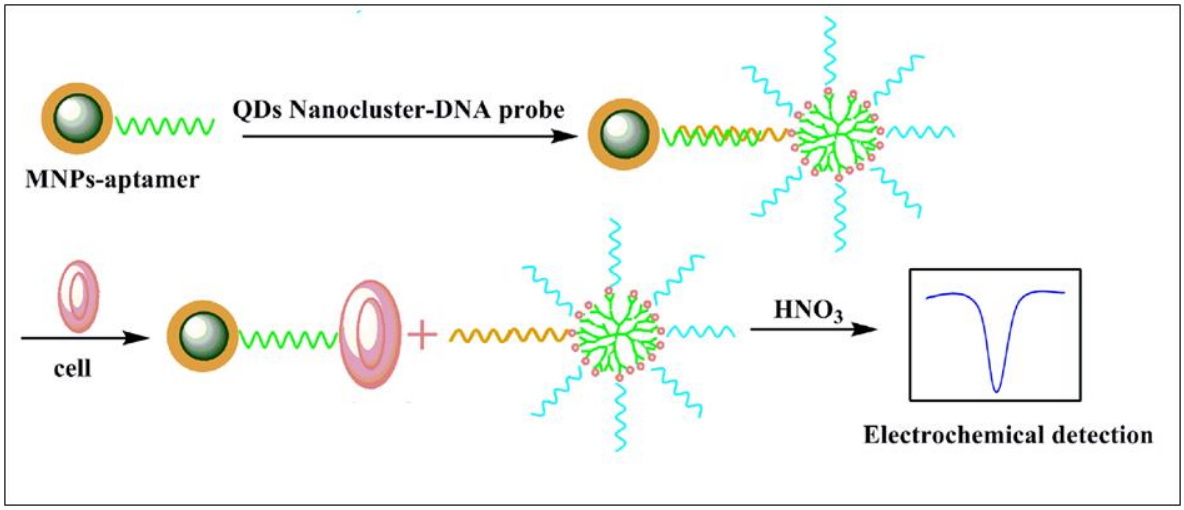

Figure 9. **Scheme of the detection of cancer cells using QDs nanoclusters**. The bond between aptamer modified magnetic nanoparticles and QDs nanoclusters via DNA hybridization is broken in the presence of the aptamer-specific target cell. The free QD nanocluster can then be electrhcemically detected. Adapted from ref. [52] with kind permission from Elsevier.

Instead, a simple approach was presented by Liu et al, where the authors detected folate receptor on the surface of cancer cells [50]. An Indium Tin Oxide ITO electrode was modified with gold nanoparticles to generate a biocompatible surface for cells; then different dilutions of cells were deposited. Using folic acid modified CdSe/ZnS QDs the authors managed to detect over-expressed folate receptor on the surface of KB cells, with a limit of detection of 2000 cells.

Our group also reported that QDs conjugated with a sweet arrow peptide (SAP) could serve as tools to study the interaction of a specific peptide with the cells [53]. In fact using the square wave voltammetry, the authors were able to discriminate the presence of QDs inside or outside the cells. In this case SAP favored the cellular uptake of the QDs conjugates, which were accumulated inside the cell. In order to obtain the specific electrochemical signal from QDs located inside cells, cells had to be lysed (Figure 10).

On contrary, QDs adsorbed onto the cell surface produced an electrochemical signal even without the lysis of the cells.

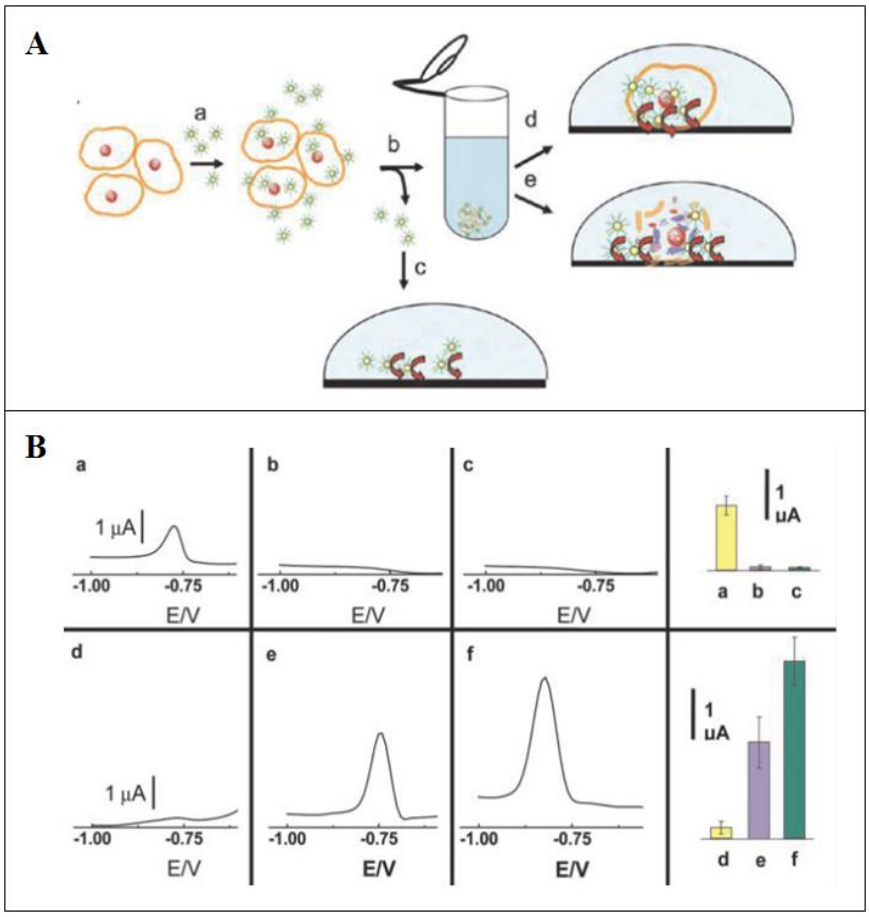

Figure 10. QDs-peptide conjugates act as tools to study cellular uptake mechanisms. A. Illustration of the assay steps: a) incubation of the cells with QDs-SAP conjugates, b) remove of excess of QDs-SAP, c) electrochemical measurement of unbound QDs, d) electrochemical detection of QDs on the cell surface, e) electrochemical detection of uptaken QDs after cell lysis. **B.** Sequential electrochemical measurement (a, b, c) of QDs accumulated on the surface of the cells (QD without SAP), and sequential electrochemical measurements (d, e, f) of uptaken QDs-SAP conjugates during lysis. Adapted from ref [53] with kind permission from ACS Publications.

1.4. Application of Quantum dots in nucleic acid recognition

In the molecular biology field, one of the mayor applications of QDs is to detect nucleic acids (DNA and RNA). The recognition of specific DNA/RNA sequences is fundamental for the early diagnosis of many diseases.

For this reason, it is of high importance to improve usual techniques and develop new cost/efficient ones. Thanks to their optical/electrochemical properties, QDs are great tools to achieve it. This is proved by the high number of published works reporting the use of QDs in methodologies used every day in molecular biology labs, such as gel electrophoresis [54], PCR [55] or fluorescent in situ hybridization (FISH) [56], but also reporting the development of novel highly sensitive and specific biosensors for nucleic acid recognition [38,57,58].

1.4.1. QDs in conventional technologies of molecular biology

Basically, QDs started to be introduced in conventional technologies as optical labels to replace organic dyes. The QD higher brightness and resistance to photobleaching compared to organic dyes, such as FITC, Cy3 or Texas Red, make them excellent labels for FISH, the standard technique to visualize DNA.

The work published by Xiao and Barker compares the stability of the fluorescent signals detected when using streptavidin-QDs or streptavidin-organic dyes at the specific band 1q12 of human metaphase chromosomes, which is the location of the breast cancer related Her2 gene. Upon 2 h of continuous illumination, QDs signals suffered a fluorescence signal decay of about 20%, whilst those of organic dyes suffered at least 70% of fluorescence decay. It was demonstrated that QDs offer a more stable and quantitative mode of FISH for research and clinical applications.

The use of QDs as labels in FISH has also been exploited for the detection of mRNA. mRNA is the product of the expression of an activated gene in cells, and being able to quantify and localize specific mRNA is of great importance for the understanding of cellular functions. Evidence of this is the work carried out by Choi et al. reporting the quantitative detection of mRNA Diptericin gene using a QD-DNA label (Figure 11) [59]. Diptericin is a Drosophila antimicrobial peptide that is induced by bacterial infection. The authors used lipopolysaccharide (LPS) to simulate an infection, since the triggering of Diptericin mRNA transcription by LPS is well known. As expected, the amount of fluorescent hybridization signals increased with the increment of the concentration of LPS added to the cell cultures. The results were further confirmed using real-time PCR as standard technique.

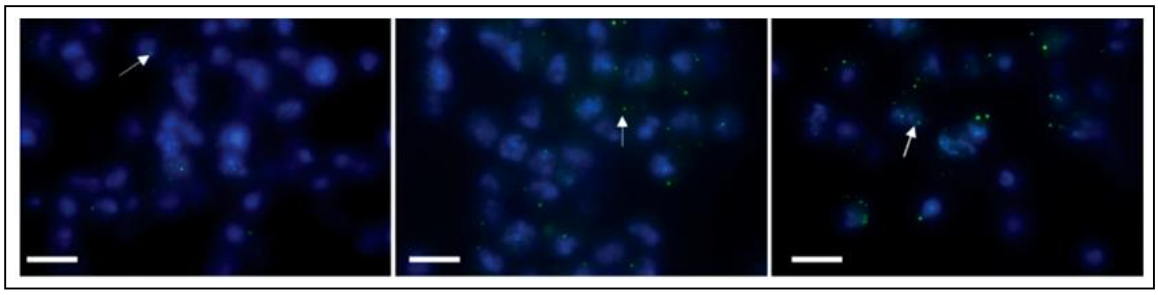

Figure 11. QD-based FISH images of Diptericin mRNA expression. The amount of QDs green fluorescence is induced by increasing the amount of lipopolysaccharide (LPS) added to the cell cultures. From left to right: 1 µg/mL, 10 µg/mL and 100 µg/mL LPS. Nuclei stained with DAPI (blue). Scale bar 20 µm. Adapted from ref [59] with kind permission from Wiley

Besides FISH applications, QDs are used in other molecular biology techniques such as gel electrophoresis. For instance, QDs can be separated and their size determined by capillary zone electrophoresis [60],showing that the mobility of QDs is inversely proportional to their size [61]. However, most importantly, gel electrophoresis has been

used to check and analyze QD conjugation to DNA molecules, an essential step for the preparation of QD-based nucleic acids sensors.

One example of that is the work done by Srinivasan et al., who successfully established the conditions for reproducible conjugation of QDs to plasmid DNA [62]. Gel electrophoresis allowed the determination of the optimal conditions to carry out this specific conjugation (Figure 12), resulting in a high efficiency cell transfection. Moreover, they showed that the intracellular trafficking of plasmid DNA conjugated to QDs could be followed through time due to their long-term photostability, in contrast with rhodamine that fade out after 50 min of continuous excitation.

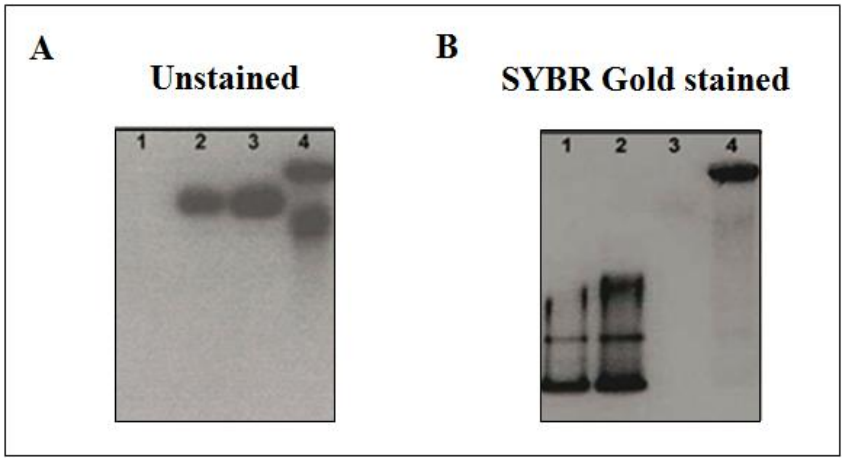

Figure 12. Characterization of QDï DNA conjugates using gel electrophoresis. A, before and **B**, after staining the gel with the DNA stain SYBR gold. Interestingly the physical mixture of QDs and plasmid DNA (lane 2) did not provoke conjugation whereas following the conjugation protocol QD-DNA conjugates were observed (lane 4). Control lanes: (lane1) plasmid DNA alone, (lane 3) QDs alone. Adapted from ref [62] with kind permission from Nature Publishing Group.

1.4.2. Use of QDs for DNA Biosensing

QDs are labels especially suitable for the detection of nucleic acids. On one hand, their functionalization with DNA can be controlled; on the other hand, they do not cause cleavage of DNA; which may occur when DNA is conjugated to organic fluorophores whose photobleaching generates free radicals [63,64]. A number of diverse approaches for QD-based DNA biosensing have been developed. Although there are few QD-based electrochemical sensors for DNA detection (using electrochemiluminescence and anodic stripping voltammetry) [65], most of the other reports are based on the Förster resonance energy transfer (FRET), with the QD as the donor and an organic fluorophore or a quencher as the acceptor [66ï 68].

A single QD-based DNA nanosensor was developed to detect a target sequence with high sensitivity and without amplification, thus reducing dramatically the time and cost of analysis [57] . The sensor consisted in a QD bioconjugated with a capture sequence and a dye-conjugated reporter sequence. When the target DNA was present in the solution, both the QD sensor and the reporter sequence formed a sandwiched structure with the target (Figure 13). This, by bringing the reporter dye very close to QD, created a FRET donor-acceptor pair and allowed a sensitive detection of as low as 50 copies of DNA.

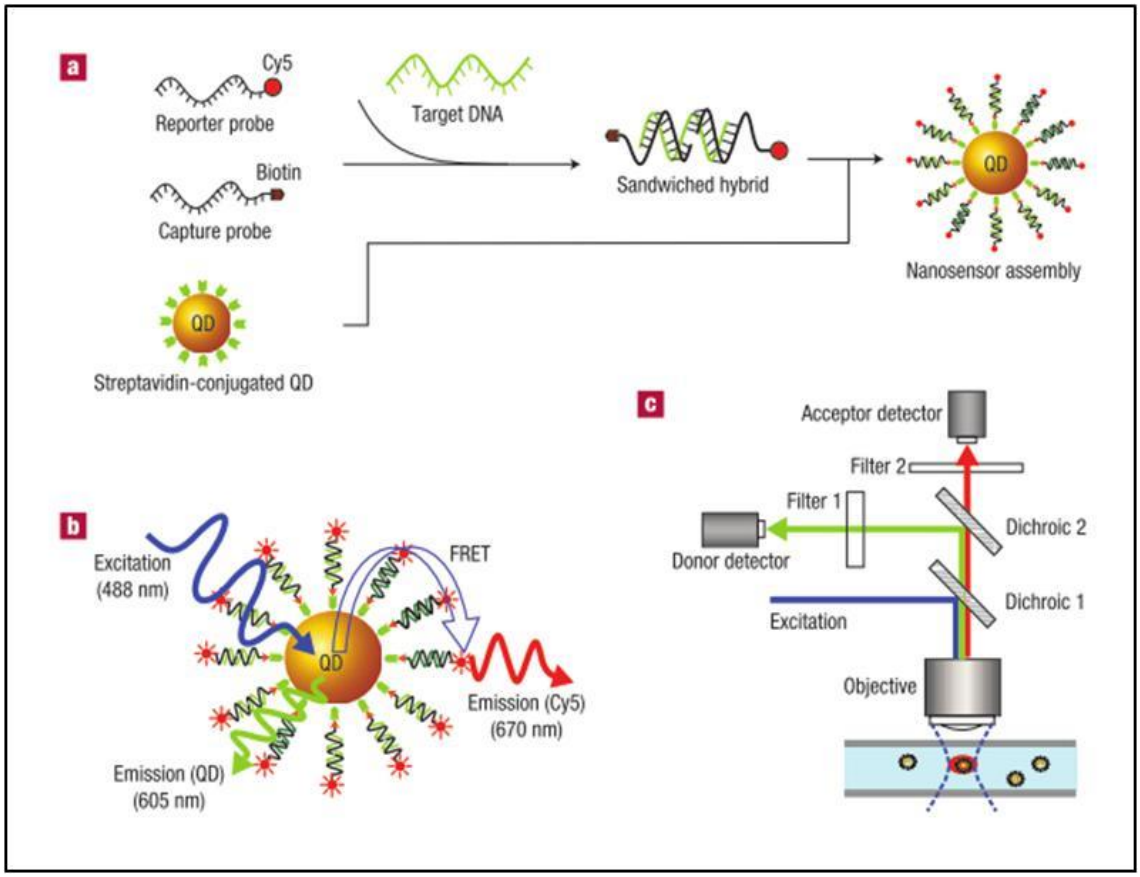

Figure 13. Schematic of single-QD-based DNA nanosensors. (a) Conceptual scheme showing the formation of a nanosensor assembly in the presence of targets. (b) Representation of FRET ocurring when Cy5-DNA target hybridizes the capture DNA of QDs surface. Illumination on QDs allow them to act as donor for hybridized Cy5-DNA. Thus Cy5 fluorescence emission can be detected although it has not been directly illuminated. (c) Experimental setup to detect the nanosensor only (using filter 1) and the nanosensor with the target Cy5-DNA hybridized (using filter 2) with a single excitation source. Adapted from ref [57] with kind permission from Nature Publishing Group.

Hairpin DNA molecules (so called molecular beacons) are used for DNA detection through FRET due to their versatility, specificity and sensitivity. Despite the superior optical properties of QDs, strategies using them in combination with MBs for DNA detection are still in their infancy and still have to be deeply explored. So far, efforts

have been focused on their engineering in order to obtain competitive performances in DNA detection assays [37,58,66]. In particular, Yeh et al demonstrated the potential and robustness of MB-QD-based probes using AuNPs as quenchers, achieving a 7.3-fold increase in fluorescent signal upon target binding, and detecting coxsackievirus B6 (CVB6) on susceptible BGMK cells [69]. To carry out the assay, QDï MBï Au NP probes were delivered into BGMK cells and then incubated with the virus. Subsequently, the increase in fluorescent signals inside cells due to hybridization of newly synthesized viral RNA with the delivered probe was tracked under a fluorescence microscope. As time passed, the fluorescence intensity inside the infected cells became higher, indicating that continual RNA synthesis and virus assembly were occurring (Figure 14). Their method made feasible the real-time monitoring of a process taking place at the intracellular level, through the indirect detection of RNA. That remarks, even more, the already highlighted photostability of QDs.

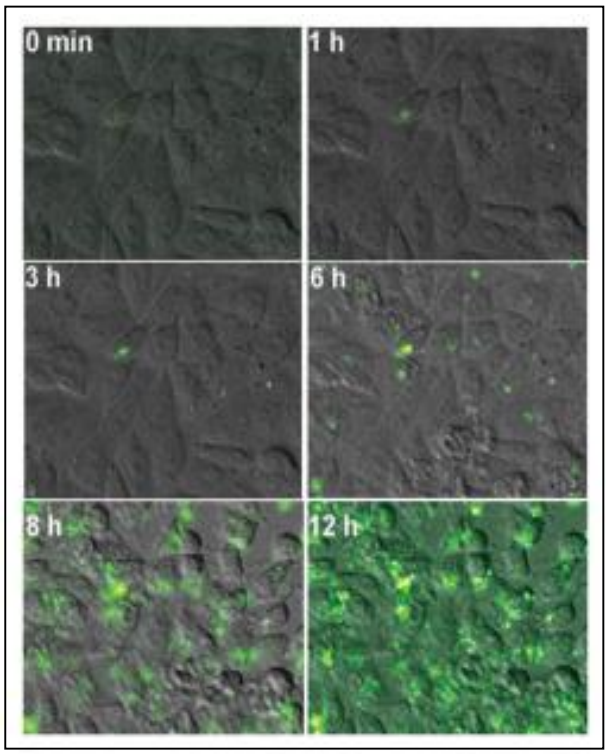

Figure 14. Real-time detection of viral infection spreading. BGMK cells were first incubated with 50 nM QDï MBï Au NP probes, infected with CVB6 at a multiplicity of infection of 0.1 Plaque-forming unit per cell, and monitored using a fluorescent microscope. Adapted from ref [69] with kind permission from RSC Publishing.

1.5. Conclusions

The advantages of QDs while used for bioapplications are related to their narrower emission bands, broad absorption spectra, higher photostability and brightness. In addition they are more stable and less affected by photobleaching than organic dye molecules. Taking these properties and the reported examples into consideration, it is clear that QDs have become a versatile and robust tool for multiple applications in biology and medicine. Nevertheless their use is mainly limited to substitute organic dyes in classical optical techniques and their utilization in combination with cutting edge technologies, such as microfluidics, has not been fully explored yet. On the other hand their specific electrochemical characteristics are still not fully applied for cell detection. Finally, very few examples combine the use of optical and electrochemical properties of QDs in the same device.

The aim of this thesis has been to try to fill in these gaps, thus addressing the objectives reported in the next section.

1.6. References

[1] X. Xu, W. Ho, X. Zhang, N. Bertrand, O. Farokhzad, *Trends Mol. Med.* **2015**, *21*, 223ï 32.

[2] A. Seth, D.-B. Oh, Y. T. Lim, *Nanomedicine (Lond).* **2015**, *10*, 959ï 75.

[3] M. Kodiha, Y. M. Wang, E. Hutter, D. Maysinger, U. Stochaj, *Theranostics* **2015**, *5*, 357ï 70.

[4] M. Singh, D. C. C. Harris-Birtill, S. R. Markar, G. B. Hanna, D. S. Elson, *Nanomedicine* **2015**, DOI 10.1016/j.nano.2015.05.010.

[5] C.-N. Lok, T. Zou, J.-J. Zhang, I. W.-S. Lin, C.-M. Che, *Adv. Mater.* **2014**, *26*, 5550ï 7.

[6] G. Franci, A. Falanga, S. Galdiero, L. Palomba, M. Rai, G. Morelli, M. Galdiero, *Molecules* **2015**, *20*, 8856ï 8874.

[7] F. Dilnawaz, S. K. Sahoo, *Drug Discov. Today* **2015**, DOI 10.1016/j.drudis.2015.06.008.

[8] A. Singh, S. K. Sahoo, *Drug Discov. Today* **2014**, *19*, 474ï 81.

[9] L. Chong, C. H. Vannoy, M. O. Noor, U. J. Krull, *Ther. Deliv.* **2012**, *3*, 479ï 99.

[10] G. Xu, S. Mahajan, I. Roy, K.-T. Yong, *Front. Pharmacol.* **2013**, *4*, 140.

[11] Y. Wang, R. Hu, G. Lin, I. Roy, K.-T. Yong, *ACS Appl. Mater. Interfaces* **2013**, *5*, 2786ï 99.

[12] P. Wu, X.-P. Yan, *Chem. Soc. Rev.* **2013**, *42*, 5489ï 521.

[13] J. Li, J.-J. Zhu, *Analyst* **2013**, *138*, 2506ï 15.

[14] A. I. Ekimov, A. A. Onushchenko, *Sov. Phys. Semicond.* **1982**, *16*, 775ï 778.

[15] L. E. Brus, *J. Chem. Phys.* **1984**, *80*, 4403.

[16] M. Amelia, T. Avellini, S. Monaco, S. Impellizzeri, I. Yildiz, F. M. Raymo, A. Credi, *Pure Appl. Chem.* **2011**, *83*, 1ï 8.

[17] D. Norris, A. Sacra, C. Murray, M. Bawendi, *Phys. Rev. Lett.* **1994**, *72*, 2612ï 2615.

[18] M. Stroh, J. P. Zimmer, D. G. Duda, T. S. Levchenko, K. S. Cohen, E. B. Brown, D. T. Scadden, V. P. Torchilin, M. G. Bawendi, D. Fukumura, et al., *Nat. Med.* **2005**, *11*, 678ï 82.

[19] W. Liu, H. S. Choi, J. P. Zimmer, E. Tanaka, J. V Frangioni, M. Bawendi, *J. Am. Chem. Soc.* **2007**, *129*, 14530ï 1.

[20] W. Liu, M. Howarth, A. B. Greytak, Y. Zheng, D. G. Nocera, A. Y. Ting, M. G. Bawendi, *J. Am. Chem. Soc.* **2008**, *130*, 1274ï 84.

[21] a P. Alivisatos, W. Gu, C. Larabell, *Annu. Rev. Biomed. Eng.* **2005**, *7*, 55ï 76.

[22] K. Zhang, H. Chang, A. Fu, A. P. Alivisatos, H. Yang, *Nano Lett.* **2006**, *6*, 843ï 7.

[23] M. Dahan, T. Laurence, F. Pinaud, D. S. Chemla, A. P. Alivisatos, M. Sauer, S. Weiss, *Opt. Lett.* **2001**, *26*, 825ï 7.

[24] http://www.thermofisher.com/es/en/home/brands/molecular-probes/key-molecular-probes-products/qdot/technology-overview.html#structure

[25] R. Gill, M. Zayats, I. Willner, *Angew. Chem. Int. Ed. Engl.* **2008**, *47*, 7602ï 25.

[26] A. M. Smith, S. Nie, *Acc. Chem. Res.* **2010**, *43*, 190ï 200.

[27] B. O. Dabbousi, J. Rodriguez-Viejo, F. V. Mikulec, J. R. Heine, H. Mattoussi, R. Ober, K. F. Jensen, M. G. Bawendi, *J. Phys. Chem. B* **1997**, *101*, 9463ï 9475.

[28] M. Grabolle, J. Ziegler, A. Merkulov, T. Nann, U. Resch-Genger, *Ann. N. Y. Acad. Sci.* **2008**, *1130*, 235ï 41.

[29] M. Bruchez, M. Moronne, P. Gin, S. Weiss, A. P. Alivisatos, *Science* **1998**, *281*, 2013ï 2016.

[30] X. Wu, H. Liu, J. Liu, K. N. Haley, J. A. Treadway, J. P. Larson, N. Ge, F. Peale, M. P. Bruchez, *Nat. Biotechnol.* **2003**, *21*, 41ï 46.

[31] Y. Zhu, H. Hong, Z. P. Xu, Z. Li, W. Cai, *Curr. Mol. Med.* **2013**, *13*, 1549ï 67.

[32] B. a Kairdolf, A. M. Smith, T. H. Stokes, M. D. Wang, A. N. Young, S. Nie, *Annu. Rev. Anal. Chem.* **2013**, *6*, 143ï 162.

[33] F. Lisdat, D. Schäfer, A. Kapp, *Anal. Bioanal. Chem.* **2013**, *405*, 3739ï 52.

[34] M. Amelia, T. Avellini, S. Monaco, S. Impellizzeri, I. Yildiz, F. M. Raymo, A. Credi, *Pure Appl. Chem.* **2010**, *83*, 1ï 8.

[35] W. W. Yu, E. Chang, R. Drezek, V. L. Colvin, *Biochem. Biophys. Res. Commun.* **2006**, *348*, 781ï 786.

[36] H. M. E. Azzazy, M. M. H. Mansour, S. C. Kazmierczak, *Clin. Chem.* **2006**, *52*, 1238ï 1246.

[37] N. C. Cady, A. D. Strickland, C. a. Batt, *Mol. Cell. Probes* **2007**, *21*, 116ï 124.

[38] C.-S. Wu, J. M. Cupps, X. Fan, *Nanotechnology* **2009**, *20*, 305502.

[39] C. Wu, J. Liu, P. Zhang, J. Li, H. Ji, X. Yang, K. Wang, *Analyst* **2015**, *140*, 6100ï 6107.

[40] A. S. Karakoti, R. Shukla, R. Shanker, S. Singh, *Adv. Colloid Interface Sci.* **2015**, *215*, 28ï 45.

[41] M.-X. Zhao, E.-Z. Zeng, *Nanoscale Res. Lett.* **2015**, *10*, DOI 10.1186/s11671-015-0873-8.

[42] C. Shi, G. Zhou, Y. Zhu, Y. Su, T. Cheng, H. E. Zhau, L. W. Chung, *Eur J Histochem* **2008**, *52*, 127ï 134.

[43] H. Chen, J. Xue, Y. Zhang, X. Zhu, J. Gao, B. Yu, *J. Mol. Histol.* **2009**, *40*, 261ï 268.

[44] Z. Zhelev, R. Bakalova, H. Ohba, R. Jose, Y. Imai, Y. Baba, *Anal. Chem.* **2006**, *78*, 321ï 330.

[45] B. Barat, S. J. Sirk, K. E. McCabe, J. Li, E. J. Lepin, R. Remenyi, L. K. Ai, T. Olafsen, S. S. Gambhir, S. Weiss, et al., *Bioconjug. Chem.* **2009**, *20*, 1474ï 1481.

[46] http://www.who.int/mediacentre/factsheets/fs297/en/

[47] Y. Zhang, J. M. Liu, X. P. Yan, *Anal. Chem.* **2013**, *85*, 228ï 234.

[48] W. Ma, L.-X. Qin, F.-T. Liu, Z. Gu, J. Wang, Z. G. Pan, T. D. James, Y.-T. Long, *Sci. Rep.* **2013**, *3*, 1537.

[49] J. Li, M. Xu, H. Huang, J. Zhou, E. S. Abdel-Halimb, J. R. Zhang, J. J. Zhu, *Talanta* **2011**, *85*, 2113ï 2120.

[50] Y. Liu, L. Zhu, J. Kong, P. Yang, B. Liu, *Electrochem. commun.* **2013**, *33*, 59ï 62.

[51] H. Liu, S. Xu, Z. He, A. Deng, J. J. Zhu, *Anal. Chem.* **2013**, *85*, 3385ï 3392.

[52] G. Jie, J. Zhang, G. Jie, L. Wang, *Biosens. Bioelectron.* **2014**, *52*, 69ï 75.

[53] S. Marín, S. Pujals, E. Giralt, A. Merkoçi, *Bioconjug. Chem.* **2011**, *22*, 180ï 185.

[54] F. Sang, X. Huang, J. Ren, *Electrophoresis* **2014**, *35*, 793ï 803.

[55] F. Sang, Y. Yang, L. Yuan, J. Ren, Z. Zhang, *Nanoscale* **2015**, DOI 10.1039/C5NR03596A.

[56] L. Ma, S. M. Wu, J. Huang, Y. Ding, D. W. Pang, L. Li, *Chromosoma* **2008**, *117*, 181ï 187.

[57] C.-Y. Zhang, H.-C. Yeh, M. T. Kuroki, T.-H. Wang, *Nat. Mater.* **2005**, *4*, 826ï 831.

[58] I. L. Medintz, L. Berti, T. Pons, A. F. Grimes, D. S. English, A. Alessandrini, P. Facci, H. Mattoussi, *Nano Lett.* **2007**, *7*, 1741ï 1748.

[59] Y. Choi, H. P. Kim, S. M. Hong, J. Y. Ryu, S. J. Han, R. Song, *Small* **2009**, *5*, 2085ï 2091.

[60] U. Pyell, *Electrophoresis* **2008**, *29*, 576ï 589.

[61] Y. Q. Li, H. Q. Wang, J. H. Wang, L. Y. Guan, B. F. Liu, Y. Di Zhao, H. Chen, *Anal. Chim. Acta* **2009**, *647*, 219ï 225.

[62] C. Srinivasan, J. Lee, F. Papadimitrakopoulos, L. K. Silbart, M. Zhao, D. J. Burgess, *Mol. Ther.* **2006**, *14*, 192ï 201.

[63] X. Michalet, F. F. Pinaud, L. A. Bentolila, J. M. Tsay, S. Doose, J. J. Li, G. Sundaresan, A. M. Wu, S. S. Gambhir, S. Weiss, *Science* **2005**, *307*, 538ï 544.

[64] H. M. E. Azzazy, M. M. H. Mansour, S. C. Kazmierczak, *Clin. Biochem.* **2007**, *40*, 917ï 927.

[65] H. Huang, J. Li, Y. Tan, J. Zhou, J.-J. Zhu, *Analyst* **2010**, *135*, 1773ï 8.

[66] J. H. Kim, D. Morikis, M. Ozkan, *Sensors Actuators, B Chem.* **2004**, *102*, 315ï 319.

[67] W. R. Algar, U. J. Krull, *Anal. Bioanal. Chem.* **2008**, *391*, 1609ï 1618.

[68] C. C. Chou, Y. H. Huang, *Sensors (Switzerland)* **2012**, *12*, 16660ï 16672.

[69] H.-Y. Yeh, M. V Yates, A. Mulchandani, W. Chen, *Chem. Commun. (Camb).* **2010**, *46*, 3914ï 3916.

Chapter 2. Objectives

2. Objective

Although in nanomedicine there are many reported quantum dots applications that take advantage of their unique properties, their stability in biological media and their availability to conjugate to diverse biomolecules, there is still a lack of optical/electrochemical QDs-based technologies that can be used for *in vitro* nanodiagnostics or drug discovery.

The main objective of this thesis is to explore different ways to use QDs for the detection of specific cells and DNA, making these new approaches valuable tools for diagnostics and drug discovery.

More in detail, specific objectives are:

- To develop a robust and reproducible strategy to use QDs as immunolabels for enhanced imaging of eukaryotic cells using fluorescence and confocal microscopy for diagnostics;

- To develop a QD-based dual optical/electrochemical technology for apoptosis detection;

- To develop a versatile platform for drug screening, by means of apoptosis detection in living cancer cells using QDs and a modular microfluidics system;

- To develop a lab-on-a-chip for monitoring of DNA hybridization assays using molecular beacons technology through the use of QDs as labels.

Chapter 3. QDs versus Alexa: reality of promising tools for immunocytochemistry

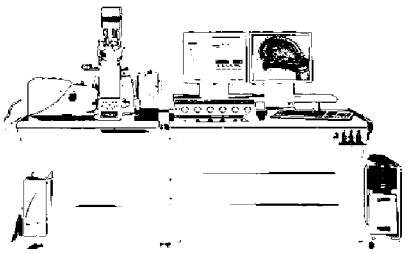

3.1. Introduction

Semiconductor nanocrystals called Quantum Dots (QDs) are fluorochromes with many advantages compared to the organic fluorescent dyes habitually used in immunocytochemistry procedures [1]. Their water solubility and capacity to be conjugated with different biomolecules have only recently been established [2]; therefore, their application in both the biological and medical research fields is still scarce.

Since the first microscope appeared up to the present day, different kinds of dyes (fluorescent proteins, small fluorescent molecules, etc.) have been used to detect or localize different biomolecules within an intracellular context. In the last decade, when nanotechnology became relevant, QDs were introduced as a promising methodological tool due to their intrinsic brightness, high photostability, high molar extinction coefficient, narrow emission band, and excitability with several wavelengths [3]. These qualities opened the possibility to handle samples labeled with different colors, preventing fluorescent signal crossing-over, using a single laser line to excite different QDs at the same time [4].

QDs are aggregates of atoms -from hundreds to tens of thousands that behave as one- of semiconductor materials that produce a crystalline matrix (nanocrystal). Composition, size and shape of this matrix determine their physical characteristics. The properties of nanocrystals vary according to their size, which ranges generally from 1 to 10 nm in diameter [5]; whereas smaller QDs emit in shorter wavelengths, bigger QDs emit in longer wavelengths. The crystalline core of QDs is composed of cadmium selenide and covered with a zinc sulfide shell. Moreover, some QDs are coated with different kinds of polymers and molecules in order to make them water-soluble and to facilitate their conjugation to different biomolecules, providing a specific functionality [6ï 9].

QDs can be linked to many molecules, such as DNA, proteins and antibodies, and therefore they have a wide range of applications in the biosciences. To date, QDs have been used to localize proteins [10,11] and mRNA within the cell [12], to label cancer markers [13], to follow in vivo metastatic cells during extravasation [14] or to track embryonic stem cells in deep tissues [15].

The aim of this study was to use QDs as secondary and tertiary antibodies in a routine immunocytochemistry procedure in which organic dyes are currently used. Therefore, we characterized the shape, size and optical properties of QD 655 (IgG or streptavidin conjugated) in order to develop a standard protocol for protein immunodetection using QDs. We have made a comparative study of fluorescence intensity, bandwidth, photostability, specificity and the quality of QD 655 versus its homologous organic fluorophore, Alexa 594 (IgG or streptavidin conjugated), to evaluate the possibility of replacing Alexa with QDs in this protein detection procedure.

3.2. Methods

3.2.1. Materials

Two types of red emission spectra QDs were used as secondary and tertiary antibodies: QD 655 Goat $F(ab)_2$ anti-mouse IgG conjugate (QD 655-IgG) and QD 655 streptavidin conjugate (QD 655-strep). Two homologous red emission Alexa Fluor Dyes: Alexa 594 Goat $F(ab)_2$ anti-mouse IgG conjugate (Alexa 594-IgG) and Alexa 594 streptavidin conjugate (Alexa 594-strep) were used to compare to QD antibodies. Secondary antibodies QD 655-IgG and Alexa 594-IgG were purchased from Molecular Probes (Invitrogen Corp; Eugene, Oregon, USA), and Anti-Ms IgG biotin from Boheringer (Mannheim; Indianapolis, USA). Primary antibody monoclonal anti-ϐ-tubulin was

purchased from Sigma-Aldrich Chemie GmbH (Steinheim, Germany). GM130 and EEA1 primary antibodies were purchased from BD Biosciences (San Jose, California, USA).

3.2.2. High Resolution Transmission Electron Microscopy (HRTEM)

To carry out a HRTEM analysis, 0.5 εl of each QD was diluted in 500 εl of MilliQ water and centrifuged for 10 minutes at 6000 rpm to eliminate all organic precipitates. A drop of each diluted QD was deposited on a carbon layer copper grid and air-dried.

Images of each type of QD were obtained with a HRTEM, using a JEOL JEM 2011 transmission electron microscope (Jeol LTD; Tokyo, Japan) operating at 200 kV. The sizes of the QDs were determined with Digital Micrograph software (Gatan Inc; Warrendale, Pennsylvania, USA) and data obtained were processed with statistics software Origin-8 (OriginLab Corporation; Northampton, Massachusetts, USA).

3.2.3. Cell cultures

Two different culture cell lines, Vero (ATCC-CCL-81) and HeLa (ATCC-CCL-2), were used. Cells were maintained in MEM (GIBCO, Rockville, Maryland, USA) supplemented with 10% Fetal Calf Serum (GIBCO) and incubated at 37°C and 5% CO_2 in a humidified atmosphere.

3.2.4. Immunocytochemistry

For immunocytochemistry analysis, cells were seeded onto glass coverslips and incubated at 37°C and 5% CO2, until confluence was reached. Cells were fixed in 4% paraformaldehyde (Electron Microscopy Sciences; Fort Washington, Pennsylvania, USA) in 0.01 M phosphate buffer saline (Sigma Aldrich Chemie GmbH; Steinheim, Germany) for 15 min, permeabilized in 0.25% Triton X-100 (Fluka Chemie AG; Buchs, Switzerland) for 15 min and blocked in 6% bovine serum albumin (Sigma Aldrich Chemie GmbH; Steinheim, Germany) for 40 min. Finally, cells were incubated with the

anti-ß-tubulin monoclonal antibody (4 ε g/ml) to detect the microtubule network, with the GM130 antibody (10 ε g/ml) to detect the Golgi complex or with the EEA1 antibody (2.5 ε g/ml) to detect the endosomal system. In all cases the primary antibody was incubated for 1 h at 37°C.

To perform secondary immunodetection, anti-Ms IgG antibody conjugated to Alexa or QDs (4 ε g/ml and 30 nM final concentration, respectively) was used. For tertiary immunodetection, cells were first incubated with Anti-Ms IgG Biotin (1 ε g/ml) for 1 h at 37°C, and then with streptavidin conjugated to Alexa or QDs (4 ε g/ml and 30 nM final concentration, respectively). Coverslips were mounted onto glass slides using Fluoprep mounting media (bioMérieux® SA, Marcy l'Etoile, France) to preserve fluorescence.

3.2.5. Confocal Laser Scanning Microscopy (CLSM)

Images were captured with a CLSM Leica TCS-SP5 AOBS spectral (Leica Microsystems Heidelberg GmbH; Mannheim, Germany) using a Plan-Apochromatic 63× objective (NA 1.4, oil).

Series of images (xyə), called lambdastacks, were taken to determine the spectra emission of QDs and Alexas and to establish their bandwidth. The excitation wavelength used was the 488 nm line of an Ar laser. The AOTF was set at 40% and 80% for QDs and Alexas, respectively.

The emission detection was set from 500 to 780 nm. The confocal pinhole for each lambdastack was fixed at 2 Airy units. For each xy focal plane, confocal microscopy measured the emission variation every 10 nm (lambda step size = 7 nm). The emission spectra analysis was processed using the CLSM software (Leica LAS AF). A Region of Interest (ROI) was delimited to determine the fluorescence intensity (FI) in the selected

area in relation to the wavelength. To analyze immunolabeled cells, 45 ROIs of 2 εm^2 were selected near cell nuclei; FI and bandwidth were calculated in the selected ROIs.

Photostability experiments were performed using the Live Data Mode function of the CLSM, which permits monitoring long time-lapse experiments. Each type of fluorophore was illuminated with a 561 nm excitation laser line for 8 minutes (100% power, zoom = 6). Images were taken at 1 second intervals, in 512 × 512 pixels with 8 bits of dynamic range. In the area where the laser was at its maximum illumination power, 45 ROIs of 2 εm^2 were selected to show the FI in the region in relation to time.

Secondary or tertiary antibody specificity was evaluated using the xyz mode of the CLSM, which permits one to scan the xy plane along the z axis. Images were captured every 0.2 εm along 3 εm of thickness, with 1 Airy confocal pinhole. From the xyz series obtained by CLSM, maximum intensity projections were achieved with Leica LAS AF software, and three-dimensional models were generated using Imaris software (Bitplane; Zürich, Switzerland).

3.2.6. Statistical analysis

To determine if there were significant differences in size between QDs conjugated to IgG or to streptavidin, a two-sample T-Student's test (T-test) for comparison of means, with 95% confidence, was carried out. Previously, a F-Fisher test was performed and equal variances were assumed due to the returned p-value of 0.389. The equality of means hypothesis was rejected when the p-value was lower than 0.05 ($p < 0.05$).

3.3. Results

3.3.1. QDs characterization by HRTEM

QD 655 showed a cone-like shape (Figure 1) with no differences in shape between QDs conjugated to streptavidin or to IgG. However, when comparing the size of the QDs conjugated to IgG with those conjugated to streptavidin, significant differences ($p < 0.05$) were found. QD 655-IgG is bigger ($15.4 \pm 0.2 \times 6.4 \pm 0.1$ nm) than QD 655-strep ($13.1 \pm 2.8 \times 6.3 \pm 0.9$ nm).

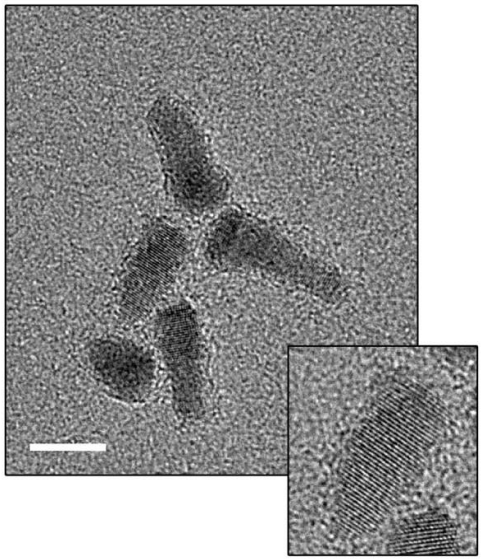

Figure 1. HRTEM QD characterization. The large image shows a general view of QD 655 dispersion. The small image shows a detail of a single QD 655 cone-like nanocrystal. Its crystalline structure core can be seen. Scale bar = 10 nm.

3.3.2. QDs characterization by CLSM

QDs have been reported to present several optical advantages in fluorescence detection regarding conventional organic fluorophores. QD 655 has been compared to Alexa 594 to evaluate differences in fluorescence intensity, bandwidth, photostability and specificity.

3.3.2.1. Emission Spectra

First, the maximum fluorescence emission peak (λ_{em}) of both fluorophores was assessed using the lambdascan function of the CLSM. QD 655 presented its maximum at 651 nm, whereas Alexa 594 had its peak at 615 nm (Figure 2, Table 1). The λ_{em} value recorded was identical for the same fluorophore independently of its conjugation (IgG or strep).

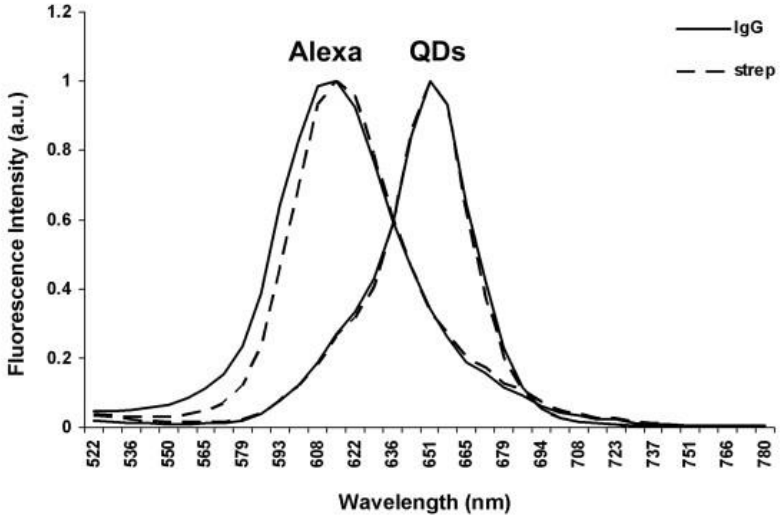

Figure 2. Fluorescence emission spectra. Spectral profile representing fluorescence intensity versus emission wavelength (500ï 780 nm) for QD 655-IgG, QD 655-Streptavidin and their Alexa homologues. Excitation wavelength = 488 nm.

Second, the fluorescence intensity (FI) level of QD 655 (Ig or Strep) and Alexa 594 (Ig or strep) was calculated. The FI level of QD 655 was higher than that of Alexa 594 (Table 1).

Table 1. Spectral properties.

	Emission peak (nm)	FI[a]	Bandwidth (nm)[b]
Q655-IgG	651	200	35.5
Q655-strep	651	180	37
A594-IgG	615	75	48
A594-strep	615	75	53

Emission peak, fluorescence intensity (FI) and bandwidth for QD 655 and Alexa 594 analyzed at 488 nm excitation wavelength.

(a) Values in gray level (0ï 255).

(b) Calculated as the full width at 50% maximum of the emission spectrum (FWHM) in the FI profile.

Differences in bandwidth, calculated from the emission profiles (Figure 2), were also found when both kinds of fluorophores were compared. QDs had narrower values of bandwidth than the homologous Alexas (Table 1).

3.3.2.2. Photostability

Photostability was assessed by exposing immunolabeled cultures for eight minutes at the maximum power laser line of 561 nm. For the first 90 seconds, the initial fluorescence intensity of ß-tubulin labeled with QD 655s was reduced by about 5%. The same laser incidence produced an intensity reduction of 90% in cultures labeled with Alexa 594s. At the end of the irradiation period, no ß-tubulin was detected in cultures labeled with Alexa 594s, whereas in cultures labeled with QD 655s, ß-tubulin still kept up to 10%ï 40% of the initial fluorescence intensity (Figure 3 and 4).

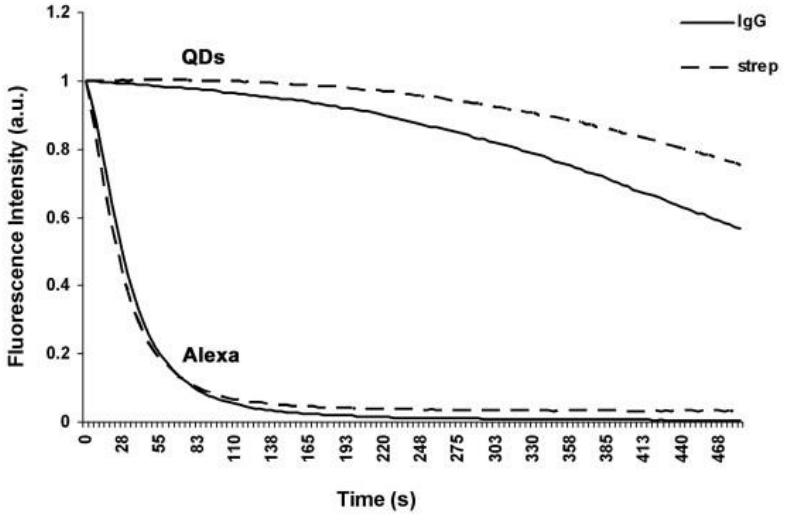

Figure 3. Photostability profile. Fluorescence intensity changes of QDs and Alexas during the irradiation period with the 561 nm laser line at maximum power.

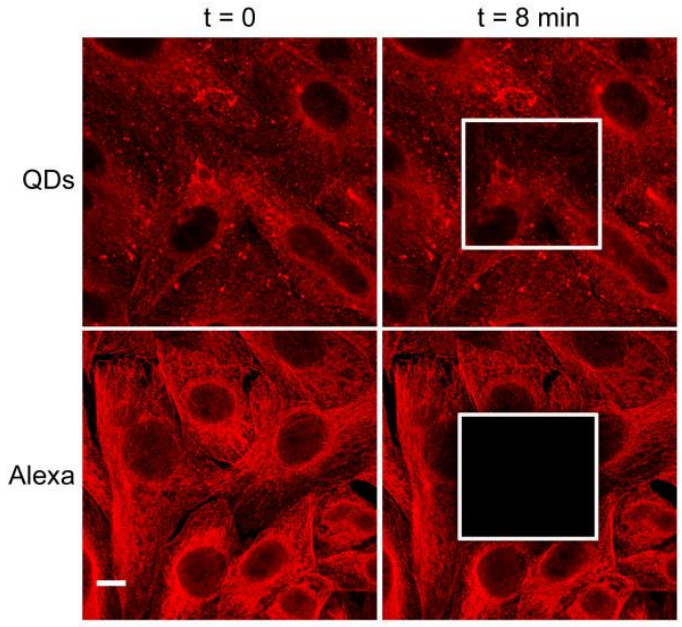

Figure 4. CLSM photostability images. Left-hand images correspond to the emission signal of QDs and Alexas conjugated to streptavidin before irradiation (t = 0 min) with the 561 nm laser line at its maximum power. Right-hand images show the emission signal of QDs and Alexas at the end of the irradiation period (t = 8 min). Note the loss of fluorescence intensity in the delimited area. Scale bar = 10 ε m.

3.3.2.3. Specificity of labeling

Staining specificity was analyzed on cell cultures labeled with primary antibody against the microtubule network (ß-tubulin), Golgi complex (GM130) or endosomal system (EEA1). Brightness of both fluorophores conjugated to IgG was similar (Figure 5). Differences in specificity were detected when QD 655-IgG was used as a secondary antibody against ß-tubulin. The network of microtubules was not well defined, with background and QD aggregates that had not selectively linked to ß-tubulin. In contrast, Alexa 594-IgG was very specific and the microtubule network was definitely detectable. When QDs and Alexas were used as tertiary antibodies, the tubulin network was clearly detected by both fluorophores, but Alexa fluorochromes were more specific in pinpointing the tubulin filament structure.

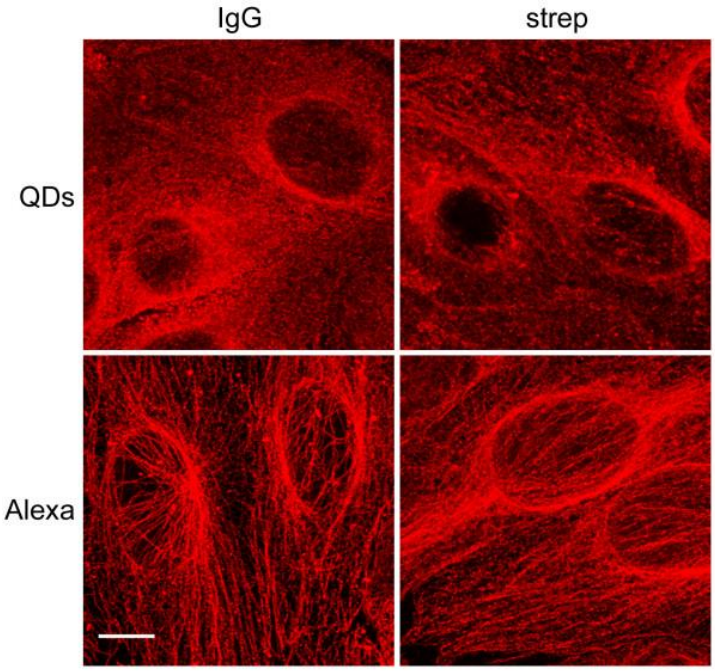

Figure 5. CLSM specificity analysis of ß-tubulin labeling. Maximum intensity projections of the distribution of the tubulin network labeled with QDs (top images) show lower specificity than their organic Alexa homologue labeling (bottom images). Scale bar = 10 ε m.

No differences in specificity were detected when QD 655 or Alexa 594 was used as a secondary or tertiary antibody against GM130 or EEA1. Both types of fluorophores showed similar specificity (Figure 6).

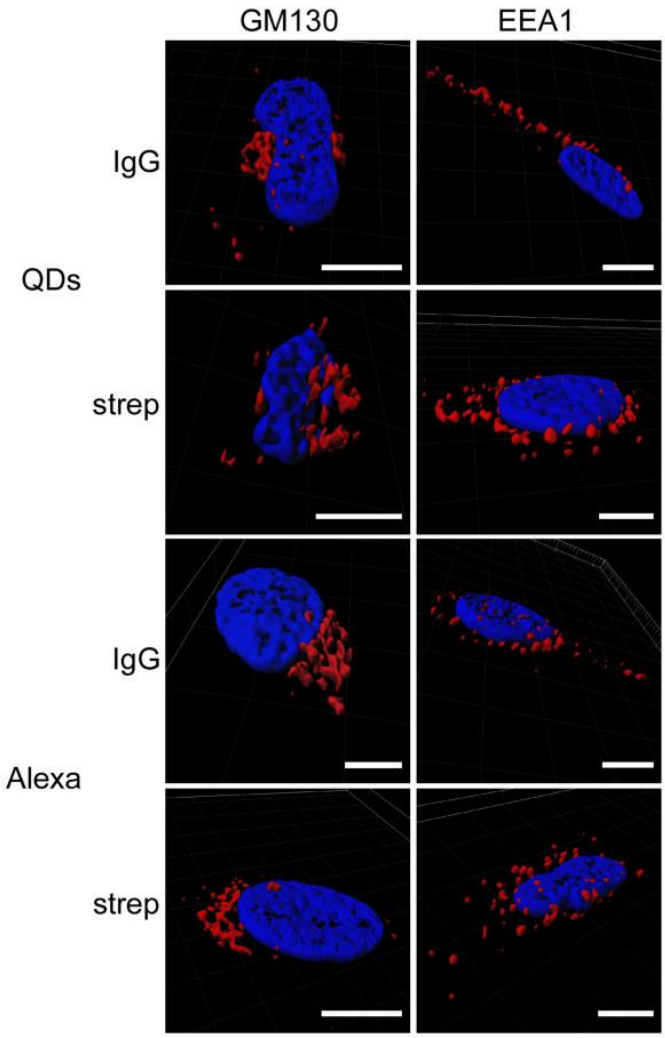

Figure 6. CLSM specificity analysis of GM130 and EEA1 labeling. Isosurface representation of the cell shows the nucleus (blue) labeled with Hoechst 33342, Golgi complex (GM130) and endosomal system (EEA1) (red) within a three-dimensional volumetric x-y-z data field. Scale bar = 10 ε m.

3.4. Discussion and Conclusions

In this work inorganic QDs were used to demonstrate their feasibility and advantages as a basic research technique in routine immunocytochemistry, as compared to Alexa

organic dyes. To our knowledge, commercial QDs are not yet standardized; neither are they completely characterized to be used without further evaluation [16,17].

HRTEM characterization of QDs demonstrated differences in core size between the two types of QDs. In theory, these differences should be due to QD manufacturing, but the current methods used to produce QD allow particle size and particle size distribution to be controlled accurately [18]. Moreover, according to the Quantum Dot Corporation [2], there are only slight size differences in a given batch of QDs. However, other authors have found some variability in CdSe QDs size distribution [19].

One of the optical properties measured was the emission spectrum, which in QDs is related to their size. QD 655 conjugated to IgG or streptavidin displays a higher emission peak and a narrower bandwidth than its Alexa homologue. These advantageous characteristics have been well documented previously by different authors [4,13,20] and offer the possibility of using different QDs simultaneously without overlapping emission bands. The bandwidth of our batch of QD 655 (IgG and strep) was similar to that described in the literature [18,20].

Slight differences in size result in slight variations in the emission wavelength. As a consequence, the emission spectrum of a certain nanocrystal ensemble will be broader than an individual QD spectrum [21]. A variation in size distribution of 5% translates into a bandwidth of approximately 25ï 30 nm, a narrow value compared to the bandwidth of many fluorescent dyes [21]. Since the size distribution of each QD analyzed in this study was about 10%, it was expected that the bandwidth would be greater (ca. 35 nm).

Another optical characteristic analyzed was the intrinsic brightness of both fluorophores. The fluorescence intensity (FI) was higher in QDs than in Alexas. Most authors agree that QDs have superior brightness than organic fluorophores [1,13,20,22]. However, other studies have found that QDs are not as bright as expected [23]. Slight

differences in FI (ca. 8%) were detected between both QDs, while in Alexas these differences were inappreciable. Other authors have found that the FI of QD 525-IgG was nearly one-third that of QD 525-streptavidin [24].

Photostability was the third optical property analyzed, and the entire scientific community agrees that this is the best advantage of QDs, as compared to other fluorescent dyes [3,5]. Our study confirms that QDs have the highest photostability. This characteristic is very important when in vivo analyses are carried out and long-term experiments are necessary and use multiple targets [25]. But photostability is also a determining factor in fixed samples in which some magnification is needed to find the best resolution to observe subcellular structures. Before QDs came out, Alexa dyes were considered to be the most photostable fluorophores [26]. Nowadays, this reality has changed: Alexa fluorophores lose almost all of their fluorescence in only 90 seconds of laser exposure, while we have demonstrated that QDs can be exposed to laser light for eight consecutive minutes and less than 40% of their initial fluorescence is lost.

All of these characteristics confirm that QDs have unique optical properties that make them powerful fluorescent dyes. In addition to the increasing interest in QDs in fluorescence techniques, their electron-dense core has potential to carry out correlated studies between CLSM and TEM, which would allow protein localization inside cells on a nanometric scale [11]. However, there is some controversy regarding the specificity of QDs as immunolabels. While some authors argue that QDs have comparable or even superior specificity in relation to organic fluorophores [27], others consider that QDs are appropriate fluorophores to be used as immunolabels, although without increasing sensitivity, and with higher, non-specific binding and aggregation than Alexa dyes [18,23]. Low specificity could be due to different reasons: i) a non-optimal concentration of QDs that could lead to a non-specific signal [1], or ii) a non-optimal surface chemistry

of QDs that would affect their spectroscopic properties and colloidal stability as well as their biomolecular function or size, which could sterically hamper access to cellular targets [20]. Several authors have pointed out the importance of QD concentration for improving the sensitivity of detecting water pathogens [22], as well as improving specific immunostaining [1]. Before starting the QD characterization, we tested three different concentrations of QD 655 in order to use the most appropriate in which to perform this study (data not shown). The optimal concentration was 30 nM because there were scarce aggregates and the QD concentration was high enough to label the tubulin network.

On the other hand, specificity was higher when QDs were used as a tertiary antibody, but still lower compared to their Alexa homologue. Other authors have reported that QD sensibility is improved when they are used as tertiary antibodies [24]; this increase in sensibility is probably due to the high affinity between streptavidin and biotin, and to the signal amplification.

Finally, the specificity of QDs in detecting ß-tubulin, GM130 and EEA1 proteins was tested. While specificity against ß-tubulin was lower than Alexa, no differences were observed when QDs were used to stain the Golgi complex (GM130 protein) or endosomes (EEA1). Specificity of QDs was higher for primary antibodies against proteins like GM130 and EEA1, which are scarce in the cell and are not involved in the composition of thin structures. Specificity was lower for proteins such as ß-tubulin which is an abundant protein in the cell and that polymerizes producing an extremely well organized thin structure. QD 655 is one of the largest QDs commercialized, and it is possible that its size could sterically obstruct its access to its target [20].

Summarizing, QDs are excellent fluorophores for labeling cellular targets as they display higher intensity, an enhanced signal to noise ratio, a narrower bandwidth and

higher photostability than organic dyes. However, the specificity of QDs depends on the target they have to bind to. More studies are needed to improve the specificity of QDs so they can be used routinely, alone or in combination with organic fluorescent dyes, in all biological applications. In this study we were able to use QDs as secondary and tertiary antibodies to clearly detect discrete localized proteins. Therefore, in these cases, they can replace fluorescent organic molecules in routine immunocytochemistry procedures.

In the future, when better control of the synthesis and functionalization of QDs is possible, the range of biological applications of these fluorophores can be extended and they can become part of basic research techniques.

3.5. References

[1] J. M. Ness, R. S. Akhtar, C. B. Latham, K. A. Roth, *J. Histochem. Cytochem.* **2003**, *51*, 981ï 7.

[2] A. Watson, X. Wu, M. Bruchez, *Biotechniques* **2003**, *34*, 296ï 300, 302ï 3.

[3] A. P. Alivisatos, *Science* **1996**, *271*, 933ï 937.

[4] P. K. Chattopadhyay, D. A. Price, T. F. Harper, M. R. Betts, J. Yu, E. Gostick, S. P. Perfetto, P. Goepfert, R. A. Koup, S. C. De Rosa, et al., *Nat. Med.* **2006**, *12*, 972ï 7.

[5] C. B. Murray, C. R. Kagan, M. G. Bawendi, *Annu. Rev. Mater. Sci.* **2000**, *30*, 545ï 610.

[6] I. L. Medintz, H. T. Uyeda, E. R. Goldman, H. Mattoussi, *Nat. Mater.* **2005**, *4*, 435ï 46.

[7] W. W. Yu, E. Chang, R. Drezek, V. L. Colvin, *Biochem. Biophys. Res. Commun.* **2006**, *348*, 781ï 786.

[8] T. Jamieson, R. Bakhshi, D. Petrova, R. Pocock, M. Imani, A. M. Seifalian, *Biomaterials* **2007**, *28*, 4717ï 32.

[9] A. M. Iga, J. H. P. Robertson, M. C. Winslet, A. M. Seifalian, *J. Biomed. Biotechnol.* **2007**, *2007*, 76087.

[10] R. Nisman, G. Dellaire, Y. Ren, R. Li, D. P. Bazett-Jones, *J. Histochem. Cytochem.* **2004**, *52*, 13ï 8.

[11] B. N. G. Giepmans, T. J. Deerinck, B. L. Smarr, Y. Z. Jones, M. H. Ellisman, *Nat. Methods* **2005**, *2*, 743ï 9.

[12] A. Matsuno, J. Itoh, S. Takekoshi, T. Nagashima, R. Y. Osamura, *J. Histochem. Cytochem.* **2005**, *53*, 833ï 8.

[13] X. Wu, H. Liu, J. Liu, K. N. Haley, J. A. Treadway, J. P. Larson, N. Ge, F. Peale, M. P. Bruchez, *Nat. Biotechnol.* **2003**, *21*, 41ï 46.

[14] E. B. Voura, J. K. Jaiswal, H. Mattoussi, S. M. Simon, *Nat. Med.* **2004**, *10*, 993ï 8.

[15] S. Lin, X. Xie, M. R. Patel, Y.-H. Yang, Z. Li, F. Cao, O. Gheysens, Y. Zhang, S. S. Gambhir, J. H. Rao, et al., *BMC Biotechnol.* **2007**, *7*, 67.

[16] D. Tonti, F. van Mourik, M. Chergui, *Nano Lett.* **2004**, *4*, 2483ï 2487.

[17] Y. Wu, S. K. Campos, G. P. Lopez, M. A. Ozbun, L. A. Sklar, T. Buranda, *Anal. Biochem.* **2007**, *364*, 180ï 92.

[18] R. E. Bailey, A. M. Smith, S. Nie, *Phys. E Low-dimensional Syst. Nanostructures* **2004**, *25*, 1ï 12.

[19] L. Li, J. Hu, W. Yang, A. P. Alivisatos, *Nano Lett.* **2001**, *1*, 349ï 351.

[20] U. Resch-Genger, M. Grabolle, S. Cavaliere-Jaricot, R. Nitschke, T. Nann, *Nat. Methods* **2008**, *5*, 763ï 775.

[21] P. Jorge, M. A. Martins, T. Trindade, J. L. Santos, F. Farahi, *Sensors* **2007**, *7*, 3489ï 3534.

[22] L. Y. Lee, S. L. Ong, J. Y. Hu, W. J. Ng, Y. Feng, X. Tan, S. W. Wong, *Appl. Environ. Microbiol.* **2004**, *70*, 5732ï 6.

[23] B. C. Ferrari, P. L. Bergquist, *Cytometry. A* **2007**, *71*, 265ï 71.

[24] T. J. Fountaine, S. M. Wincovitch, D. H. Geho, S. H. Garfield, S. Pittaluga, *Mod. Pathol.* **2006**, *19*, 1181ï 91.

[25] A. Fu, W. Gu, C. Larabell, A. P. Alivisatos, *Curr. Opin. Neurobiol.* **2005**, *15*, 568ï 75.

[26] N. Panchuk-Voloshina, R. P. Haugland, J. Bishop-Stewart, M. K. Bhalgat, P. J. Millard, F. Mao, W. Y. Leung, *J. Histochem. Cytochem.* **1999**, *47*, 1179ï 88.

[27] M. A. Hahn, J. S. Tabb, T. D. Krauss, *Anal. Chem.* **2005**, *77*, 4861ï 9.

Chapter 4. Annexin-V/quantum dot probes for multimodal apoptosis monitoring in living cells: improving bioanalysis using electrochemistry

---

4.1. Introduction

The development of new techniques to detect and study the apoptosis is crucial to fully understand how its deregulation leads to disorders such as cancer [1,2], neurodegenerative diseases [3] and myocardial infarction [4], among others. Nowadays, most techniques used to detect apoptotic cells aim to label phosphatidylserine (PS), a negatively charged aminophospholipid, whose translocation from the inner to the outer plasma membrane is a distinctive hallmark of early stages of apoptosis [5ï 8]. Methods based on PS recognition are useful clinical tools for early diagnosis, evaluation of diseases progression, and monitoring therapy efficacy, besides providing excellent quantitative analysis in living cells and new potential targets for drug discovery [9,10]. To date, Annexin-V (AnnV), a phospholipid-binding protein with high affinity for PS [11], has been widely used as an imaging tool to monitor the apoptosis progression when conjugated to a fluorescent dye [12ï 15]. Nevertheless, its applicability is restrained by the properties of common fluorescent dyes, which have a limited photostability and a tendency to photobleach [16,17].

Considering this framework, CdSe/ZnS Quantum Dots (QDs) are excellent tools to overcome organic dye inconveniences; in fact, they have size-dependent tunable narrow fluorescence emission spectra, high-resistance threshold to chemical and photo degradations, high extinction coefficient and high quantum yield [18,19]. They are already widely used in fluorescence based technologies such as fluorescence microscopy and confocal laser scanning microscopy (CLSM) [20ï 22], flow cytometry [23], spectroscopy [24,25] and microarrays [26ï 28]. Another unique characteristic of QDs, over dyes and enzymes, is that their high electron density allows for their use also as electron microscopy labels. Although fluorescence-based and electron microscopy methods provide an accurate detection of apoptosis, most of them are time-consuming,

troublesome, expensive and require qualified staff to analyze the results. A complementary and quantitative electrochemical detection of apoptosis would solve those inconveniencies. Several works reported the use of voltammetry to detect QDs as electrochemical labels, taking advantage of their redox properties [29ï 32].

Herein, we describe the use of AnnV-QDs conjugates as dual optical/electrochemical labels for fully monitoring apoptosis in living leukemia-derived THP1 cells (Figure 1). Using this label, we achieved to: i) make the labeling process easier (single-step) and faster (30 min) than most commercially available kits, ii) study the same sample with classical cell biology techniques (CLSM, Scanning Electron Microscopy (SEM) and flow cytometry) obtaining a deep overview of the cell status, and iii) develop a cheap, easy-to-use, fast and quantitative electrochemical technique, which results are in fully agreement with those obtained by flow cytometry.

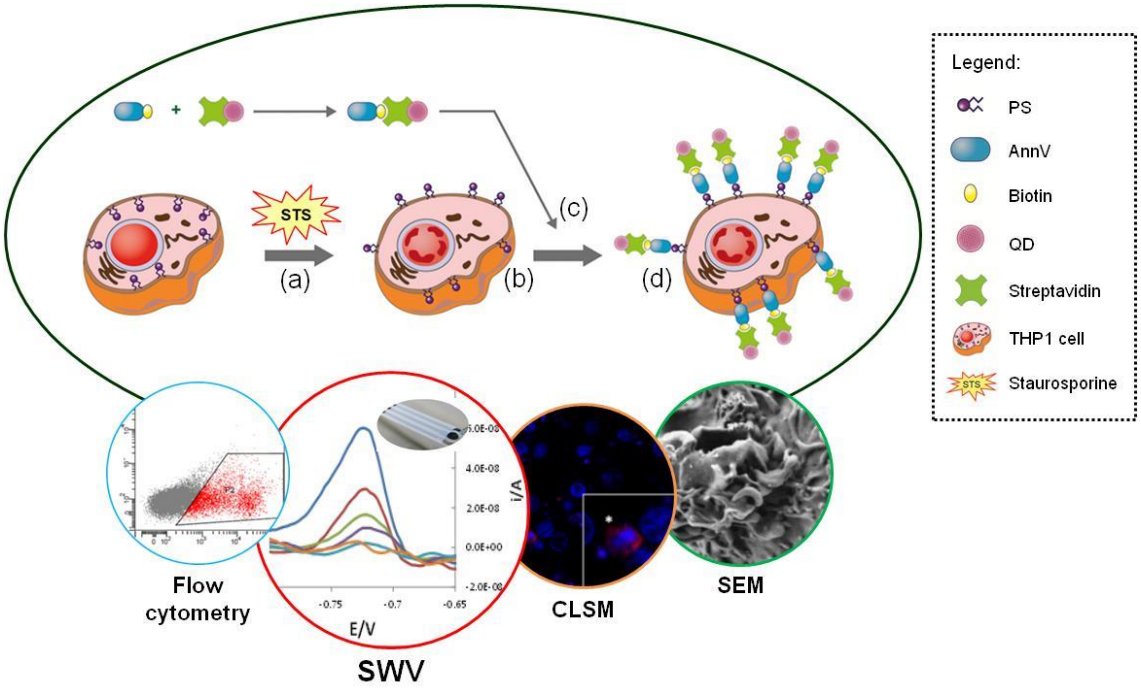

Figure 1. Use of Annexin-V/Quantum dot probes for optical and electrochemical detection of apoptotic cells. THP1 cell cultures are incubated with Staurosporine (STS) (a), a pro-apoptotic drug, and as a consequence phosphatidylserine (PS) is externalized (b). AnnV-QD

conjugates previously prepared are added to the cell cultures (c) and bound to PS expressed in the outer membrane of apoptosis induced THP1 cells (d). Due to the properties of QDs (they are fluorescent, electroactive and electron dense) diverse analyses can be performed.

4.2. Methods

4.2.1. Reagents and instruments

RPMI-1640 (Gibco), Foetal Bovine Serum (FBS) (Gibco) and L-Glutamine (Gibco), for cell cultures, and Qdot® 655 Streptavidin Conjugates (Invitrogen), dimer EthD (Invitrogen) and Hoechst 33342 (Invitrogen), for labeling the cells, were purchased from Life Technologies S.A. (Spain). T-25 and T-75 flasks (Nunc) were purchased from Thermo Scientific and the hemocytometer with a Bürker grid was purchased from Brand Gmbh + Co KG (Germany). A HERAcell 150 incubator (Heraeus, Spain) and an Eppendorf Centrifuge 5804 R (Eppendorf Ibérica S.L. Spain) were used for cell culture maintenance and in some steps of the experimental procedure.

Staurosporine (STS) and Dimethyl sulfoxide (DMSO) for the apoptosis induction step were purchased from Sigma (Spain) and Annexin-V biotin (Biovision Inc.) was purchased from Deltaclon S.L. (Spain). Sample shaker used for preparation of the conjugate was a TS-100 Thermo shaker (Spain).

Reagents for PBS and AnnexinV binding buffer preparation were purchased from Sigma, Aldrich or Fluka. All the solutions were prepared using mQ water, produced using Milli-Q system (>18.2MÝcm^{-1}) purchased from Millipore (Sweden).

4.2.2. Cell culture and induction of apoptosis

The human monocytic THP-1 cell line (ATCC® TIB-202TM) was maintained at a density of 5-8 x 10^5 cells/mL in 75 cm^2 flasks in RPMI-1640 medium supplemented with 2 mM L-Glutamine and 10% FBS in standard conditions (5% CO^2 at 37 ºC).

For apoptosis induction, 2 mL of cell suspension at a concentration of 5 x 10^5 cells/mL were transferred to 25 cm^2 flasks where 3 µL of 0.5 mg/mL of STS diluted in DMSO were added into the flasks (induced cultures). The equivalent volume of DMSO was added into the control flasks (control cultures). Cultures were kept in standard conditions for 6 h. Two washing cycles with PBS were performed in order to remove any presence of STS in the cell cultures transferring cell suspensions to centrifuge tubes and spinning at 300 x g for 5 min. Final pellets were resuspended in 200 µL PBS.

During the incubation with STS, THP-1 cell cultures were checked using an inverted microscope with a phase-contrast objective. We took images of control and apoptosis-induced cell cultures in order to observe changes occurring in the cells due to the effect of STS such as cell shrinkage and membrane blebbing (Figure SI 1).

4.2.3. AnnexinV-QD conjugates preparation

AnnV-QD conjugates were prepared according to the manufacturerôs protocol. Briefly, 3 µL of 2 µM streptavidin-QDs solution were incubated with 187 µL of QD conjugation buffer and 10 µL of biotinylated Annexin-V for 45 min in a thermo-shaker at 500 rpm at 25ºC and stored at 4ºC until used.

4.2.4. Simple labeling protocol for apoptosis

A simple one-step labeling procedure was carried out by adding 200 µL of AnnV-QD conjugate and 200 µL of Ca^{2+} containing binding buffer to the cell suspensions

(prepared in 200 µL PBS). Then it was incubated at room temperature (RT) in a rocker shaker for 30 min. Thereafter, in order to eliminate the unbound AnnV-QD conjugates two washing cycles with PBS were performed.

4.2.5. Confocal Laser Scanning Microscopy

A 10 µL drop of the labelled cell suspension was placed in a bottom glass petri dish for confocal imaging. Images were captured with a CLSM Leica TCS-SP5 AOBS spectral (Leica Microsystems Heidelberg GmbH; Mannheim, Germany) using Plan-Apochromatic 20× and 40× objectives (NA 0.9 and NA 1.2 respectively).

Simultaneous excitation of the PS-expressing cells (labeled with AnnV-QD) and their nuclei (Hoechst staining) was performed using a 405 nm blue laser diode and simultaneous detection was done using two different photomultipliers (PMT), one per each corresponding spectral range. CLSM software (Leica LAS AF) was used to obtain overlapped images of nuclei and AnnV-QD labeling. Stacks of XY images at different Z planes were processed with ImageJ (NIH, Maryland, USA) and Imaris 3D rendering software (Bitplane AG, Switzerland). In order to perform semiquantitative analyses, fluorescence intensity data from the images were obtained with ImageJ extracting the sum of intensities of all pixels for the nuclei (FIN) and the QD (FIQD) labeling, separately for each given image. Average intensities of 3 pair of images, from different areas, were calculated and the average ratio FIQD/FIN was used to quantify the cell death. Further projections and 3-D views of apoptotic cells were performed using Imaris software.

4.2.6. Sample preparation for SEM analysis

Labeled-cell suspensions were washed in 0.1 M cacodylate buffer for 1 min and then fixed with 2.5% glutaraldehyde in 0.1 M cacodylate buffer, during 1 h at RT. Cells were

incubated again with 0.1 M cacodylate buffer for 1 min and then dehydrated sequentially in increasing concentrations of cold ethanol (50, 70, 90% during 8 min each). To complete the dehydration process samples were incubated two times in 100% ethanol (8 min each, 25ºC) and finally resuspended in hexamethyl disilazane solution (Sigma-Aldrich) for 15 min at RT. A 50 µL of each sample was placed in separate glass coverslips and let dry for 15 min at RT. SEM samples were kept in a desiccator at 25 ºC until analysis.

The volume of all reagents used in the sample preparation was 1 mL and after each of the above-mentioned steps cells were recovered by centrifugation (300 x g, 5 min).

Prior to SEM analysis (Magellan®FE-SEM, FEI), glass coverslips were placed over a typical SEM sample holder and the edges of the coverslips were painted with silver ink in order to increase their conductivity and facilitate the analysis of the samples.

This protocol avoids the use of metallization steps keeping intact the cellular structure and allows a direct visualization of small metallic nanoparticles such as QD on the cell surface.

4.2.7. Flow Cytometry

AnnV-QD labeled cells (20,000 cells) were analyzed to quantify the number of apoptotic cells in both induced and control cultures using a FACSCanto II flow cytometer (BD Biosciences, Franklin Lakes, NJ) equipped with the BD Biosciences FACSDivaÊ software.

4.2.8. Electrochemical detection of apoptotic cells

The electrochemical detection of apoptotic cells was done using mercury-modified screen printed electrodes (from ItalSens, acquired through PalmSens) placing 30 εL of

the AnnV-QD labeled cells onto the working electrode. Apoptotic cells were detected electrochemically though the presence of Cd ions (as defects at Cd QDs surface) contained in the QDs structure by direct voltammetric detection. This methodology has been previously reported by our group [33] and applied now with some minimal modifications. Briefly, the Cd(II) contained in the QDs was reduced to Cd(0) applying a potential of -1.1V for 5 min. After that, a square wave voltammetry (SWV) was performed scanning the potential from -1.1 to -0.4 V (step potential 10 mV, modulation amplitude 30 mV, frequency 15 hz) and measuring the current value (analytical signal) due to the oxidation of Cd(0) to Cd(II). The oxidation process generates a peak of current at ī 0.8 V which intensity is related with the quantity of QDs in contact with the working electrode surface. The electrochemical detection in the samples was directly performed in PBS pH 7,4.

Different concentrations of cells ranging from 20,000 to 1,250 were measured and three measures using three different electrodes (represented as error bars in the graphs) were performed per each number of cells.

4.3. Results and Discussion

4.3.1. Optimization of apoptosis induction and labeling with AnnV-QD probes

In this study, we used a human monocytic leukemia cell line, THP-1 as target of Staurosporine (STS), a commonly used drug to induce apoptosis in cell-based assays [34,35]. Although several works report the apoptotic effect of STS, concentrations and incubation times change depending on the cell line and specific assay requirements [36,37]. We observed that 5 µg/mL of STS during 6 hours provoke the expected effect in THP-1 cell cultures by exhibiting early apoptotic symptoms such as cell shrinkage or

membrane blebbings. We also optimized the labeling step in order to make the method faster and easier than the use of Annexin-V-biotin kits in conjuction with conventional streptavidin or avidin-dye reagents. In fact, using commercial kits, cells are first incubated with Annexin-V-biotin followed by a second incubation with a fluorescently labeled streptavidin; besides, after each incubation step several washing steps are necessary, making the overall labeling process at least longer than 1 h. In the proposed method the Annexin-V-biotin is pre-incubated with streptavidin-QDs and the resulting conjugates can be stored at 4ºC, protected from light, until use. In this way we minimized the number of steps, decreasing the overall assay to 30 min.

4.3.2. *In vitro* CLSM monitoring of apoptosis in THP-1 cell cultures

In order to study the efficiency and specificity of AnnV-QDs conjugates to detect apoptotic cells, we analyzed the sample both with CLSM and SEM. In particular, taking advantage of the fluorescent emission of QDs, we used CLSM to obtain qualitative information of the assay by comparing images of the control and apoptosis-induced samples (Figure 2a). Images in Figure 2a show the differences in the amount of AnnV-QD labeled-cells (in red) between the two samples. Nuclear staining (in blue; using Hoechst 33342 dye) confirms the apoptotic status of cells in the induced cultures, where DNA condensation and nuclear fragmentation are evident (insert box in Figure 2a). We used ImageJ software to analyze three random areas in both samples (control and induced), to attain the integrated fluorescence intensity of nuclear (FI_N) and QDs (FI_{QD}) staining. The histogram in Figure 2b displays the FI_{QD}/FI_N ratio of control and induced samples, respectively 0.022±0,001 and 0.06±0,001 A.U.. The higher ratio observed in the induced sample indicates a prevalence of apoptotic cells in the culture incubated with STS. Furthermore, by scanning the sample along the Z axis, we obtained information of the whole-cell labeling. A cross section of a selected stack of an

apoptotic cell is shown in Figure 2c. XZ and YZ plane projections show the relative localization of AnnV-QD labeling, which is restricted to the periphery of the cells, as expected, and also the fragmentation of the nucleus. Finally, this peripheral localization can also be seen in a surface-rendered 3-D reconstruction of an apoptotic cell, which gives a more complete volumetric view of the same labeling information (Figure 2d).

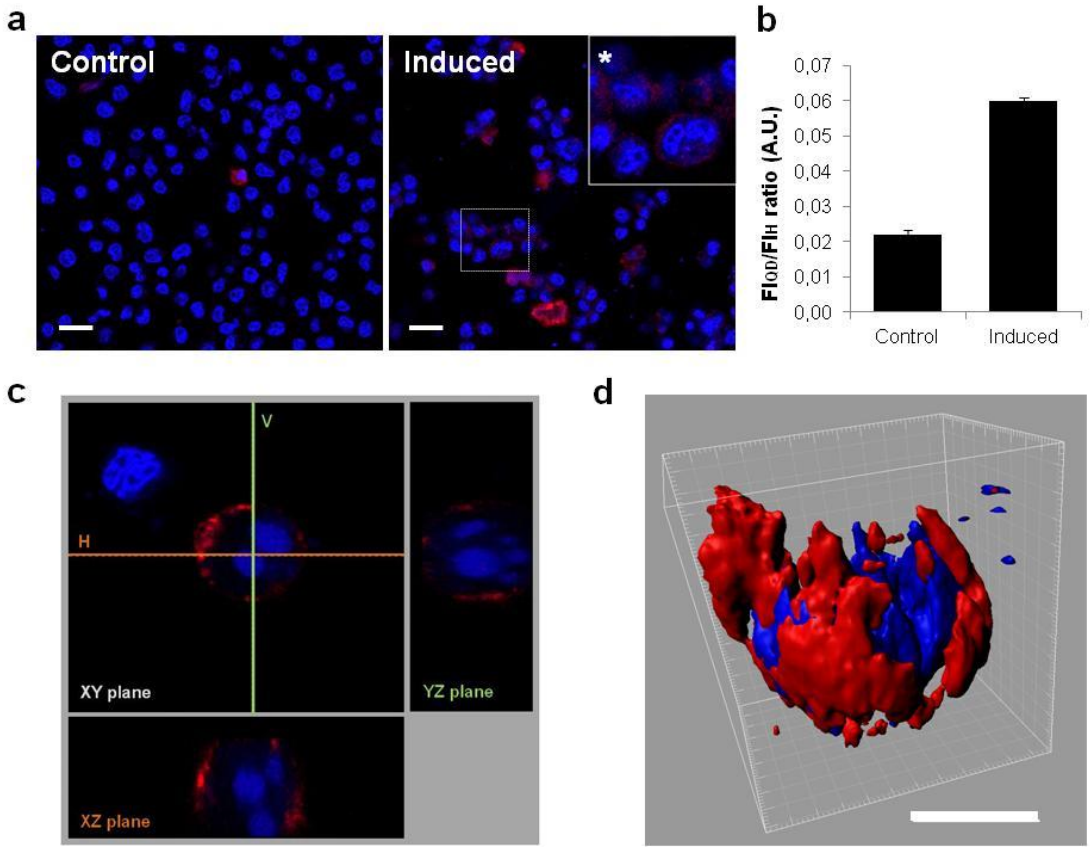

Figure 2. CLSM analysis. (**a**) Images of THP1 cells after AnnV-QD labeling (red) show few apoptotic cells in control cultures and many in induced ones. Nuclei were counterstained with Hoechst (blue). A zoom in a selected region (dashed line) is displayed in a box for more detail (*). Scale bars 20 µm. (**b**) Apoptosis in control and induced cultures was established from the images acquired. Fluorescence intensities of nuclei ($FI_{H,}$ Hoechst stain) and of AnnV-QD ($FI_{QD,}$ QDs) bound to cells were quantified and the ratio FI_{QD}/FI_{N} was calculated. This ratio was twice in induced cultures compared to control ones. (**c**) A cross section projection allows the visualization of an XZ plane (horizontal -H- section) and a YZ plane (vertical -V- section),

where DNA condensation and nuclear fragmentation can be clearly observed. (**d**) 3-D rendered projection shows the peripheral localization of the AnnV-QDs in a volumetric view. Scale bar 5 µm.

4.3.3. SEM analysis of apoptotic THP-1 cells and AnnV-QD labeling at the plasma membrane

We performed SEM analysis both to see in detail the external morphology of the cells, and to evaluate the presence or absence of QDs in the plasma membrane surface (CdSe/ZnS QDs can be visualized by SEM thanks to their electron dense composition). Figure 3a and 3b show respectively non-apoptotic and apoptotic cells at 20,000X magnification: whereas non-apoptotic cells (Figure 3a) had usual morphologies, apoptotic cells (Figure 3b) decreased in size (shrinkage) and presented membrane blebbings (pointed out in the picture by yellow arrows), which are typical of apoptotic processes. Moreover at 50,000X magnification, the presence of QDs was evaluated: no QDs were observed in non-apoptotic cells (Figure 3aô). However, in apoptotic cells, QDs (displayed as bright dots in the image) were present in their membranes (yellow arrowheads in Figure 3bô), corresponding to what was expected, due to the interaction of AnnV-QD with the externalized PS.

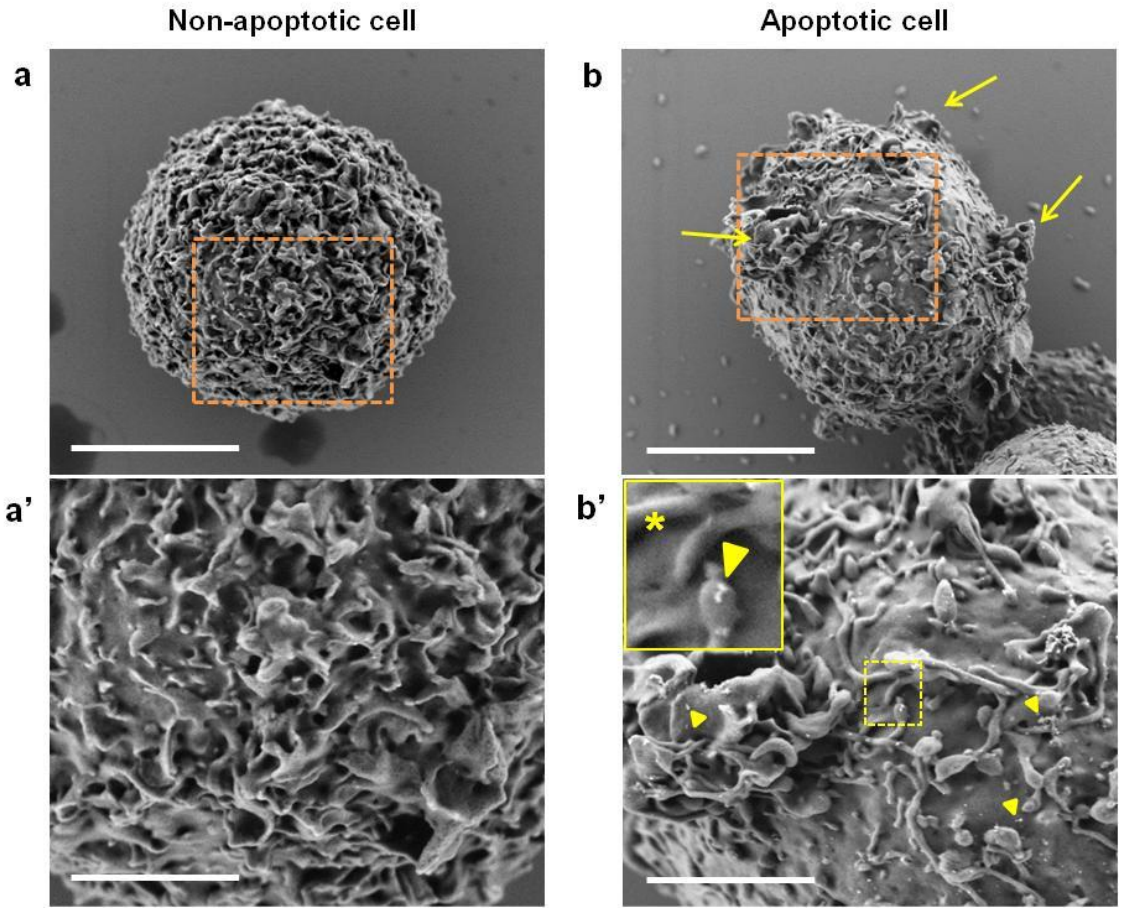

Figure 3. SEM analysis. Morphology of control and apoptotic cells and presence of QDs in the outer membrane of cells were evaluated by SEM imaging. Images a and b were taken at 20,000X to check the size and morphology of cells, scale bar 5 µm. Apoptotic cells (b) shown to be smaller in size (shrinkage) and presented also big evaginations or blebbings (indicated by arrows), typical of apoptotic processes. Images aô and bô were taken at 50,000X in a selected area (dashed square in top images) in order to evaluate the presence of QD in the membrane (bright dots indicated by arrowheads), scale bar 2 µm. No QDs were present in non-apoptotic cells (aô) whereas in apoptotic cells (bô) dispersed or groups of QDs were observed. In the inset (*) a detail of a selected area (dashed square) is displayed and two QDs in the membrane of the cell can be clearly observed.

4.3.4. Quantification of AnnV-QD labeled apoptotic THP-1 cells by Flow Cytometry

We also used flow cytometry to analyze the same samples used for CLSM and SEM; in this way we could prove both, the versatility of AnnV-QD labels using a different technique, and the acquisition of quantitative data to be used for evaluating the performances of the new electrochemical detection. In particular, for each culture, 20,000 cells were analyzed and representative plots were obtained for each sample. Figure 4 shows the distribution of the total cell culture population. The red colored area corresponds to the apoptotic cell population labeled with AnnV-QD, which was determined according to the negative control analyzed under the same conditions. Comparing both plots, a more condensed red area is observed in the apoptosis induced culture than in the control one, as expected. We extracted numerical data from the plots and calculated the percentage of apoptosis for each sample. Apoptotic cells constituted 5% of the control sample, as usual in normal healthy or untreated cell cultures [38], whereas for induced cultures it was 17.1%. These results indicate that apoptosis was successfully induced by STS and that AnnV-QD label method allowed the specific detection of apoptotic cells via flow cytometry.

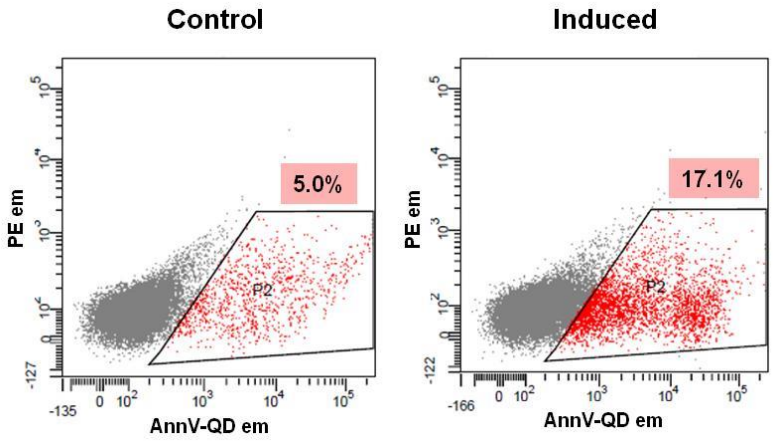

Figure 4. Flow cytometry analysis. A total of 20,000 cells from control and induced cultures were analyzed and the number of cells emitting fluorescence (AnnV-QD labelled cells) were quantified (P2 area; red dots). The population of AnnV-QD labelled cells (P2) increased substantially in induced cell cultures (17.1% in front of 5.0% of the control). AnnV-QD em = fluorescence intensity emitted at 655 nm. PE em = fluorescence intensity emitted at 585 nm (used as control).

4.3.5. Electrochemical stripping detection of apoptotic THP-1 cells through QDs

Finally, we developed an electrochemical method, based on the stripping voltammetry of QDs (Figure 5a), to detect apoptotic cells. It is based on the redox properties of the CdSe/ZnS QDs, which produced a characteristic oxidative peak at -0.720 V. The peak intensity can be used to estimate the amount of QDs in the sample that in turn can be related to the quantity of apoptotic cells present. The stripping voltammetry was performed in PBS using disposable screen printed electrodes and a potentiostat, as shown in Figure 5b. In this way, an entire population of cells can be screened, checking the effect of the drug upon their viability. In Figure 5c, the histogram displays the peak values obtained by electrochemical detection of serial dilutions of control and apoptotic-induced cells. Considering the same number of cells, the apoptotic-induced cells generated higher peaks compared to control samples, due to the higher amount of QDs present in their plasma membrane, indicating the specific binding of AnnV-QDs to the externalized PS. The difference is observable in a range from 20,000 to 1,250 cells (inset of Figure 5c shows a classical read-out of the electrochemical stripping detection of different dilutions of apoptotic cells). Control cell cultures, as observed by CLSM and flow cytometry, also gave low intensity signals due to the basal apoptotic activity of a normal cell culture.

This electrochemical method allows quantitative comparison of the effect of a drug on an induced sample and a control one, and, when used in correlation with flow cytometry data, allows us to estimate the number of apoptotic cells in the sample. In the present case, the flow cytometry results indicate that 17% of cells analyzed in the induced sample are apoptotic cells, thus, we can assume that in the smallest concentration used in the electrochemical detection, consisting of 1250 cells, about 212 cells were apoptotic cells.

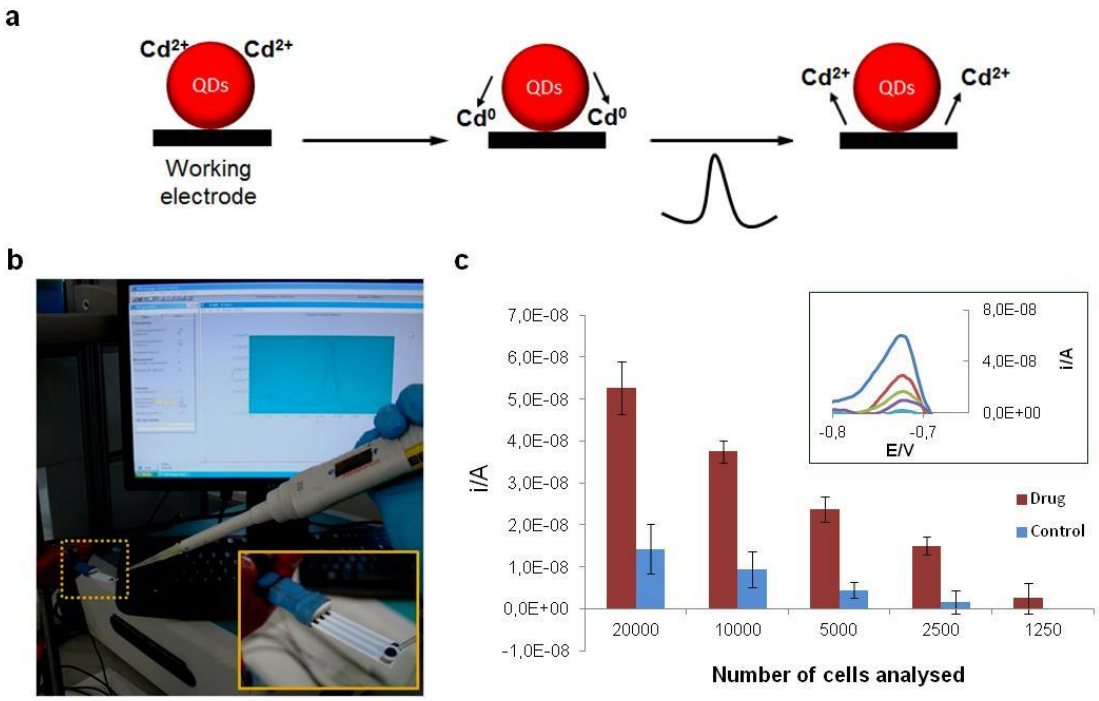

Figure 5. Electrochemical detection. (**a**) Schematic of the electrochemical detection by SWV of QDs. First Cd ions (as defects at CdSe QDs surface) are reduced to Cd^0 and the subsequent oxidation to Cd^{2+} generates a peak, the intensity of which corresponds to the amount of QDs present on the electrode surface. (**b**) Photo of the set-up for the electrochemical detection. (**c**) Electrochemical stripping peak currents obtained measuring different amounts of induced-apoptotic cells (red columns) and control cells (blue columns). In the inset typical electrochemical stripping curves obtained for the apoptotic cells are shown.

4.3.6. Correlation between electrochemistry and other quantitative techniques

We compared the results obtained analyzing 20,000 cells by flow cytometry and electrochemistry, as well as with those from CLSM (Table 1). Data collected showed an excellent correlation (~97.7%) between flow cytometry and electrochemistry, with almost the same value of fold-increase between the control and apoptosis induced sample, respectively 3.42 and 3.50. The 2.72 fold increase obtained with CLSM is also in a good agreement with the previous ones (~78%) (although it cannot be used as a quantitative result, due to the lack of statistical significance of the technique). This new electrochemical method can be considered as a faster (readout obtained in less than 5 minutes), cheaper and easier-to-use alternative or complementary method to flow cytometry. Unlike other electrochemical methods for heavy metal detection (such as those incorporating QDs) all measurements are carried out in a cell-friendly saline solution instead of using strong acidic conditions. Other advantages of this method include the fact that it can be used by untrained personnel, that is easily miniaturizable and that does not limit the user to working with samples containing high number of cells.

Table 1. Apoptosis analysis. Correlation between electrochemistry, flow cytometry and confocal laser scanning microscopy (CLSM) measures.

Technique	Control cells	Induced cells	Fold increase
Electrochemistry (nA)	15,0	52,50	3,50
Flow Cytometry (%)	5,0	17,10	3,42
CLSM (A.U.)	0.022	0.06	2,72

4.4. Conclusions

We have explored the use of AnnV-QD probes as optical and electrochemical labels to easily carry out correlative studies of the same sample using different techniques such as voltammetry, flow cytometry, CLSM and SEM. The complementary information obtained from the different methods allows for greater insight into the apoptotic process compared to data obtained from single techniques using other dyes or enzymes. The proposed quantitative, electrochemical-based method is faster, cheaper and more versatile than most of those currently in use and can be easily miniaturized into a point-of-care, micro-fluidic device, making it useful for both research and industrial settings. We expect this technique to be extended not only to other cell toxicity studies with interest for clinical industries, but also to the detection of any disease-biomarker expressed in the plasma membrane, with clear relevance for diagnostic applications.

4.5. References

[1] J. F. Kerr, C. M. Winterford, B. V Harmon, *Cancer* **1994**, *73*, 2013ï 2026.

[2] S. R. MacEwan, A. Chilkoti, *Nano Lett.* **2014**, *14*, 2058ï 64.

[3] M. P. Mattson, *Nat. Rev. Mol. Cell Biol.* **2000**, *1*, 120ï 129.

[4] G. Takemura, H. Fujiwara, *J. Cell. Mol. Med.* **2006**, *10*, 56ï 75.

[5] S. J. Martin, C. P. Reutelingsperger, A. J. McGahon, J. A. Rader, R. C. van Schie, D. M. LaFace, D. R. Green, *J. Exp. Med.* **1995**, *182*, 1545ï 1556.

[6] G. Rimon, C. E. Bazenet, K. L. Philpott, L. L. Rubin, *J. Neurosci. Res.* **1997**, *48*, 563ï 570.

[7] S. M. Van den Eijnde, L. Boshart, C. P. Reutelingsperger, C. I. De Zeeuw, C. Vermeij-Keers, *Cell Death Differ.* **1997**, *4*, 311ï 316.

[8] P. A. Leventis, S. Grinstein, *Annu. Rev. Biophys.* **2010**, *39*, 407ï 427.

[9] K. Schutters, C. Reutelingsperger, *Apoptosis* **2010**, *15*, 1072ï 82.

[10] H. Shi, R. T. K. Kwok, J. Liu, B. Xing, B. Z. Tang, B. Liu, *J. Am. Chem. Soc.* **2012**, *134*, 17972ï 81.

[11] H. A. Andree, C. P. Reutelingsperger, R. Hauptmann, H. C. Hemker, W. T. Hermens, G. M. Willems, *J. Biol. Chem.* **1990**, *265*, 4923ï 4928.

[12] I. Vermes, C. Haanen, H. Steffens-Nakken, C. Reutelingsperger, *J. Immunol. Methods* **1995**, *184*, 39ï 51.

[13] H. van Genderen, H. Kenis, P. Lux, L. Ungeth, C. Maassen, N. Deckers, J. Narula, L. Hofstra, C. Reutelingsperger, *Nat. Protoc.* **2006**, *1*, 363ï 367.

[14] D. M. Monsalve, T. Merced, I. F. Fernández, S. Blanco, M. Vázquez-Cedeira, P. a Lazo, *Cell Death Dis.* **2013**, *4*, e513.

[15] L. Quinti, R. Weissleder, C.-H. Tung, *Nano Lett.* **2006**, *6*, 488ï 90.

[16] U. Resch-Genger, M. Grabolle, S. Cavaliere-Jaricot, R. Nitschke, T. Nann, *Nat. Methods* **2008**, *5*, 763ï 775.

[17] H. Montón, C. Nogués, E. Rossinyol, O. Castell, M. Roldán, *J. Nanobiotechnology* **2009**, *7*, 4.

[18] A. P. Alivisatos, W. Gu, C. Larabell, *Annu. Rev. Biomed. Eng.* **2005**, *7*, 55ï 76.

[19] R. Gill, M. Zayats, I. Willner, *Angew. Chem. Int. Ed. Engl.* **2008**, *47*, 7602ï 25.

[20] S. Le Gac, I. Vermes, A. van den Berg, *Nano Lett.* **2006**, *6*, 1863ï 9.

[21] Y. Wang, L. Chen, *Nanomedicine* **2011**, *7*, 385ï 402.

[22] X. Wu, H. Liu, J. Liu, K. N. Haley, J. A. Treadway, J. P. Larson, N. Ge, F. Peale, M. P. Bruchez, *Nat. Biotechnol.* **2003**, *21*, 41ï 46.

[23] P. K. Chattopadhyay, S. P. Perfetto, J. Yu, M. Roederer, *Wiley Interdiscip. Rev. Nanomedicine Nanobiotechnology* **2010**, *2*, 334ï 348.

[24] E. Petryayeva, W. R. Algar, I. L. Medintz, *Appl. Spectrosc.* **2013**, *67*, 215ï 252.

[25] Y. Luo, C. Wang, T. Jiang, B. Zhang, J. Huang, P. Liao, W. Fu, *Biosens. Bioelectron.* **2014**, *51*, 136ï 142.

[26] G. Rousserie, A. Sukhanova, K. Even-Desrumeaux, F. Fleury, P. Chames, D. Baty, V. Oleinikov, M. Pluot, J. H. M. Cohen, I. Nabiev, *Crit. Rev. Oncol. Hematol.* **2010**, *74*, 1ï 15.

[27] E. Morales-Narváez, H. Montón, A. Fomicheva, A. Merkoçi, *Anal. Chem.* **2012**, *84*, 6821ï 7.

[28] E. Morales-Narváez, A. R. Hassan, A. Merkoçi, *Angew. Chemie - Int. Ed.* **2013**, *52*, 13779ï 13783.

[29] S. Marin, A. Merkoçi, *Nanotechnology* **2009**, *20*, 055101.

[30] M. Medina-Sánchez, S. Miserere, S. Marín, G. Aragay, A. Merkoçi, *Lab Chip* **2012**, *12*, 2000.

[31] M. Amelia, T. Avellini, S. Monaco, S. Impellizzeri, I. Yildiz, F. M. Raymo, A. Credi, *Pure Appl. Chem.* **2011**, *83*, 1ï 8.

[32] J. Wang, G. Liu, A. Merkoç i, *J. Am. Chem. Soc.* **2003**, *125*, 3214ï 3215.

[33] A. Merkoçi, L. H. Marcolino-Junior, S. Marín, O. Fatibello-Filho, S. Alegret, *Nanotechnology* **2007**, *18*, 035502.

[34] Y. Wu, D. Connors, L. Barber, S. Jayachandra, U. M. Hanumegowda, S. P. Adams, *Toxicol. Vitr.* **2009**, *23*, 1170ï 1178.

[35] W.-T. Li, H.-W. Tsao, Y.-Y. Chen, S.-W. Cheng, Y.-C. Hsu, *Photochem. Photobiol. Sci.* **2007**, *6*, 1341ï 1348.

[36] A. H. Heussner, D. R. Dietrich, *Open J. Apoptosis* **2013**, *02*, 25ï 30.

[37] N.-S. Chang, *BMC Cell Biol.* **2002**, *3*, 8.

[38] P. Kameritsch, N. Khandoga, U. Pohl, K. Pogoda, *Cell Death Dis.* **2013**, *4*, e584.

Chapter 5. A Versatile Modular Microfluidic Platform for Monitoring Anti-cancer Drug Effect in Human Carcinoma Cells Using Quantum Dot-based Probes

---

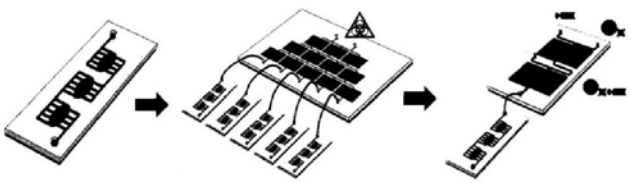

5.1. Introduction

Drug discovery is a field of research in constant development due to the need of new and improved drugs to treat different kinds of disorders, diseases or illnesses. Up to date, several methods for drug development have been reported,[1] and specific efforts have been focused in the development of new strategies to study the effect of specific drugs on biological samples and to verify the function for which the drug was developed before conducting the clinical trials.[2],[3]

One of the most important fields in drug development research is the related to cancer treatment.[4],[5],[6] Most anticancer drugs such as Camptothecin (CAMPT) induce apoptosis,[7],[8] with some common characteristics (endonucleolytic cleavage of DNA, chromatin condensation, caspases activity, phospholipids translocation, etc.),[9] which can be used to develop different methods for cell apoptosis detection by the recognition of a specific apoptotic marker. Several scientific contributions on apoptotic cell detection have been reported being the detection of phosphatydilserine (PS), a phospolipid located in the inner face of the plasma membrane (PM) that translocates to the outer leaflet of the PM at early stages of apoptosis, one of the most common methods currently in use.

Detection of PS through the specific phospholipid-binding protein Annexin V (AnnV) has been widely used for diagnosis[10],[11] and as an imaging tool to monitor the cell death progression when conjugated to a fluorescent dye.[12],[13] This non-invasive technique for the cell is a good alternative for drug screening assays. However, one of the main problems of AnnV-based fluorescent probes is the limited photostability of the organic dyes conjugated to the AnnV and the small diversity commercially available of them, to avoid spectral overlapping. These problems can be solved using Quantum Dots (QDs) as fluorescent reporters instead of typical organic dyes.[14]

Companies are producing commercially QDs due to their unique optical properties and their great potential in diagnostic imaging with particular interest in cancer diagnosis.[15] We have

already reported the superiority of QDs over organic dyes for labeling intracellular structures through double or triple immunocytochemistries showing higher intensity, narrower bandwidth and higher photostability[16] and we have as well demonstrated the efficient employment of QDs as labels in microarray technology for either protein[17] (Alzheimerôs disease biomarker screening) or bacteria[18] (e-coli detection in a digital like response via fluorescence quenching with graphene oxide). Thereby, the use of QDs conjugated to AnnV provides a unique candidate to monitor apoptosis in time-lapse imaging due to their high photostability.[19]

QD-based labeling strategies can improve conventional technologies but, modifications in the assay platform such as the use of microfluidics would allow the development of a cheaper and more efficient method[20],[21] by down-scaling the cell environment, making biological interactions more dynamic (microflows), and decreasing sample, reagents and time of analysis.[22]

As a result of the micro and nanofabrication progresses, new tools have been introduced in the biomedicine field in order to improve current methodologies used in diagnosis, drug screening, etc.[23] For instance, one of the most interesting alternatives is the development of lab-on-a-chip platforms whose aim is to integrate various laboratory functions on a small chip taking advantage of the microfluidics and microelectronics.

Microfluidic devices are basically known as integrative platforms to carry out diverse and complex experiment.[24] Although many researchers are proposing highly integrated and sophisticated platforms,[25],[26] the complexity of the experiments for non-experienced personnel can be a drawback due to their multiple components. However, the use of a modular configurations brings the opportunity to couple different kind of chips depending on the requirements of each experiment in a versatile and simple way, resulting in a large number of combinations.[27],[28] The main idea is that several microfluidic components can be connected in a motherboard to perform a larger integrated system.[29],[30]

DNA detection,[31],[32] protein immunoassays,[33],[34] and cell-based experiments[35],[36],[37],[38], by using microfluidic platforms have been widely reported in the literature. Focusing on cell studies using microfluidics, several platforms for cytotoxicity evaluation and drug discovery have been also described.[39],[40] The above mentioned platforms cover functionalities such as parallelization, appropriated microenvironments, multidetection, etc., however they usually require more complex fabrication, including control system and implementation procedures. In addition, these approaches for cell-based analysis mainly use organic dyes which are not stable and not sensitive enough for long-term studies.

In the present work we report the development of a versatile platform based on modular microfluidics to carry out cell-based assays for drug discovery revealing PS externalization, occurring in early apoptosis, by using QDs as signalling probes. To achieve such an anti-cancer drug effect monitoring system we designed a flexible modular system composed of three different modules (Figure 1): i) a concentration gradient generator (CGG) to automatically generate a gradient of concentration of CAMPT, ii) a cell apoptosis detection chip (CELL) to seed the cells and detect optically the AnnV-QD labeled apoptotic cells, and iii) a mixer (MIX) to create the AnnV-biotin-streptavidin-QD (AnnV-QD) probes in the appropriate buffer.

The integration of different chips (modules) with various functionalities allows to obtain a more versatile and simple platform, being possible to interchange upon demand one or more modules. As a proof-of-concept, we show the monitoring of the effect of CAMPT in human carcinoma cells using AnnV-QDs probes as high sensitive fluorescent labels for cell apoptosis quantification through specific recognition of PS.

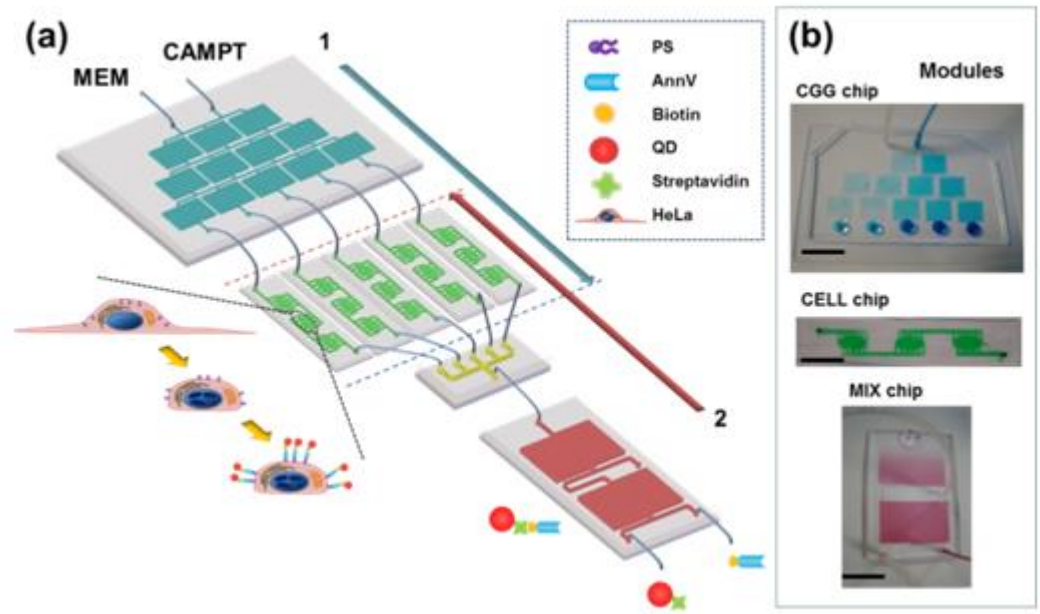

Figure 1. Complete modular microfluidic platform for cell death monitoring. (a) Schematic representation and connections between the three different modules: i) CGG (concentration gradient generator), ii) CELL (cell chamber), and iii) MIX (AnnV-biotin and QD-streptavidin mixer). 1) Direction of the flow when the generated drug concentrations [0 to 20 µM] are introduced into the CELL chip, and 2) direction of the flow in order to label translocated PS with AnnV-QDs when apoptosis is induced by the drug (after 4h of incubation in presence of the drug, see cell schematic). (b) Corresponding pictures of the three modules filled in with coloured inks.

5.2. Methods

5.2.1. Design and chip features

The design of each module (CGG, MIX and CELL) was done taking into account the required functionality (concentration gradient generation, mixing and immunoassay performance and cell seeding and analysis) in terms of modularity, versatility, easy assembly, among others, as reported previously.[45]

CGG and MIX chips were designed with long paths through serpentine shapes. Each serpentine sector of the CGG chip was 100 µm depth, 125 µm width and 172 mm of

path length whereas each serpentine sector of the MIX chip was 100 µm depth, 200 µm width and 1,500 mm of path length. In the CELL chip, several ramifications were included in each chamber in order to minimize the stress that the flow can produce in the cells growing inside the chips. All chips were fabricated by soft-lithography as previously described by Whitesidesô group.[46]

5.2.2. Fabrication of PDMS/glass chips

All chips were fabricated by soft-lithography as previously described.[47] Briefly, a 4-inch silicon wafer was spin coated with a negative photoresist (SU8-50, from Microchem, USA) and patterned by photolithography by using a flexible mask (Microlitho, UK). Poly-dimethylsiloxane (PDMS, from Ellsworth, Spain) was poured onto the resulting mould and cured at 65 ºC for 2 h. After this, the PDMS channel and glass substrate were assembled; both surfaces, glass and PDMS were activated for 1 min by air plasma 30 W (Harrick Plasma, USA), and put into contact to achieve irreversible bonding.

5.2.3. Hydrodynamic optimization of CGG chips

Design of the CGG chip was based on previous work.[48] The fabricated chip consists on sequential mixers to be used for producing a gradient of concentration in the corresponding outlets. Experimental data with our CGG chip were obtained to compare the relative concentrations with the theoretical ones. Quantification of relative concentrations at the outlets was performed by introducing through inlet 1 cell culture medium MEM (Minimum Essential Medium, Gibco) supplemented with 10 % Foetal Bovine Serum (FBS, Gibco) and with a 25 % dimethyl sulfoxide (DMSO, Sigma), which is the Camptothecin (CAMPT) solvent in stock solutions. Through the inlet 2, MEM supplemented with 10% FBS and with a 10% of Trypan blue (Fluka by Sigma

Aldrich, Spain) was introduced. Trypan blue was used during the optimization experiments to allow measurements of colour intensity because although MEM has phenol red in its composition it is transparent at small volumes. For filling-up the chips, 1 mL syringes (Hamilton, USA) and syringe pumps (Harvard Apparatus USA) were used. To determine optimal flow rate and time of infusion different settings were tested in order to find the less time-consuming configuration allowing the obtaining of desired values of relative concentrations.

Image processing and determination of relative concentrations generated in CGG chips

Images at the outlets of CGG chips were captured with an optical microscope (Olympus IX71, Germany) coupled with a CCD camera (Olympus DP72, Germany) using the bright field mode, 4x magnification objective.

Image J (U. S. National Institutes of Health, Maryland, USA) was used for the image post-processing in order to determine the relative concentrations at the outlets. Two regions of interest (ROIs) inside (X, Xô) and outside (Y, Yô) the channel were selected for quantification. First of all a division between the intensities of the paired areas X/Y and Xô/Y' was done respectively in order to avoid errors due to differences attributed to imaging itself such as a change of environmental light. Then the mean of the two obtained values was calculated and, in order to normalize the results, the colour intensity in the outlets was compared with intensities in the intersection of the two inlets. Two ROIs in inlet 1 (Ŭ, inside, and ɓ, outside the channel) and two ROIs in inlet 2 (Ŭô, inside, and ɓô, outside the channel) were considered. Considering all parameters the following equation (Eq. 1) was established to obtain normalized intensities at the outlets:

$$\text{Normalized relative intensity} = \frac{Mean\left(\frac{X}{X'};\frac{Y}{Y'}\right)-\frac{\alpha'}{\beta'}}{\frac{\alpha}{\beta}-\frac{\alpha'}{\beta'}} \quad \text{(Eq. 1)}$$

5.2.4. Hydrodynamic optimization of MIX chips

Optimizations for the MIX chip were carried out in order to determine convenient mixing factors inside the channels which would later allow the formation of AnnV-QD conjugate and the mixing with the appropriate buffer. Different solutions were introduced through the inlets to establish mixing factors at different points along the channel path (0; 50; 100 and 150 mm approximately): streptavidin QD655 (Life Technologies, Spain) at a 120 nM from a stock solution prepared in QD incubation buffer (Borate buffer pH 9.2, Life Technologies, Spain) were introduced through one of the inlets, whereas QD incubation buffer and Ca^{2+} containing AnnexinV binding buffer were introduced through the second and third inlet respectively. To determine optimal flow rate and time of infusion different settings were tested in order to find the less time-consuming configuration allowing the obtaining of the best mixing factor.

5.2.5. Image processing and determination of mixing factors

Images at different points along the channel path were captured using an optical microscope (Olympus IX71, Germany) coupled with a CCD camera (Olympus DP72, Germany) using the fluorescence mode, 4x magnification objective. An HBO mercury lamp was used as UV-light excitation source and a TRITC filter cube was set to select convenient emission wavelength coming from QDs.

The mixing factor at each selected point was calculated by measuring the mean fluorescence intensity of two ROIs per side of the channel (See Figure S4A for more details), the so-called I_{max} (X and Xô) and I_{min} (Y and Yô), due to maximum and minimum fluorescence observed at the origin in the inlet cross where solutions have not yet been mixed. First the mean intensity between X and Xô, and between Y and Yô were calculated separately then the mixing factor was obtained as follows:

$$\text{Mixing factor} = \frac{I_{min}}{I_{max}} \quad \text{(Eq. 2)}$$

The closer to 1 the better was the resulting mixture. Mixing factors were normalized after calculating I_{min} (mean Ŭ, Ŭô) and I_{max} (mean ɓ, ɓô) at the inlet cross (See Figure S4 B for more details) allowing to obtain the mixing factor at this point as reference, the so-called Normalized Mixing Factor (NMF) in the inlet. Then, normalized values of mixing factors at each selected point were calculated as follows:

$$\text{NMF} = \frac{Mixing\ \ factor - Mixing\ \ Factor\ in\ the\ inlet}{1 - Mixing\ \ Factor\ in\ the\ inlet} \quad \text{(Eq.3)}$$

5.2.6. Cell culture

Human adenocarcinoma HeLa cell line (ATCC®) was used as a model of adherent cell culture to carry out cell-based assays. Cells were maintained as a monolayer of cells in 25 cm^2 flasks in MEM medium supplemented with 2 mM L-Glutamine and 10% FBS in standard conditions (5% CO_2 at 37 ºC).

Cells in exponential phase of growth were used in the assays. Cells were detached by trypsinization, that is, MEM was removed and flasks were washed twice with 2 mL of 1X Hankôs Balanced Saline Solution (HBSS, Gibco) without Ca^{2+} and Mg^{2+}. Then 1 mL of 1X trypsin/EDTA solution (Gibco) was added and incubated at standard conditions for 3 min. Once cells were detached and could be seen individualized under an optical microscope 4 mL of fresh supplemented MEM was added to neutralize the effect of trypsin. Cells were quantified using a Neubauer chamber.

5.2.7. Optimization of CELL chip sterilization

Chips must be sterilized before cell seeding to avoid contaminations. Sterilization method was optimized in CELL chips and the optimal method was implemented to sterilize the rest of the chips. Different sterilization procedures were evaluated: i) chips were filled in 70 % ethanol, ethanol was removed and then chips exposed to UV light for 1h, ii) chips were filled in 70 % ethanol and exposed to UV light for 1h (no ethanol removal), and iii) chips were filled with 70 % ethanol until use (no UV light exposure). In all cases, after sterilization, MEM was introduced in the chips to replace ethanol which is toxic for the cells. Then, cells growing in flasks were counted as described previously and seeded into the chips manually using 1 mL plastic syringes (Sigma Aldrich, Spain). To optimize the sterilization method three different chips were used and 60,000 cells per chip were seeded and incubated in standard conditions. Images of each of the three chambers of the chips were taken at 4 h and 24 h after cells were seeded in the chips to evaluate cell adhesion and proliferation.

5.2.8. On-chip apoptosis induction by CAMPT in cell-based assays

All material required to carry out this step (syringes, syringe pumps, connector tubes, etc) was introduced to the safety cabinet in order to be sterilized for 15 min under UV light. Then, CGG chip was sterilized, as mentioned in the main text, by introducing 70 % ethanol first and replacing it by fresh MEM until use. Each of the outlets of the CGG chip was connected with a plastic connector tube to one CELL chip so finally 5 CELL chips were connected to the CGG chip. Then, supplemented MEM was introduced in one of the inlets and a 20 εM CAMPT solution in the other one at a flow rate of 10μL/min during 15 min. A range of CAMPT concentrations (0; 2.5; 10; 17.5 and 20 εM) was produced and automatically distributed to different CELL chips.

5.2.9. Cell labeling with AnnV-QD conjugates in cell-based assays

Before connecting MIX and CELL chips, AnnV-QD conjugation in an appropriate buffer was formed in the MIX chip and then CELL chips were filled in with the already created label, one by one. To fulfill this, biotinilated AnnV (diluted half with QD incubation buffer) and streptavidin QDs at 120 nM were introduced through the first and second inlets with a flow rate of 5 µL/min during 12 min whereas 2X AnnV binding b (diluted in MEM) was introduced through the third inlet with a flow rate of 10 µL/min during 12 min. After 12 min, the MIX chip was completely filled. Flow rate and time of infusion was changed to 4 µL/min and 7 min in order to fill in each of CELL chips previously incubated with CAMPT. CELL chips were incubated during 30 min in the CO_2 incubator at 37ºC to ensure the binding of the AnnV-QDs conjugate with the PS expressed in apoptotic cells. After that time, the unbound QDs were removed from inside the CELL chips by introducing supplemented MEM at a flow rate of 4 µL/min during 7 min.

5.2.10. Cell apoptosis detection using Fluorescence Microscopy

Optical detection of AnnV-QD labelled apoptotic cells was performed using an inverted microscope. CELL chips were placed in the stage of the microscope and 3 ROIs per chamber (9 ROIs per chip) were selected in order to obtain images for the analysis. A 10x objective coupled with a phase contrast lens was used to obtain bright field images of all cells and UV light in combination with a TRITC filter cube were used to obtain fluorescence images of apoptotic cells due to the maximum emission wavelength at 655 nm of QDs used.

5.2.11.Quantification of apoptosis level

To determine the level of apoptosis present in each chip bright field and fluorescence images were analysed. Total number of cells was obtained by counting individual cells in bright field images whereas the number of apoptotic cells was established counting cells in fluorescence images, where they can be easily identified for their red colour due to the QD emission at 655 nm.

The ratio between apoptotic cells and total number of cells was established for each chamber of the chip dividing the number of AnnV-QD labelled cells (in red) and the number of total cells. The closer to 1 the value was the higher percentage of apoptosis found. Mean values per chip were determined considering the values obtained in the three chambers of a CELL chip. The level of apoptosis found in each CELL chip was related graphically with the concentration of CAMPT to which it was exposed previously.

5.3. Results

5.3.1. Optimization of the CGG chip

To optimize the working performance of the modules, each chip was analysed separately and specific settings were established to run the final assay. First, flow rate and duration of liquid injection for the CGG chip were evaluated.

To simulate the real composition of the solutions, supplemented cell culture medium (Minimum Essential Medium, MEM) was introduced by one of the inlets, and a combination of MEM, dimethyl sulfoxide and trypan blue was introduced through the other one. To evaluate the gradient of concentrations obtained with the CGG chip, microscope images were taken in the outlets (Figure 2a) and further processed with ImageJ software to obtain the relative intensities of colour (Annex I Figure S1) which would be related to a specific solution concentration introduced in the inlets.

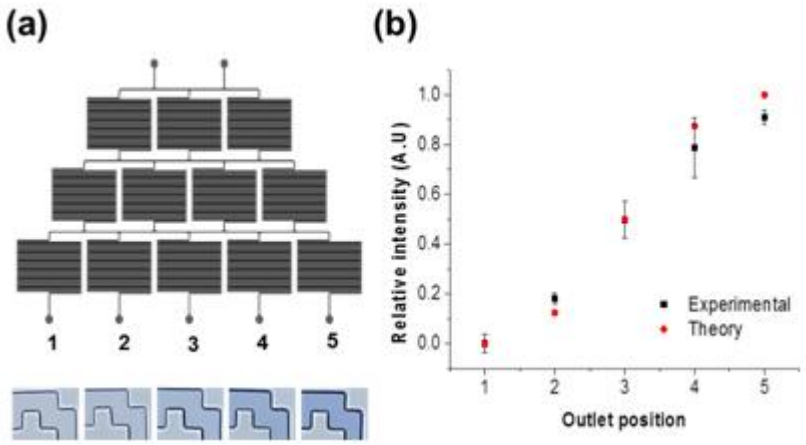

Figure 2. Optimization of the gradient of concentration in the CGG chip. (a) Schematic of the CGG chip with the corresponding outlets (optical images of the trypan blue dilutions at the end of the channel of each outlet), and (b) Comparison between theoretical and experimental concentration data resulted from the obtained solutions at the outlets.

According to theoretical predictions for such design (Annex I Figure S2), the relative concentrations in the outlets should be 0; 0.125; 0.5; 0.875 and 1. Experimental values obtained at different flow rates and times (Table 1) were compared with the predicted theoretical values (Figure 2b) and the most convenient settings to perform the complete assay were established at 10 µL/min flow rate during 3 min.

Repeatability and reproducibility studies were carried out by repeating measurements in the same chip and in three different chips respectively (Annex I Figure S3) showing negligible differences between measures thus demonstrating the functionality of the CGG chip in generating a gradient of concentrations of CAMPT.

Table 1. Flow rate and time settings to optimize the performance of the CGG chip.

	Flow rate (µl/min)	**Time (min)**	**Experimental concentration***	**Theoretical concentration***
Setting 1	10	3	0; 0.18; 0.5;	0; 0.125; 0.5;

	Both inlets		0.79 and 0.91	0.875; and 1
Setting 2	5	6	0; 0.41; 0.7;	
	Both inlets		0.84; and 0.93	

** Experimental and theoretical concentration values are given as arbitrary units (A.U.)*

5.3.2. Optimization of the MIX chip

Similar optimization procedure was done to establish the parameters for the MIX chip and several flow rates and injection times were tested (Table 2). Conjugation of AnnV-biotin with Streptavidin-QDs will be performed in the first section of the chip (C sector -conjugation-, Figure 3a), and once it is conjugated, the mixing of the AnnV-QD with the medium for cell incubation will take place in the second section (M sector -mixing-, Figure 3a).

Table 2. Flow rate and time settings to optimize the MIX chip performance.

Flow rate settings: (µl/min)	***Inlet 1*: 1** ***Inlet 2*: 1** ***Inlet 3*: 2**	***Inlet 1*: 5** ***Inlet 2*: 5** ***Inlet 3*: 10**	***Inlet 1*: 10** ***Inlet 2*: 10** ***Inlet 3*: 20**
C sector time (min)	40	8	4
M sector time (min)	20	4	2
Total time (min)	60	12	6

First of all, streptavidin-QDs at a concentration of 120 nM were introduced through inlet 1 (Figure 3a) and AnnV-biotin through inlet 2 (Figure 3a, Annex I Figure S4. Fluorescence images were taken at certain points (0 -C0-, 50 -C50-, 100 -C100- and 150 -C150- cm) from the beginning of the inlet path of C sector (see inset images in Figure 3b) in order to evaluate the fluorescence intensity in several Regions of Interest (ROIs) with the aim to calculate the mixing factor. Mixing factor reflects the

homogeneity of the solution and thus the best conditions to perform the AnnV-QD conjugation.

A flow rate of 5 µl/min during 12 min was found to be the optimal parameters to obtain a mixing factor value of almost 1 at the end of the C sector of the chip (Figure 3b). Repeatability and reproducibility studies for C sector were carried out and negligible differences between measurements or chips were observed (Annex I Figure S5a).

To start the analysis of the M sector of the MIX chip (Figure 3a), AnnV binding buffer was introduced through inlet 3. AnnV binding buffer contains Ca^{2+} that provides the appropriate environment for the specific binding between PS and AnnV which is Ca^{2+} dependent. Similarly to the analysis of C sector, fluorescence images along the channel path in M sector (0 -M0-, 50 -M50-, 100 -M100- and 150 -M150- cm: see, inset images in Figure 3c) were taken and the mixing factors determined at each of these points. A good compromise was found between the duration of the assay (6 min) and the obtaining of good mixing factors at 20 µL/min flow rate (Figure 3c). As for the C sector, repeatability and reproducibility for M sector of the chips were evaluated and no significant differences between repeated measurements neither in a same chip nor in different ones were found (Annex I Figure S5b).

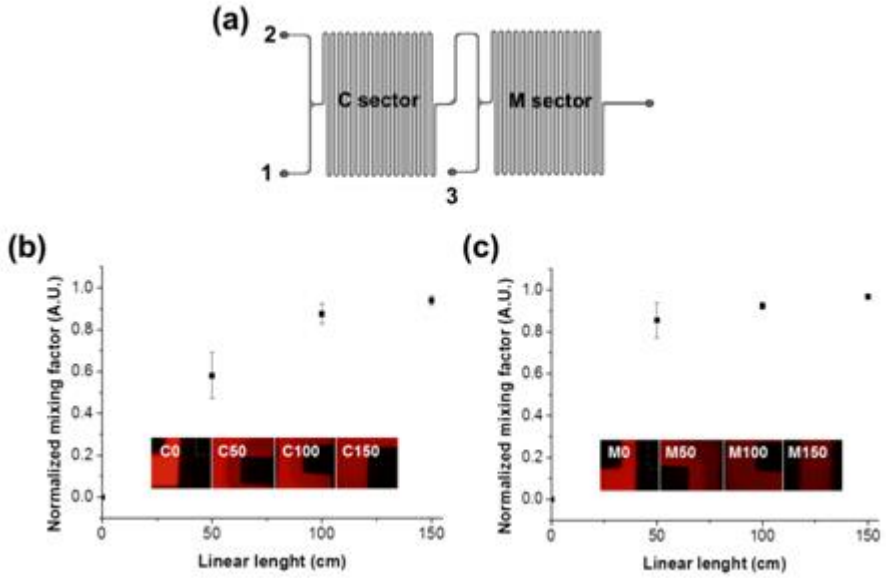

Figure 3. Optimization of the MIX chip. (a) Schematic of the MIX chip with the corresponding inlets (1, 2 and 3) and sectors analyzed. (b) Graph of mixing factors obtained from images taken at 0 -C0-, 50 -C50-, 100 -C100- and 150 -C150- cm of the channel path in the C sector (conjugation of AnnV and QDs), and (c) Graph of mixing factors calculated along the M sector of the chip from images taken at 0 -M0-, 50 -M50-, 100 -M100- and 150 -M150- cm, where conjugated AnnV-QDs are mixed with the binding buffer.

5.3.3. Optimization of the CELL chip

For the CELL chip a sterilization method and an optimum number of seeded cells were established. On one hand, a single step sterilization consisting in filling in the chip with ethanol 70% showed the best cell culture growth after 24 h of cell seeding (Annex I Figure S6). The number of cells growing in each chamber of the chip (1, 2, or 3 in Figure 4a) was analysed to ensure that the cells were uniformly distributed in the CELL chip and no differences were found among chambers (Figure 4b), therefore each chamber is considered a replicate in the final assay. On the other hand, different number of cells was seeded in the chips to find the optimal concentration of cells after 24 h incubation (data not shown). We chose to seed 120,000 cells per chip to almost

reach a monolayer of cells in the chambers at the moment of running the experiment (24 h post seeding).

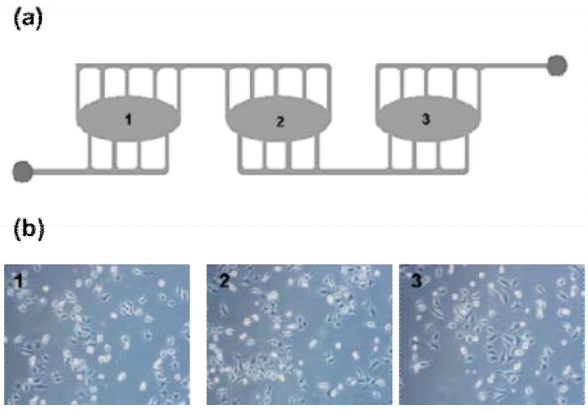

Figure 4. CELL chip optimization. (a) Schematic of the CELL chip with the three chambers where cells are seeded for analysis, and (b) Cells uniformly distributed in the three chambers of the same chip 24 h post-seeding.

5.3.4. Cell-based assay for drug discovery application

Once the three modules were optimized separately, the aim was to demonstrate the suitability of the developed modular platform to carry out a real cell-based assay by exploring the apoptotic effect of CAMPT in HeLa cells through labelling of the translocated PS with AnnV-QD probes. To fulfil the assay three sequential steps were performed (Annex I Figure S7a). First, cells were seeded in 5 different CELL chips and incubated overnight in a CO_2 incubator to allow cell proliferation. Secondly, CAMPT was used to induce cell apoptosis by introducing 20 µM CAMPT and 1X MEM through the inlets of the CGG chip that was previously connected to the CELL chips (See Annex I Figure S7 b). As a result, different concentrations of CAMPT from 0 to 20 µM (See details of time and flow rate in Table 3) were introduced in the CELL chips.

Table 3. Flow rate and time settings to perform the full assay

	CGG chip[a]	**MIX chip (C sector)[b]**	**MIX chip (M sector)[c]**	**CELL chip[d]**
Flow rate (µl/min)	10	5*(inlet 1)* 5*(inlet 2)*	10 *(outlet C sector)* 10 *(inlet 3)*	4
Time of injection (min)	3	8	4	5

[a)] Generation of CAMPT concentration, b)Conjugation of Annexin V and QD, c)Mixing with Annexin V binding buffer, d)Injection of AnnV-QD labeling into CELL chips.

CELL chips were disconnected from the CGG chip and placed again in the incubator for 4 h in order to allow the induction of apoptosis in the cell cultures by CAMPT. The third step of the assay was to label positive-apoptosis, which is cells with the translocated PS to the outer leaflet of the membrane, with the AnnV-QD probe. To achieve this, biotinylated AnnV and streptavidin-QD were introduced through the two inlets (1 and 2) of the C sector of the MIX chip followed by the introduction of AnnV binding buffer through the third inlet (3) located in the M sector of the MIX chip in order to dilute the AnnV-QD probe in the appropriate buffer for cell incubation. The MIX chip was then sequentially connected to each of the CELL chips in order to let the probe interact with the cells. CELL chips were incubated with the AnnV-QD probe solution for 30 additional minutes in order to label translocated PS in apoptotic cells, followed by a washing step which consisted in the introduction of supplemented MEM for 7 min at a flow rate of 4 µL/min, to remove unbound AnnV-QD.

Each CELL chip was then analysed by fluorescence microscopy (Annex I Figure S7c) in order to determine the percentage of apoptotic cells. Three areas per chamber of

each chip were selected to acquire bright field images (Figure 5a) and fluorescence images (Figure 5b).

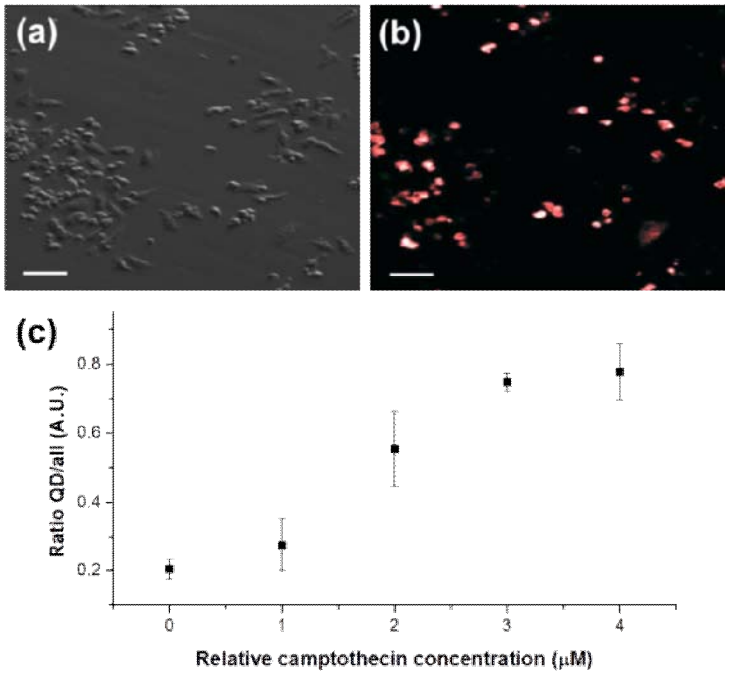

Figure 5. Apoptosis induction by different CAMPT concentrations. (a) Typical bright field image of a selected area of the chamber. (b) Fluorescence image of the same selected area. (c) Graph showing the increment of the apoptotic cells (QD-labeled cells/total number of cells) in relation to the CAMPT concentration.

Images were processed to establish the apoptosis ratio for each concentration of CAMPT used. As expected, the higher the concentration of CAMPT used to induce apoptosis the higher the number of cells labelled with AnnV-QD (Figure 5c). Two replicates of this experiment were carried out in different days and results obtained were similar (Annex I Figure S8) showing the good reproducibility of the method.

5.4. Discussion

The presented obtained results indicate that all modules of the platform fulfilled the role for which they were designed and therefore the complete modular system allows the successful monitoring of such a complex cell-based assay.

CGG chip plays a key role in the whole system since efficient mixing of two compounds (drug and buffer), to obtain the desired concentration of the analysed compound (in our case CAMPT) at the outlet of the chip, must be very efficient. Different geometrical changes (increasing the channel length and including additional serpentines into the channels) were done in the CGG chips to optimize the gradient generation. As it can be seen in Figure 2 using this design, we have attained a substantial agreement between the theoretical model and the obtained experimental results. The small deviations observed are probably caused by bubble generation in the channel affecting the liquid behaviour. Similar results can be obtained using a wide range of flow rates (data not shown). The 10 µL/min flow rate allowed the reduction of time of analysis without causing detachment of the cells from the surface of CELL chip when CAMP was injected. The MIX chip, designed to perform conjugation of QDs and Ann-V was optimized in the same way as for CGG chip. In this case the addition of a very long serpentine channel (up to 172 mm of path length) allows a good mixing of the reagents and holds an appropriate volume of the probe inside the chip, for filling in all the CELL chips to carry out the labelling step. In the same way, CELL chip was also optimized. The oval-shaped chambers with channel ramifications showed a more uniform distribution of cells within all chambers of the chip. In addition, this design helps to avoid a possible cell detachment caused by high flow, which is very important for obtaining reproducible results during microscope images captures.

Results from the full cell-based drug screening assay (Figure 5) indicate an appropriated correlation between concentration of CAMPT and relative number of apoptotic cells (labelled with AnnV-QD probes). As a proof-of-concept the applicability of the modular platform to carry out cell-based assays for drug screening has been demonstrated with a standard deviation that usually varied from 3 to 8 %.

Considering the factors that a cell-based assay for drug discovery should feature such as sensitivity of detection and reagent stability,[41] an important advantage of the developed system is the use of QD instead of fluorescent dyes to reveal apoptosis. QDs are the most robust bioassay labels to carry out long optimizations and quantifications which require high sensitivity and stability of signal (in this case, fluorescence) that other labels such as dyes canõt provide. Their compatibility in biological media, long-term stability and resistance to photobleaching make them ideal tools to monitor real time events thereby obtaining sensitive and reliable measures of apoptosis. Moreover, although for this work CELL chips were designed for optical detection they can be easily fabricated with integrated electrodes, being this functionality the future direction of our work. The versatility of QDs offers this possibility to evolve this work in other applications or in different ways involving electrochemistry to fulfil the specific goal depending on the bioanalytical/bioassay scenario. For instance, electrochemical-based microfluidic platforms with an easy monitoring capability thanks to the use of redox properties of QDs[42] has been reported by our group as an efficient alternative to detect very low levels of a biomarker with interest for diagnostics.[43] Therefore, an important advantage of the presented QDs-based system and approach is the possibility to be used also in a dual optical/electrical detection that may allow a fast quantitative following up and to study the apoptosis process upon a chemical stimulus (in this case, the effect of an anticancer drug at different concentrations could be in-chip electrochemically detected as demonstrated recently in batch mode).[44]

This work confirms that using microfluidic platforms and quantum dots give rise to stable and sensitive cell assay for drug discovery applications, which is one of the main goals of nanomedicine. In addition it leads to significant both time and reagent saving due to the in-chip preparation of the reagents (drug dilutions, labelling probe formation, etc.) and to the small volumes necessaries to perform the cell-based assay. For example, experiments performed in the presented modular microfluidic system uses 4 times less volume of CAMPT stock solution (1 µL of stock solution is sufficient to prepare all working solutions in CGG chip) comparing with common techniques based on multiple well plates. Similarly, smaller volumes of QDs, cells suspensions and buffers are used in microfluidic chips than in plate-based assays.

Moreover, this cell-based assay performed in microfluidic chips is characterized by a shorter duration of the experiment (at least 40% shorter in our platform) and by less manual steps which may introduce variability in the system. In this modular system assay, syringe pumps were used as fluid driving units. Due to the limited control of liquid behaviour, air introducing and bubble creation is one of the major problems which may affect the assay due to disruption of the fluid flow that would interfere in the mixing step. This can be prevented by using commercial pressure-driven flow controllers which work by applying an appropriate pressure on the inlet and outlet of the chip which would reduce bubble formation and moreover facilitates automation of the whole assay.

In addition, in the case of multi well plates if used during the complete experiment, several steps should be followed. Some of them are simplified by the use of microfluidics, as we explain further. This conjugation protocol would include various washings steps in between various other steps, which can be easily performed by flowing buffer through the channel in a more reproducible way, reducing time, and avoiding damage on the cell culture. First the cells should be adhered onto the plate

bottom surface or microchannel and the cell medium removed. Each different concentration of the drug should be prepared individually in the case of multi well, while with the microchannel we just introduce the stock solution and the buffer, and by using the gradient chip, the dilutions are generated right away. Then those dilutions are introduced, and incubated for 1hr in the case of micro wells and 12 min for the microchannel, and the conjugate (which should have been previously prepared when the experiment is in batch, increasing the time of conjugation) is added and incubated again followed by the remove of its excess, proper rinsing and finally observation in the microscope. These various steps if done manually could easily introduce errors. There is no doubt that the use of the proposed microfluidic chip avoids wrong manipulation and contamination of cells in addition of offering of a robust and easy to use system even for use out of a specialized lab and even by non-professional users.

As mentioned earlier, one of the main advantages of using modular microfluidics is the versatility it provides. Each chip can be modified, replaced by other or removed to obtain a suitable system for each new application. Also, microfluidics does not require large volume of samples, time-consuming steps or highly skilled users. For these reasons and considering that the developed microfluidic approach can be potentially automated and is easy-to-use, the presented platform is suitable for point-of-care applications as well.

5.5. Conclusions

In summary, we have designed and fabricated various PDMS/glass-based chips with different functionalities using common microfabrication techniques. All together they form a modular microfluidic system that has been applied in a cell-based assay for anti-cancer drug screening. Moreover, a simple optical detection of apoptotic human carcinoma cells has been achieved using QD-based probes.

The main advantages of the presented method rely on the ease of use, miniaturization/portability and versatility of the platform which in combination with QD-based probes make the system appropriate for point-of-care applications besides the above demonstrated drug screening applicability. For this reason we think that this platform can meet the needs of different labs looking for diverse applications with adaptability to specific requirements. For instance, QD can be conjugated to other biomolecules therefore changing their specificity allowing the detection of cell receptors of interest. In addition, having separate chips for cell seeding may allow the evaluation of a drug effect on different cell types.

The presented system opens the doors to the evaluation of new drugs to be tested in preclinical stages given the fact that this principle can be easily adapted to specific requirements by redesigning the geometries of the chips, the conjugated nanoprobes or the target cells.

5.6. References

[1] M. Koel, M. Kaljurand, *Pure Appl. Chem.* **2006**, *78*, 1993.

[2] C. Lledo-Fernandez, C. E. Banks, *Anal. Methods* **2011**, *3*, 1227.

[3] G. W. Peng, W. L. Chiou, *J. Chromatogr. B Biomed. Sci. Appl.* **1990**, *531*, 3.

[4] C. Rodwell, *Nat. Rev. Cancer* **2013**, *13*, 78.

[5] M. Suggitt, M. C. Bibby, *Clin. Cancer Res.* **2005**, *11*, 971.

[6] M. M. Lieberman, G. M. Patterson, R. E. Moore, *Cancer Lett.* **2001**, *173*, 21.

[7] R. K. Lin, C. W. Ho, L. F. Liu, Y. L. Lyu, *J. Biol. Chem.* **2013**, *288*, 7182.

[8] J. Han, T. P. N. Talorete, P. Yamada, H. Isoda, *Cytotechnology* **2009**, *59*, 45.

[9] W. R. Sellers, D. E. Fisher, *J. Clin. Invest.* **1999**, *104*, 1655.

[10] K. Schutters, C. Reutelingsperger, *Apoptosis* **2010**, *15*, 1072.

[11] G. A. F. Van Tilborg, E. Vucic, G. J. Strijkers, D. P. Cormode, V. Mani, T. Skajaa, C. P. M. Reutelingsperger, Z. A. Fayad, W. J. M. Mulder, K. Nicolay, *Bioconjug. Chem.* **2010**, *21*, 1794.

[12] H. A. Andree, C. P. Reutelingsperger, R. Hauptmann, H. C. Hemker, W. T. Hermens, G. M. Willems, *J. Biol. Chem.* **1990**, *265*, 4923.

[13] I. Vermes, C. Haanen, H. Steffens-Nakken, C. Reutelingsperger, *J. Immunol. Methods* **1995**, *184*, 39.

[14] U. Resch-Genger, M. Grabolle, S. Cavaliere-Jaricot, R. Nitschke, T. Nann, *Nat. Methods* **2008**, *5*, 763.

[15] W. R. Algar, U. J. Krull, *Anal. Bioanal. Chem.* **2010**, *398*, 2439.

[16] H. Montón, C. Nogués, E. Rossinyol, O. Castell, M. Roldán, *J. Nanobiotechnology* **2009**, *7*, 4.

[17] E. Morales-Narváez, H. Montón, A. Fomicheva, A. Merkoçi, *Anal. Chem.* **2012**, *84*, 6821.

[18] E. Morales-Narváez, A. R. Hassan, A. Merkoçi, *Angew. Chemie - Int. Ed.* **2013**, *52*, 13779.

[19] S. Le Gac, I. Vermes, A. Den Van Den Berg, *Nano Lett.* **2006**, *6*, 1863.

[20] V. A. Online, Q. Wu, D. Gao, J. Wei, F. Jin, W. Xie, Y. Jiang, H. Liu, **2014**, 2762.

[21] J. Chen, J. Li, Y. Sun, *Lab Chip* **2012**, *12*, 1753.

[22] D. Janasek, J. Franzke, A. Manz, *Nature* **2006**, *442*, 374.

[23] M. Medina-Sánchez, S. Miserere, A. Merkoçi, *Lab Chip* **2012**, *12*, 1932.

[24] G. M. Whitesides, *Nature* **2006**, *442*, 368.

[25] Y.-H. Jang, M. J. Hancock, S. B. Kim, S. Selimović, W. Y. Sim, H. Bae, A. Khademhosseini, *Lab Chip* **2011**, *11*, 3277.

[26] G. S. Du, J. Z. Pan, S. P. Zhao, Y. Zhu, J. M. J. Den Toonder, Q. Fang, *Anal. Chem.* **2013**, *85*, 6740.

[27] P. K. Yuen, *Lab Chip* **2008**, *8*, 1374.

[28] P. K. Yuen, J. T. Bliss, C. C. Thompson, R. C. Peterson, *Lab Chip* **2009**, *9*, 3303.

[29] W. Li, J. Greener, D. Voicu, E. Kumacheva, *Lab Chip* **2009**, *9*, 2715.

[30] P. Skafte-Pedersen, C. G. Sip, A. Folch, M. Dufva, *J. Micromechanics Microengineering* **2013**, *23*, 055011.

[31] K. Hsieh, A. S. Patterson, B. S. Ferguson, K. W. Plaxco, H. T. Soh, *Angew. Chemie - Int. Ed.* **2012**, *51*, 4896.

[32] S. H. Yazdi, K. L. Giles, I. M. White, *Anal. Chem.* **2013**, *85*, 10605.

[33] H. C. Tekin, M. a M. Gijs, *Lab Chip* **2013**, *13*, 4711.

[34] A. H. Diercks, A. Ozinsky, C. L. Hansen, J. M. Spotts, D. J. Rodriguez, A. Aderem, *Anal. Biochem.* **2009**, *386*, 30.

[35] L. Hajba, A. Guttman, *TrAC - Trends Anal. Chem.* **2014**, *59*, 9.

[36] R. J. Meagher, A. V Hatch, R. F. Renzi, A. K. Singh, *Lab Chip* **2008**, *8*, 2046.

[37] D. L. Englert, M. D. Manson, A. Jayaraman, *Nat. Protoc.* **2010**, *5*, 864.

[38] G. Pasirayi, S. M. Scott, M. Islam, L. O¸Hare, S. Bateson, Z. Ali, *Talanta* **2014**, *129*, 491.

[39] J. El-Ali, P. K. Sorger, K. F. Jensen, *Nature* **2006**, *442*, 403.

[40] E. Jedrych, S. Flis, K. Sofinska, Z. Jastrzebski, M. Chudy, A. Dybko, Z. Brzozka, *Sensors Actuators, B Chem.* **2011**, *160*, 1544.

[41] T. Riss, *Cell Note Issue* **2005**, 16.

[42] M. Medina-Sánchez, S. Miserere, S. Marín, G. Aragay, A. Merkoçi, *Lab Chip* **2012**, *12*, 2000.

[43] M. Medina-Sánchez, S. Miserere, E. Morales-Narváez, A. Merkoçi, *Biosens. Bioelectron.* **2014**, *54*, 279.

[44] H. Montón, C. Parolo, A. Aranda-Ramos, A. Merkoçi, C. Nogués, *Nanoscale* **2015**, *7*, 4097.

[45] L. Tang, N. Y. Lee, *Lab Chip* **2010**, *10*, 1274.

[46] K. Ziolkowska, E. Jedrych, R. Kwapiszewski, J. Lopacinska, M. Skolimowski, M. Chudy, *Sensors Actuators, B Chem.* **2010**, *145*, 533.

[47] J. C. McDonald, D. C. Duffy, J. R. Anderson, D. T. Chiu, H. Wu, O. J. Schueller, G. M. Whitesides, *Electrophoresis* **2000**, *21*, 27.

[48] E. Jedrych, M. Chudy, A. Dybko, Z. Brzozka, *Biomicrofluidics* **2011**, *5*, 1.

Chapter 6. Aminosilane-functionalized PDMS/glass chips for real-time monitoring of DNA hybridization assays using Quantum dot-modified molecular beacons

---

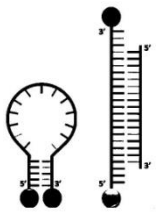

6.1. Introduction

Physico-chemical properties of Quantum dots (QDs) have made them one of the greatest focuses of interest in the scientific community over the last decades. Specifically, their unique optical properties have been exploited in bioanalytical and biomedical applications giving rise to new advancements in biological imaging and diagnostics[1ï4]. Development of diagnostic tools are on the agenda not only to build up a more complete scenario in drug discovery or biomarker detection, but also to improve the understanding of a certain disease pathogenesis decreasing associated costs at the same time. So far, QD-based probes have been successfully designed and used to achieve these purposes. For instance, we described in 2012 the use of streptavidin conjugated QDs as reporters in an immunocomplex microarray format assay designed to detect apolipoprotein E, a potential biomarker for Alzheimerôs disease, proving them to be highly effective and providing five times more sensitivity than common fluorescent dyes [5]. More recently, as reported in chapter 4, we have shown the use of Annexin V-QD probes as specific and versatile contrast agents in dual electrochemical/optical detection for the study of apoptosis[6], which is a key factor of several diseases[7][8] and a target for drug development[9].

Nowadays, another important active area of research where QDs properties are of great value is nucleic acid diagnostics. Conjugated with oligonucleotides QDs have been indistinctly used as optical or electrochemical probes and as scaffolds to carry out the detection of the corresponding target nucleic acid sequences *via* hybridization [10,11].

Among all probes developed for nucleic acid detection, Molecular Beacons (MBs) are one of the most exploited due to their versatility, specificity and sensitivity. MBs were first introduced by Tryagi and Kramer in 1996 [12] who reported the first use of a

binding-induced conformational change in a DNA molecular beacon for sensing puroposes. Specifically, they designed hairpin-shaped DNA structures with an internally quenched fluorophore that produced a robust optical response when the hybridization of target DNA sequences opened the double-stranded stem (the principle of operation of molecular beacons is shown in Figure 1).

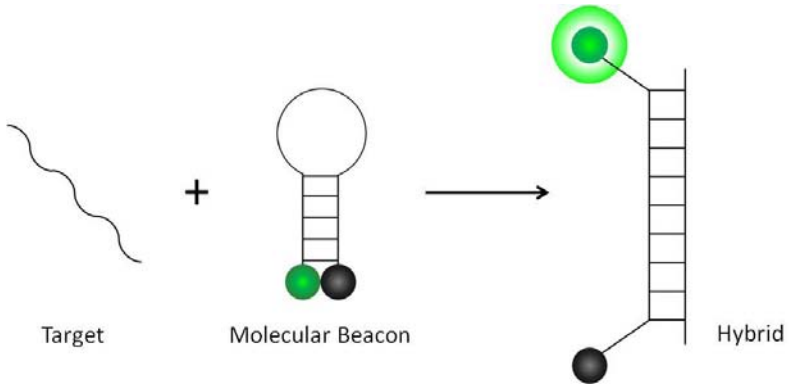

Figure 1. Hairpin-shaped DNA structures, so called molecular beacons, are designed to have a fluorophore (drawn in green) close to a quencher (drawn in black). Only when the hybridization of target DNA sequences takes place, an optical response is produced due to the opening of the double-stranded stem which provokes the quencher to move away from the fluorophore.

Since then, many labs worldwide have been using and adapting this new DNA nanotechnology for diverse applications such as PCR, molecular biology techniques (electrophoresis gel), bioassays, intracellular imaging, or pathogen detection [13,14].

However, remarkable improvements have arrived with the combination of DNA nanotechnology and QDs for sensing applications using both Förster Resonance Energy Transfer (FRET), and quenching principles [10,15,16]. Dark quenchers are dyes with no native fluorescence used as acceptors in quenching-based FRET. In fact one of the

most used dark quenchers are black hole quenchers (BHQ) because they are capable of quenching across the entire visible spectrum depending on their structure [17] .

Such DNA detection nanotechnology, as shown in many applications, requires a high level of control over the distance between the acceptor/donor or the dye/quencher [18ï 20]. For that reason, many works have been focused towards this direction and have described different strategies to get QDs conjugated to MBs (QD-MB) basically through carbodiimide chemistry [21,22] and have demonstrated its potential in different applications. Some recent works reported the use of QD-MB as tools for pathogens and transgenes detection [23], for PCR amplicons detection [24], for fluorescence enhancement in biosensors for DNA detection [25] or even for an in vitro and in vivo detection of matrix metallopeptidase 2 (MMP2) on tumoral cells [26].

Some of the works mentioned above used microfluidics approaches to carry out nucleic acid detection. So far, lab-on-a-chip platforms have been widely used for several applications including sample preconcentration or pretreatment [27,28] and detection of different analytes such as proteins, virus or nucleic acids among others [29] in addition of other interesting applications involving nanomaterials [30]. For instance, in our group, several works have been reported in the use of microfluidics such as in-chip manipulation and electrochemical detection of QDs [31], on-chip electrochemical detection of an Alzheimer related biomarker [32] and even including paper-based devices as simple lateral flow assays for pathogen detection using quenching strategies [33].

Microfluidics-based lab-on-chips meet the requirements that clinical and point-of-care diagnostics should have. This technology provides platforms which offer reduction of sample and reagent volumes, and of time of reactions and analysis [34] and more interestingly simple use for non-specialized personnel [35]. Thus, assembling DNA

nanotechnology with QDs in a miniaturized system such as microfluidics-based lab-on-chip platforms creates the perfect scenario for the development of a possible game changer technology. Moreover, in the development of microfluidic-based systems, the application of deposition techniques makes possible to configure the presence of biomolecules in glass substrates, as the lately reported on-the-spot immobilization using hydrophobins in our group [36], providing a powerful tool for biomedical and environmental applications [37].

In this chapter we present how the combination of MBs and QDs can be used in a diagnostic microfluidic device for the detection of nucleic acids through fluorescence microscopy (in Figure 2A the setup is shown). A simple and functional microfluidic chip, which contains a single line array of spots made with aminosilanes through APTES deposition, is applied. This allows the monitoring, in real-time, of a complete DNA hybridization assay starting from the conjugation of QDs with MBs up to the interrogation of target samples. All the in-channel occurring events (immobilization of QDs, conjugation with MBs and hybridization of specific or nonspecific oligonucleotides) are monitorized through fluorescence microscopy (Figure 2B) and further quantified by image processing in order to obtain numerical data of the whole assay.

With this method we were able to: i) reduce sample volumes and time of reactions by using a small microdevice, ii) make the complete monitoring easier by functionalizing specific areas of the chip with aminosilanes and, iii) carry out a stable and robust long-term monitoring with high accuracy of quantification by using QDs as detection probes.

Alltogether, MBs with QDs within lab-on-a-chip, provide a reliable system to reveal nucleic acid markers for clinical and point-of-care diagnostics applications.

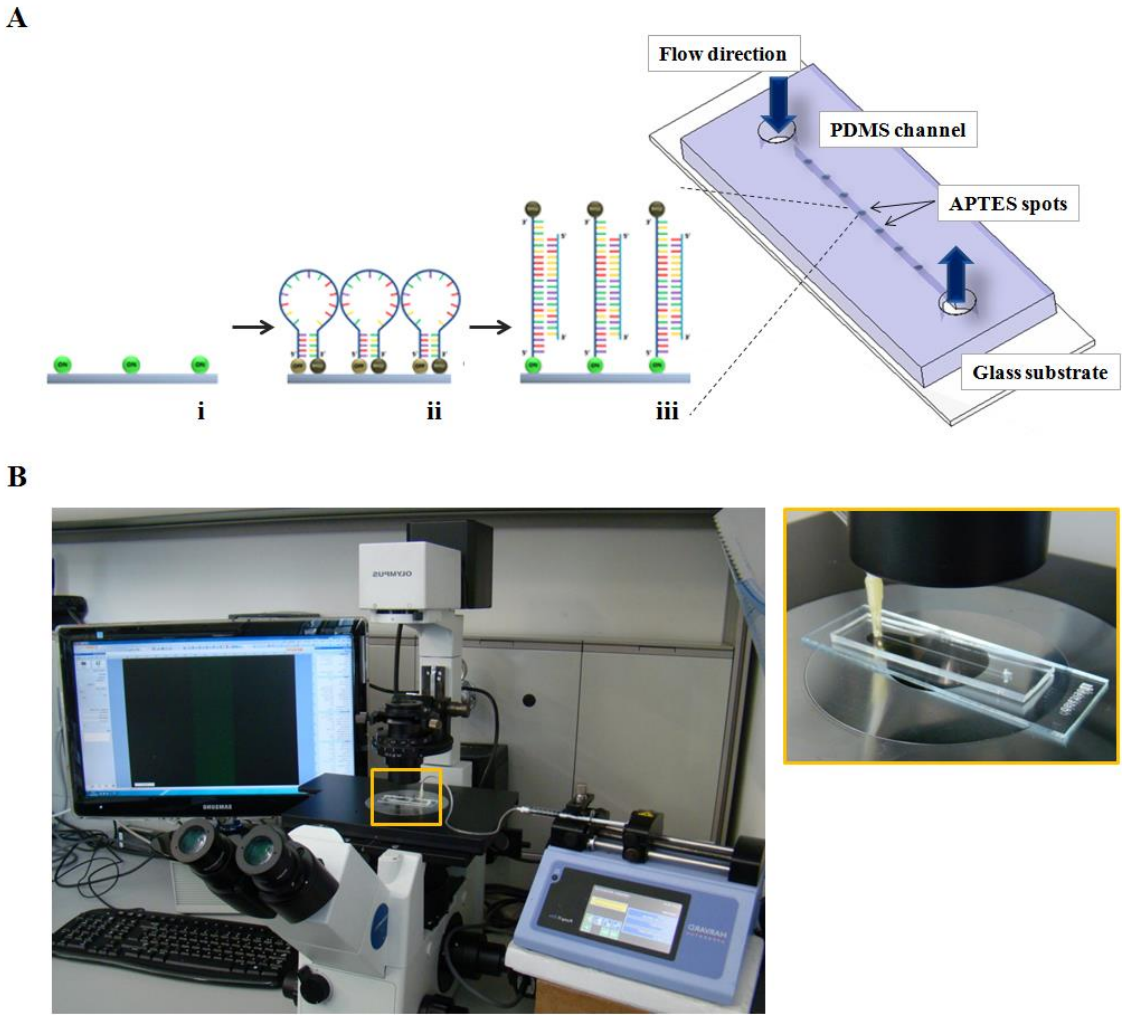

Figure 2. A. Schematic draw of the lab-on-a-chip that performs the whole assay from (i) immobilization of QDs in the APTES spots, (ii) conjugation of MBs with the immobilized QDs provoking their quenching and (iii) hybridization of the DNA target with the loop of the MB moving away the quencher from the QDs, thus causing the recovery of the fluorescence . **B**. Photo of the set-up for in-chip detection of nucleic acids through fluorescence microscopy including the syringe pump and the optical microscope coupled with a CCD camera and specific software for results processing. A closer view of the PDMS/glass chip is shown in the upper-right corner.

6.2. Methods

6.2.1. Materials and instruments

Qdot® 525 ITKÊ Carboxyl Quantum Dots (QDs) were purchased from Life Technologies S.A. (Spain). Molecular Beacons (MBs) modified with Black Hole Quencher (see structure at Table 1), specific or nonspecific 17mer target (t17) oligonucleotides, 3-aminopropyltriethoxylane (APTES), 1-Ethyl-3-(3-dimethylaminopropyl)carbodiimide (EDC), *N*-hydroxysuccinimide (NHS), Saline-Sodium Citrate buffer 20X (SSC 20X) and 1 mL plastic disposable syringes were purchased from Sigma-Aldrich (Spain).

Negative photoresist (SU8-50) for the fabrication of chips was purchased from Microchem (USA), flexible masks from Microlitho Ltd (UK), Poly-dimethylsiloxane (PDMS) from Ellsworth (Spain). Syringe pumps were purchased from Harvard Apparatus (USA) and Plasma Cleaner from Harrick Plasma (USA).

A Milli-Q system (>18.2MÝcm^{-1}) purchased from Millipore (Sweden) was user to produce mQ water.

6.2.2. Design and fabrication of PDMS channels

Microchips consisting on a linear channel (cross section of 500 X 100 µm, length of 2 cm) were fabricated by rapid prototyping using softlithography, which has been widely described in the literature.[37] Briefly, a 4 inch silicon wafer was spin coated for 50 s at 2000 rpm with a negative photoresist (SU8-50) and patterned by photolithography through exposition under UV light for 50 s and then revealed. All of these steps were done in cleaning room conditions. Consequently, PDMS was deposited onto the resulting SU8 master and cured at 65 ºC during 2 h.

6.2.3. Aminosilane (APTES) functionalization of glass substrates

Glass substrates were treated by air-plasma for 1 min and then several drops of 0.1 µL of 10% (v/v) APTES solution in milliQ water were deposited manually onto the glass drawing a linear array of spots in the substrate. APTES drops were incubated for 30 min at room temperature in order to allow the functionalization of the glass surface with the amino groups previous to the immobilization of QDs. Glass substrates were rinsed gently with water and then air-dried with compressed N_2 air to remove any trace of humidity.

6.2.4. Assembly of PDMS channels with APTES-functionalized glass substrates

To achieve the assembly of the microchips, PDMS channels were first treated by air-plasma for 1 min and then put in contact with the glass substrate. Finally, the irreversible bonding was achieved by keeping the assembled microchips 15 min at 65 ºC in a hotplate.

6.2.5. Immobilization of carboxyl-QDs

Prior to immobilization of carboxyl-QDs into the microchannels a 100 µL suspension containing QDs, EDC and NHS was prepared. 0.2 µL of QDs from the stock suspension were added into a microtube containing 97.8 µL of milliQ water, pipette mixed and vortexed. Then 1 µL of freshly prepared EDC at 30 mM and 1 µL of freshly prepared NHS at 15 mM were added into the tube and the suspension was pipette mixed and vortexed.

Immobilization of QDs on the APTES-functionalized areas was carried out introducing the already prepared QDs suspension inside the microchannel using a 1 mL syringe and controlling the flow rate at 2.5 $\mu L \cdot min^{-1}$ during 5 min with the syringe pump. Finally, a

washing step was carried out by introducing milliQ water into the microchannels at a flow rate of 5 µL·min^{-1} during 5 min.

6.2.6. Conjugation with BHQ-modified Molecular Beacons

A solution of 1 µM amino-terminated MBs modified with BHQ (see **Table 1**) was prepared in order to conjugate them with the in-channel already immobilized carboxyl-QDs. 1 µL of MBs solution at 100 µM was added into a microtube containing 97 µL of milliQ water. A vigorous vortex of the solution was carried out and then 1 µL of freshly prepared EDC at 30 mM and 1 µL of freshly prepared NHS at 15 mM were introduced into the microtube and mixed by gently pipetting.

Conjugation of MBs with QDs was performed introducing the MBs solution inside the microchannel using a 1 mL syringe and keeping the flow rate at 2.5 µL·min^{-1} during 5 min. A final washing step was carried out by introducing mQ water into the microchannels at a flow rate of 5 µL·min^{-1} during 5 min.

Table 1. Oligonucleotide sequences of the Molecular Beacon and target DNAs used in the assays

Name	Sequence
Molecular Beacon (MB)	NH2-5ô-CTCTCGATCGGCGTTTTAGAGAG-3ô-BHQ
Specific t17	3ô-AGCTAGCCGCAAAATCT-5ô
Nonspecific t17	3ô-AGCT**GG**T**GAG**A**C**A**T**TCT-5ô

The 5ô and 3ô modifications in the MB backbone used are shown. NH2, amine group; BHQ, black hole quencher; t17, 17mer target. Underlined are nucleotides bases that constitute the stem of the MB. Mismatch bases of nonspecific target are represented in bold.

6.2.7. Hybridization with target oligonucleotides

Specific or nonspecific target oligonucleotides (see **Table 1**) were used to carry out hybridization assays. A solution of each of them was prepared at a concentration of 100 µM in SCC buffer 2X, previously diluted from a 20X stock solution in mQ water.

Hybridization of target oligonucleotides with the QD-MB already conjugated in the APTES- modified areas of the microchannel was carried out introducing target solutions at a flow rate of 2.5 $\mu L \cdot min^{-1}$ during 10 min.

6.2.8. Monitoring and quantification using fluorescence microscopy

Live monitoring of fluorescent changes associated to immobilization, conjugation and hybridization was carried out using an inverted fluorescence microscope (Olympus IX71, Germany) coupled with a CCD camera (Olympus DP72, Germany). An HBO mercury lamp was used as excitation source and a FITC filter cube was set to select the emission wavelength of the QDs.

Images of a selected APTES functionalized spot inside the microchannel were acquired at different time intervals depending on the process being monitored: every 15 sec for immobilization and conjugation steps, and every 30 sec for hybridization.

Image J (U. S. National Institutes of Health, Maryland, USA) was used for the image post-processing in order to determine the fluorescence intensity variation over time corresponding to each event taking place inside the microchannel. Three squared regions of interest (ROI) were randomly selected in the immobilization area and the pixel sum intensity was quantified in each ROI. The average intensity of the three ROIs was normalized and used as a comparative value between images acquired at different time intervals of the immobilization, conjugation and hybridization steps.

6.3. Results and Discussion

6.3.1. Aminosilane functionalization of PDMS/glass chips

A relevant issue to consider for point-of-care devices is the possibility of analyzing small volumes of sample. That goal was achieved by using microfluidic channels in combination with deposition of APTES to preconcentrate the sample. We deposited APTES linearly in microspots onto the glass substrates to match the path with the PDMS channel thus facilitating the monitoring of the events by preconcentrating the reagents required in specific areas of interest. Microscope images of the assembled PDMS/glass chips confirmed their correct position along the channel (Figure 3.A). We also confirmed that APTES spots were not fluorescent in the wavelength range of the QDs emission (Figure 3.B.) thus not interference was expected in the monitoring of the immobilization, conjugation and hybridization processes.

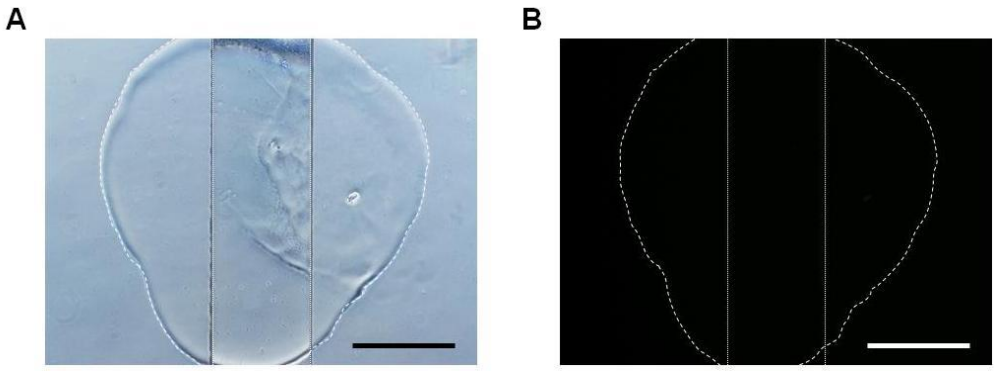

Figure 3. A. Brightfield images along the channel path were acquired in order to confirm that APTES spots were correctly deposited. This image shows an APTES spot covering a specific area of the channel. **B.** Fluorescence image of the same spot were acquired using the settings for QDs imaging. This shows that no fluorescence is emitted by APTES in this specific range and that this would not interfere the monitoring of events involving QDs. Scale bars = 500 µm.

Spot diameters of about 1.5 mm were determined by manually depositing APTES drops of 0.1 µL. That was the minimum volume allowed by the pipette in order to obtain spots as much separated as possible in a single channel. The aim was to develop a platform that allowed us to monitorize sequential events, but also a device that can be used in future applications to carry out highly parallel analyses. Different concentrations of APTES were checked and we observed that 10% was the optimal concentration to obtain a good coverage of the spot surface with QDs. Lower percentages of APTES gave place to a poor amount of QDs immobilized in the area of interest and higher percentages did not resist the continous flow and the spots were detached before the end of the experiment (Annex II.A).

6.3.2. Monitoring of full assay in-chip: immobilization, conjugation and hybridization

Monitoring the immobilization of QDs, their conjugation with BHQ-modified MBs and the hybridization with specific targets with QD-MBs was done under a fluorescence microscope (Figure 4A). Flow rates and incubation times for each step were optimized and were established at the fastest speed of the stream at which the spots remain stable during the whole assay, which was 2.5 $\mu L \cdot min^{-1}$ for a maximum of 5 $\mu L \cdot min^{-1}$.

Immobilization of carboxyl-QDs with APTES could be followed due to the fluorescence emission of QDs which made APTES modified spots inside the channel visible as QDs were being immobilized onto them (schematic and corresponding image in Figure 4A-a). The immobilization time was determined by the minimum time (5 min) to obtain a homogenous coverage of QDs that would not induce any QDs aggregation, which would skew the quantification.

Interestingly with both the silanization method through APTES deposition exposing amino groups and the use of EDC-NHS chemistry to immobilize QDs and conjugate them to MBs, the covalent binding of QDs onto the silanized areas, firstly, and between already immobilized QDs and MBs, later on, was ensured to take place in a more efficient and immediate way.

As BHQ-modified MBs started being conjugated to QDs, the fluorescence of the spots dramatically decreased due to the proximity of the BHQ to the QDs provoked by their conjugation (schematic and corresponding image in Figure 4A-b). The incubation time required for the conjugation step was determined as the time when no more decreasing of fluorescence was observed (5 min) which meant that the system could not accept more binding of MBs indicating that it was already saturated. A QD:MB ratio of approximately 1:60 was used to prepare initial solutions of QDs and MBs for the immobilization and conjugation steps, respectively. An excess of MBs in relation with the amount of QDs favored a fast conjugation step due to the high number of available MBs per QDs already immobilized in the areas of interest. After each incubation step, excess of either QDs or MBs inside the channel were washed away to avoid the interference with the binding events occurring in the specific areas.

Finally, hybridization of target oligonucleotides specific for the loop sequence of the QD-MB was performed and monitored. As specific t17 hybridized with the QD-MB, the stem-loop structure of the MB opened moving away the BHQ from the QD thus causing progressive recovery of the fluorescence (schematic and corresponding images i to iii in Figure 4A-c). Incubation time for the hybridization step was also optimized in terms of the incubation time necessary to have a significant recovery of fluorescence.

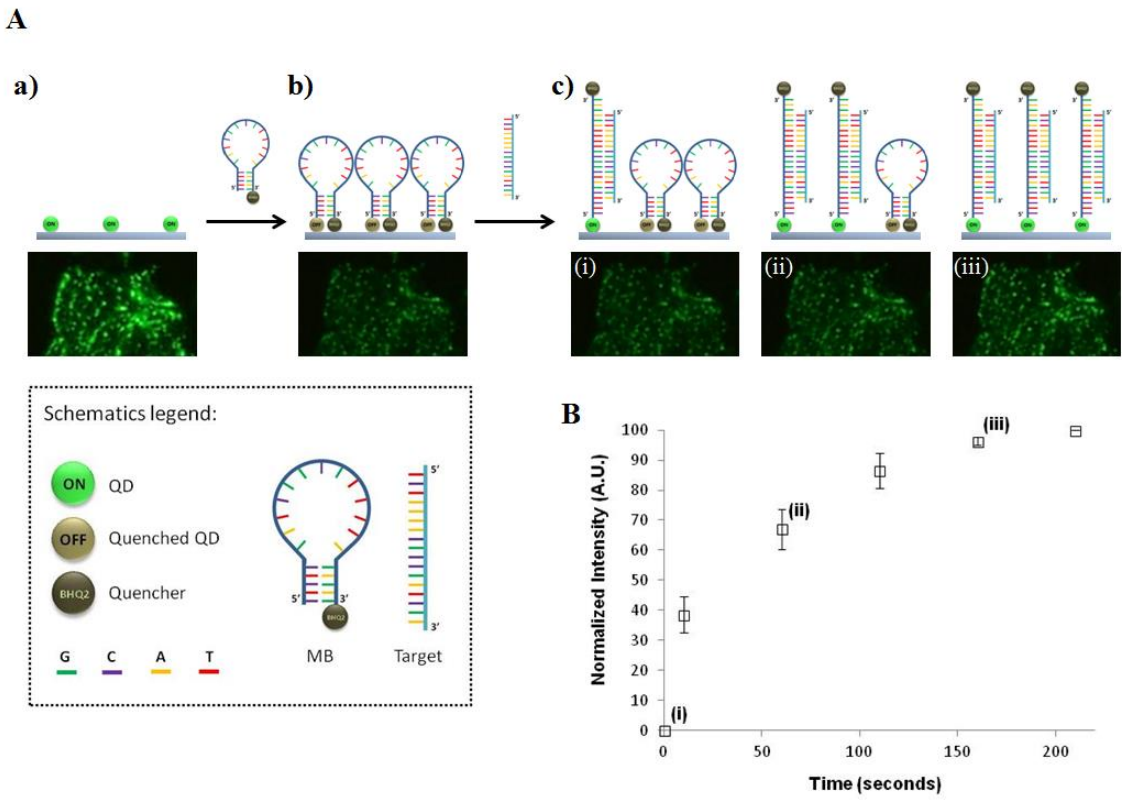

Figure 4. A. Schematics and corresponding images of a full assay monitoring. **a)** Immobilization of QDs on APTEs modified areas. **b)** Conjugation of QDs with MB showing a fluorescence decrease due to the proximity of QD with the BHQ present in the MB. **c)** Hybridization with specific target oligonucleotides made a progressive recover of the fluorescence proportional to the amount of target hybridized with the MB (i, ii, iii). **B.** Binding curve obtained from hybridization assays with specific t17. Normalized mean values of fluorescence were calculated from images acquired at different timepoints (timepoints (i), (ii) and (iii) correspond to data obtained from images shown in A-c. Error bars represent differences between quantified areas of the same chip.

Hybridization of the specific t17 with the QD-MB was quantified, and binding curves were obtained (Figure 4B). The increment on fluorescence observed over time time corresponds to the increment of hybridization between specific t17 and QD-MBs. Incubation times for hybridization ranged from 6 up to 20 min and eventually it was

possible to detect fluorescence recovery by naked-eye during the monitoring process. However by analyzing and quantifying images at different timepoints we were able to obtain consistent results for typical binding curves after 10 min of incubation for all experiments. Therefore 10 min were established as the incubation time necessaty, with target oligonucleotides, to complete the hybridization assay.

Fluorescence was quantified for each timepoint by selecting three random regions of interest (ROIs) of each image and the mean value of fluorescence intensity was calculated. Normalized mean values, obtained for each image, were displayed in graphs showing the trend of a typical binding curve. The same trend was observed in hybridization performances obtained for different chips (Annex II.B). As an example, three different timepoints are depicted in the graph as (i), (ii) and (iii) in Figure 4B, that correspond to the images shown in Figure 4A-c and, as expected, differences in fluorescence intensity are more evident in the graph than in the images.

We believe that the variability in incubation time for the hybridization is due to the temperature at which the experiment is carried out. Whereas immobilization and conjugation did not show temperature-dependence, DNA hybridization is known to be sensitive to temperature and it is usually performed at higher temperatures such as 60ºC. Although carrying out the assay at room temperature can slightly delay obtaining the results it allows having an easy-to-use platform for potential point-of-care device.

6.3.3. Specificity of the assay (specific target vs nonspecific target)

We evaluated the specificity of the assay by comparing two target oligonucleotides; one with the exact recognition sequence for the loop of the MB (specific t17) and the other which contained seven mismatches with the loop of the MB (nonspecific t17).

A complete hybridization assay from the immobilization of the QD and conjugation with the MB up to the introduction of the specific or nonspecific target was carried out to study the specificity of the system. As explained above, hybridization of specific t17 or nonspecific t17 with the QD-MB was quantified. The data obtained from two different chips tested for two different targets (specific and nonspecific hybridization) are shown in Figure 5. As it can be observed in the graph, a recovery of fluorescence typical of a binding curve is obtained for the specific t17 hybridization whereas small or negligible recovery of fluorescence (shown as a flat curve) is observed when the nonspecific t17 is introduced. These results show undoubtedly the specificity of the system since no relevant hybridization was taking place when the target introduced is nonspecific for the loop of the MB.

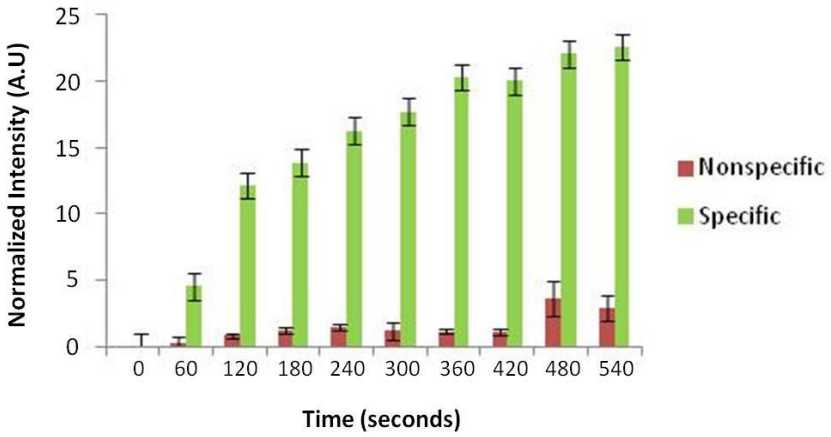

Figure 5. Comparative fluorescence intensity at different timepoints of hybridization assays carried out with specific or nonspecific target oligonucleotides. When a specific target is introduced (green) a recovery of fluorescence resulting in the trend of a typical binding curve is observed, whereas a flat curve with no or negligible fluorescence recovery is obtained when a nonspecific target oligonucleotide (red) is introduced.

6.4. Conclusions

In this chapter, we have shown how the combination of different technologies i.e., molecular beacons with QDs-based fluorescence and microfluidics can lead to the development of a simple and easy-to-use integrated device able to reveal the presence of a nucleic acid biomarker in an unknown sample. This device was achieved by using a single channel platform in which APTES was previously deposited. Through this silanization process amino groups were exposed in localized spots where all reactions took place and afterwards selective fluorescence changes were monitorized.

Specificity and sensitivity are basic elements of point-of-care diagnostics devices that at our platform are achieved thanks to the use of MBs. We chose a MB structure with a number of bases and complementarities well studied and previously optimized with proven results by Plaxco and collaborators[38ï 40]. Coupling /conjugating now MB with QDs contributed to have a robust optical detection which, far from complicating the readout of the signal, provided a more intuitive technique for diagnostic application based on the internally quenched structure. Undoubtfully, introduction of QDs was the key step to monitorize the entire assay from immobilization up to the hybridization of the MBs with the target oligonucleotide. In fact, the stability of the emitted fluorescence by QDs allows having reliable measures at any time during long-term experiments [41], something that other labels can not provide [42,43].

In addition, we were able to minimize immobilization, conjugation and hybridization times because of the high surface-to-volume ratio and the constant flow associated to microfluidics that increases the sensitivity due to the higher number of available binding events. Moreover, the use of microfluidics allows integration and automation of the system making it more attractive in terms of possible future commercialization.

Summarizing, the results presented in this chapter show that we successfully applied QD-MB based technology to detect nucleic acids by carrying out hybridization assays in specific areas of a microfluidic channel. The assay consisting in different steps, including the immobilization of QDs as a fluorescent labeling, MB conjugation with QD and target oligonucleotide hybridization in-flow mode, allowed real time monitoring of the process through continous analysis of fluorescence changes. Combining a simple deposition method with microfluidics and using QD-MB technology, a proof-of-concept platform for nucleic acid detection with reliable results is developed.

Considering that there is a strong demand for clinical and point-of-care diagnostics that can reveal nucleic acid sequences the developed proof-of-concept DNA detection technology may be useful for future applications. The developed lab-on-a-chip systems, based on microchannels easy to be fabricated using conventional soft-lithography, [44] make the proposed QD-MB technology of interest for mass production which combined with further automatization of the whole process will be with great interest for real sample applications.

6.5. References

[1] J.-J. Xu, W.-W. Zhao, S. Song, C. Fan, H.-Y. Chen, *Chem. Soc. Rev.* **2014**, *43*, 1601ï 11.

[2] M. Wei, R. Liang, D. G. Evans, X. Duan, *Chem. Commun.* **2014**, *50*, 14071ï 14081.

[3] J. Li, J.-J. Zhu, *Analyst* **2013**, *138*, 2506ï 15.

[4] B. a Kairdolf, A. M. Smith, T. H. Stokes, M. D. Wang, A. N. Young, S. Nie, *Annu. Rev. Anal. Chem.* **2013**, *6*, 143ï 162.

[5] E. Morales-Narváez, H. Montón, A. Fomicheva, A. Merkoçi, *Anal. Chem.* **2012**, *84*, 6821ï 7.

[6] H. Montón, C. Parolo, A. Aranda-Ramos, A. Merkoçi, C. Nogués, *Nanoscale* **2015**, *7*, 4097ï 104.

[7] R. E. Castro, M. M. M. Santos, P. M. C. Glória, C. J. A. Ribeiro, D. M. S. Ferreira, J. M. Xavier, R. Moreira, C. M. P. Rodrigues, *Curr. Pharm. Des.* **2010**, *16*, 2851ï 2864.

[8] A. L. Hunter, J. C. Choy, D. J. Granville, *Methods Mol. Med.* **2005**, *112*, 277ï 289.

[9] S. W. Fesik, *Nat. Rev. Cancer* **2005**, *5*, 876ï 885.

[10] R. Freeman, J. Girsh, I. Willner, *ACS Appl. Mater. Interfaces* **2013**, *5*, 2815ï 34.

[11] W. R. Algar, U. J. Krull, *Anal. Bioanal. Chem.* **2008**, *391*, 1609ï 1618.

[12] S. Tyagi, F. R. Kramer, *Nat. Biotechnol.* **1996**, *14*, 303ï 8.

[13] N. E. Broude, *Trends Biotechnol.* **2002**, *20*, 249ï 256.

[14] G. Goel, a. Kumar, a. K. Puniya, W. Chen, K. Singh, *J. Appl. Microbiol.* **2005**, *99*, 435ï 442.

[15] J. E. Ghadiali, S. B. Lowe, M. M. Stevens, *Angew. Chem. Int. Ed. Engl.* **2011**, *50*, 3417ï 20.

[16] L. C. Grigsby, Y.-P. Ho, K. W. Leong, *Nanomedicine* **2012**, *29*, 997ï 1003.

[17] ñbiosearchtech,ò can be found under https://www.biosearchtech.com/bhq, **n.d.**

[18] F. Wang, B. Willner, I. Willner, *Curr. Opin. Biotechnol.* **2013**, *24*, 562ï 574.

[19] F. Zhang, J. Nangreave, Y. Liu, H. Yan, *J. Am. Chem. Soc.* **2014**, *136*, 11198ï 11211.

[20] V. Linko, H. Dietz, *Curr. Opin. Biotechnol.* **2013**, *24*, 555ï 561.

[21] D. a Hines, P. V Kamat, *ACS Appl. Mater. Interfaces* **2014**, *6*, 3041ï 57.

[22] L. Liu, H. Li, T. Qiu, G. Zhou, K.-Y. Wong, Z. He, Z. Liu, *Chem. Commun. (Camb).* **2011**, *47*, 2622ï 2624.

[23] K. P. Burris, T. C. Wu, M. Vasudev, M. A. Stroscio, R. J. Millwood, C. N. Stewart, *IEEE Trans. Nanobioscience* **2013**, *12*, 233ï 238.

[24] X. He, N. Ma, *Anal. Chem.* **2014**, *86*, 3676ï 3681.

[25] N. C. Cady, *Methods Mol. Biol.* **2009**, *544*, 367ï 379.

[26] X. Li, D. Deng, J. Xue, L. Qu, S. Achilefu, Y. Gu, *Biosens. Bioelectron.* **2014**, *61*, 512ï 518.

[27] C. C. Lin, J. L. Hsu, G. B. Lee, *Microfluid. Nanofluidics* **2011**, *10*, 481ï 511.

[28] J. H. Jung, B. H. Park, Y. K. Choi, T. S. Seo, *Lab Chip* **2013**, *13*, 3383ï 8.

[29] C. A. Baker, C. T. Duong, A. Grimley, M. G. Roper, *Bioanalysis* **2009**, *1*, 967ï 975.

[30] M. Medina-Sánchez, S. Miserere, A. Merkoçi, *Lab Chip* **2012**, *12*, 1932.

[31] M. Medina-Sánchez, S. Miserere, S. Marín, G. Aragay, A. Merkoçi, *Lab Chip* **2012**, *12*, 2000.

[32] M. Medina-Sánchez, S. Miserere, E. Morales-Narváez, A. Merkoçi, *Biosens. Bioelectron.* **2014**, *54*, 279ï 284.

[33] E. Morales-Narváez, T. Naghdi, E. Zor, A. Merkoçi, *Anal. Chem.* **2015**, *87*, 8573ï 8577.

[34] D. Mark, S. Haeberle, G. Roth, F. Von Stetten, R. Zengerle, *NATO Sci. Peace Secur. Ser. A Chem. Biol.* **2010**, 305ï 376.

[35] C. Liberale, G. Cojoc, F. Bragheri, P. Minzioni, G. Perozziello, R. La Rocca, L. Ferrara, V. Rajamanickam, E. Di Fabrizio, I. Cristiani, *Sci. Rep.* **2013**, *3*, 1ï 6.

[36] A. M. Gravagnuolo, E. Morales-Narváez, C. R. S. Matos, S. Longobardi, P. Giardina, A. Merkoçi, *Adv. Funct. Mater.* **2015**, n/aï n/a.

[37] E. Blinka, K. Loeffler, Y. Hu, A. Gopal, K. Hoshino, K. Lin, X. Liu, M. Ferrari, J. X. J. Zhang, *Nanotechnology* **2010**, *21*, 415302.

[38] A. Vallée-Bélisle, F. Ricci, K. W. Plaxco, *Proc. Natl. Acad. Sci. U. S. A.* **2009**, *106*, 13802ï 13807.

[39] H. M. Watkins, A. Vallée-Bélisle, F. Ricci, D. E. Makarov, K. W. Plaxco, *J. Am. Chem. Soc.* **2012**, *134*, 2120ï 2126.

[40] D. Kang, A. Vallée-Bélisle, A. Porchetta, K. W. Plaxco, F. Ricci, *Angew. Chemie - Int. Ed.* **2012**, *51*, 6717ï 6721.

[41] C. Srinivasan, J. Lee, F. Papadimitrakopoulos, L. K. Silbart, M. Zhao, D. J. Burgess, *Mol. Ther.* **2006**, *14*, 192ï 201.

[42] X. Wu, H. Liu, J. Liu, K. N. Haley, J. A. Treadway, J. P. Larson, N. Ge, F. Peale, M. P. Bruchez, *Nat. Biotechnol.* **2003**, *21*, 41ï 46.

[43] H. Montón, C. Nogués, E. Rossinyol, O. Castell, M. Roldán, *J. Nanobiotechnology* **2009**, *7*, 4.

[44] Y. Xia, G. M. Whitesides, *Annu. Rev. Mater. Sci.* **1998**, *28*, 153ï 184.

Chapter 7. Conclusions and Future Perspectives

7.1. Conclusions

This PhD thesis demonstrates how the use of QDs can improve current methodologies of biology and bring also novel ones. We exploited both the optical and electrochemical properties of QDs to develop novel labels and biosensing systems for the detection of cells and DNA.

First of all, we demonstrated that QDs can be used routinely as fluorescent labels to visualize several proteins in eukaryotic cells. This technology proved to have several advantages over classical organic dyes: the same source of excitation can be used to detect different markers and their higher brightness and photostability allows to visualize samples for longer times and to optimize their visualization without damaging the samples or decreasing the resolution of the signal.

Following the first work, we applied the QDs for the specific detection of apoptotic cells. Combining QDs and Annexin-V, we managed to develop an optical-electrochemical label that has been used to improve the detection and quantification of apoptosis in living cells. The peculiar properties of QDs have been exploited to study the same sample of apoptotic induced cells using classical techniques, such as SEM, CLSM, flow cytometry, and an electrochemical technique such as stripping voltammetry. While SEM and CLSM gave us qualitative information about the apoptotic status of a limited number of cells, flow cytometry and stripping voltammetry gave us a more quantitative insight over the sample population. Combining the data from the 4 different techniques it is possible to evaluate the efficiency of a specific drug in inducing apoptosis, and to have also a closer look on the process taking place in order to understand it better.

A further step towards the use of QDs in biological application has been done with the development of a microfluidic chip for drug screening. The idea behind the project was to

demonstrate that QDs can be part of an integrated system that would facilitate the work done by the operator making it more reliable, and would also allow the analysis and comparison of different drugs saving materials and time. In this first prototype, we decided to combine several steps of the protocol developed for the detection of apoptotic cells into a series of microfluidic chips. We designed a chip for the conjugation of QDs and Annexin-V, in which the main feature is the serpentine-shaped long channel that improves the mixing and thus the conjugation efficiency; a second chip for the generation of different drug concentrations; and a third chip for the cell culture and apoptosis detection. The results obtained for drug screening proved that, on one hand, the chips work properly, making easier and faster the whole process if compared to the manual work; and, on the other hand, QDs are compatible with this integrated system, showing their robustness, which is essential to expand their use to new biological fields.

Finally we showed how QDs can be used as labels for DNA detection using DNA origami structures. Taking advantage of the nanoscale precision of DNA molecular beacons and the optical properties of the QDs, we managed to develop an optical biosensor based on fluorescence quenching, integrating it into a microfluidic channel to further optimize its performances. In this case, the narrow emission band of the QDs is a great tool to develop a sensitive and specific quenching-based DNA sensor, in which the donor and acceptor wavelengths can be perfectly matched, minimizing non-specific results. The further integration of the QD-Molecular Beacon complex into a microfluidic channel enabled us not only to use less material, thus lowering the cost, but also to be able to achieve a continuous monitoring of the whole process, from the conjugation of the QDs with the molecular beacon to the target hybridization. Being able to perform such a continuous following up of the whole process gives the user much more control over the experiments and consequently to respond to possible encountered problems faster and more efficiently. The achievement of

such level of control is due exclusively to the high resistance to photobleaching of the QDs; in fact the use of organic dyes would considerably limit the possibility of live monitoring, since after a while the fluorescence begins to fade to finally disappear.

To conclude, we have demonstrated that QDs are not only able to replace organic dyes as fluorescent labels, but they can also be combined with electrochemical methods and microfluidics, generating whole new alternatives in biosensing and drug screening.

Summarizing:

1. We set up an optimal protocol for the use of QDs as optical immunolabels in routine immunocytochemistries allowing a robust confocal microscopy imaging of HeLa cells for diagnostics applications.

2. We developed a specific optical-electrochemical label combining QDs to Annexin V in order to detect apoptosis by using classical techniques such as SEM, CLSM and flow cytometry but also through biosensing using electrochemical stripping voltammetry.

3. We developed a modular microfluidic platform for drug screening consisting in the combination of three different chips with specific functionalities to finally detect apoptosis in living cancer cells through the use of QDs as optical labels.

4. We developed an optical biosensor using DNA molecular beacons and QDs in a lab-on-a-chip based on microfludics for nucleic acid detection.

7.2. Future Perspectives

As shown in chapter 4, we believe that the combination of different sources of information by the use of different optical and electrical techniques can give a more accurate insight over biological interactions. The aim of the work done in this thesis was to create the basis for a future fully integrated platform, where QDs would be simultaneously used as dual optical-electrochemical labels for diverse applications.

We envisage a platform that is based on microfluidics and novel transparent electrodes. The microfluidics will minimize the waste of reagents and the number of steps done by the operator (as shown in chapter 5). In this way the final device will be cheaper, easier to use and, possibly, will be used at the point of care. The use of transparent electrodes, such ITO or graphene-based electrodes, will enable the simultaneous optical and electrochemical detection. The possibility of observing in real time how a specific process is occurring (such as the DNA hybridization monitoring shown in chapter 6) and, based on that, be able to better understand reactions taking place, will be an invaluable tool for future research in nanomedicine.

From a wider perspective on the use of QDs, although they are becoming more and more common in research labs, the time in which they will be used for *in-vivo* applications, is still far away. The main concern is about their toxicity. Toxicity and the interaction of QDs with the human body are not trivial questions to answer, and it is not just related to QDs, but in general to nanomaterials as for any chemical reagent or other material in use so far. However, although toxicity issues on the nanotechnology field for *in vivo* applications have to be addressed, the use of nanomaterials for *in vitro* applications is widely extended. In regards with the use of QDs, their superior properties as optical (and electrochemical) labels, compared to those of organic dyes, are and will be further exploited for their use in

diagnostics, drug screening, and *in vitro* imaging. There are already works reporting the use of QDs in point-of-care sensors, such as paper-based sensors. This type of sensors is well known by the general public (i.e. pregnancy tests) and the use of QDs along with it will prove how stable and efficient they are, and will also improve the overall acceptance of nanotechnology-based products.

Annex I. Supporting information of Chapter 5

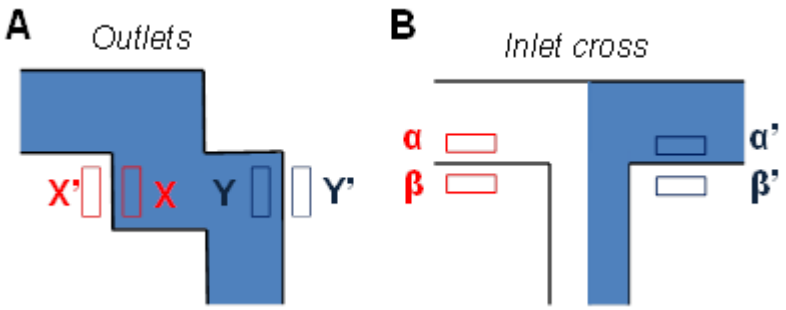

Figure S1. Quantification of relative concentrations in CGG chip. In order to evaluate the performance of the CGG chip, relative concentrations at the outlets were calculated. (A) Two regions of interest (ROIs) inside (X, X') and outside (Y, Y') the channel were selected in each outlet for quantification, and (B) In order to obtain normalized data, color intensity at the outlets was compared with two ROIs of inlet 1 (α, inside, and β, outside the channel) and two ROIs in inlet 2 (α', inside, and β', outside the channel).

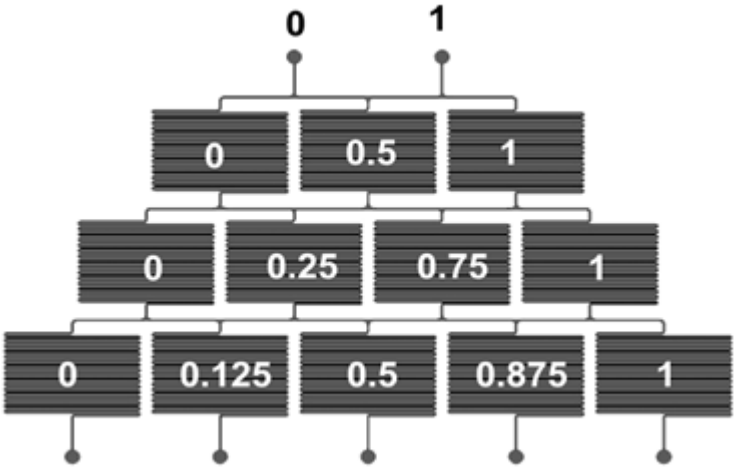

Figure S2. Calculation of theoretical concentrations in the CGG chip. According to the distribution of mixers in the CGG chip, considering 0 and 1 the values of relative concentrations at the inlets, the relative concentrations at the outlets will be: 0; 0.125; 0.5; 0.875 and 1.

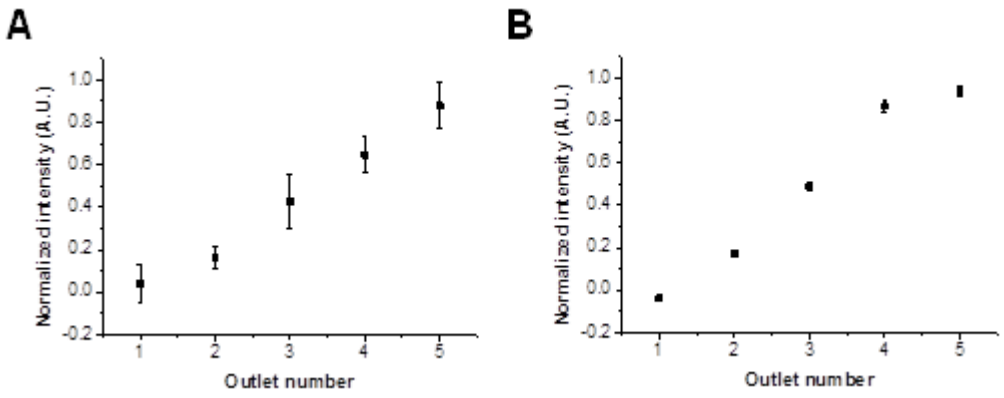

Figure S3. Reproducibility and repeatability studies in CGG chips. (A) Graphics corresponding to the assays performed in three different (CGG) chips. The values of the graphics represent the relative intensity obtained in each of the outlets and the error bars the standard deviation obtained by doing the evaluation three times, and (B) Reproducibility results for the (CGG) chip. The error bars correspond to the standard deviation obtained from the results of the evaluations done in three different chips.

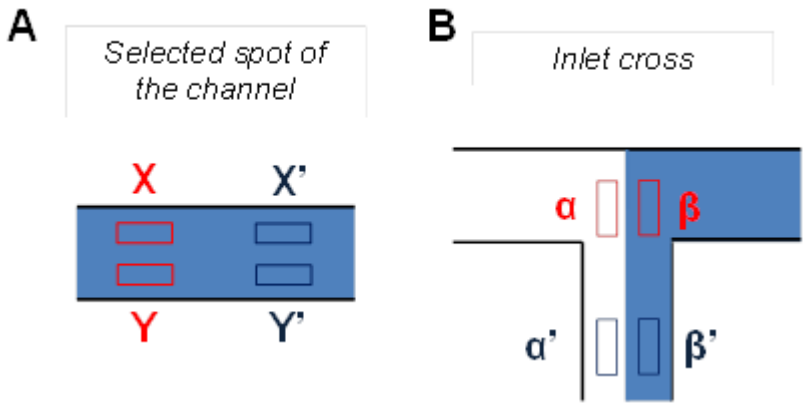

Figure S4. Fluorescence Intensity quantification of MIX chip. The mixing factor at each selected spot of the channel was calculated by measuring the mean fluorescence intensity of two ROIs selected in each side of the channel (A), the so-called I_{max} (mean: X, X') and I_{min} (mean: Y, Y') due to maximum and minimum fluorescence observed at the inlet cross, where solutions have not yet been mixed , and (B) I_{min} (mean α, α') and I_{max} (mean β, β') in the inlet cross were also calculated and further used in order to normalize the mixing factors obtained in each selected spot of the channel.

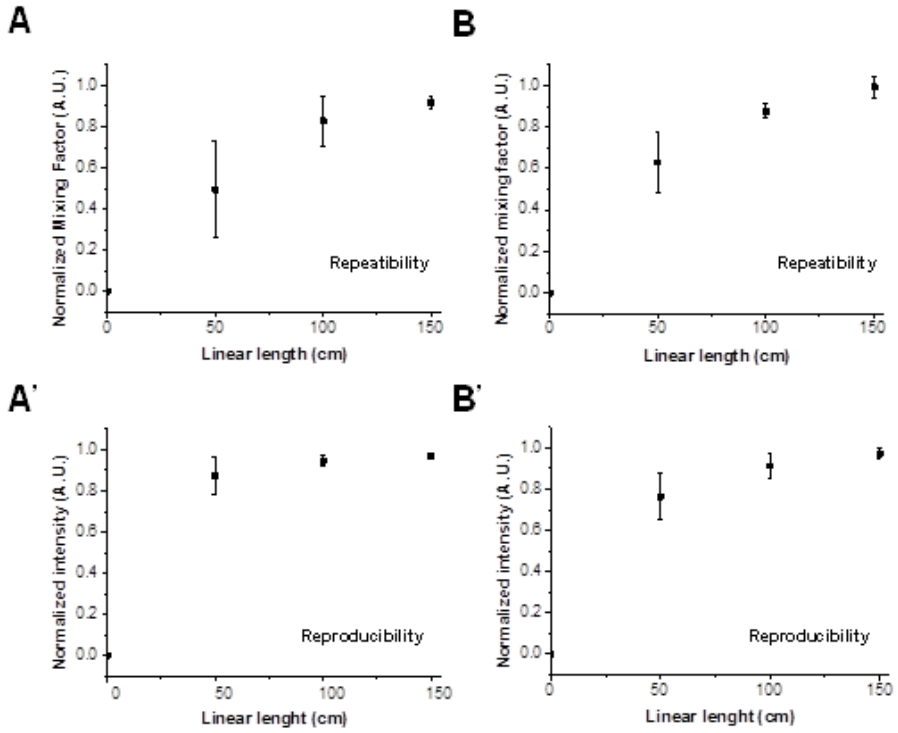

Figure S5. Reproducibility and repeatability in MIX chips. **(A)** Graphics corresponding to three different repeatability assays performed in three different MIX chips. The values of the graphic correspond to the normalized mixing factor obtained at different positions of the chip and the error bars to the standard deviation obtained by doing the evaluation three times, and **(B)** Reproducibility results for the (MIX) chip. The error bars correspond to the standard deviation obtained from the results of the evaluations done in three different chips.

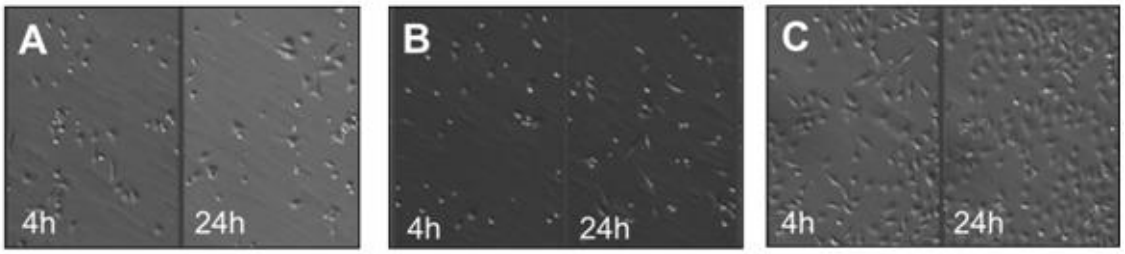

Figure S6. Comparison between sterilization methods. (A) Chips were filled in with 70 % ethanol, ethanol was removed and then chips exposed to UV light for 1h, (B) Chips were filled in with 70 % ethanol and exposed to UV light for 1h (no ethanol removal), and (C) Chips were filled in with 70 % ethanol until use (no UV light exposure).

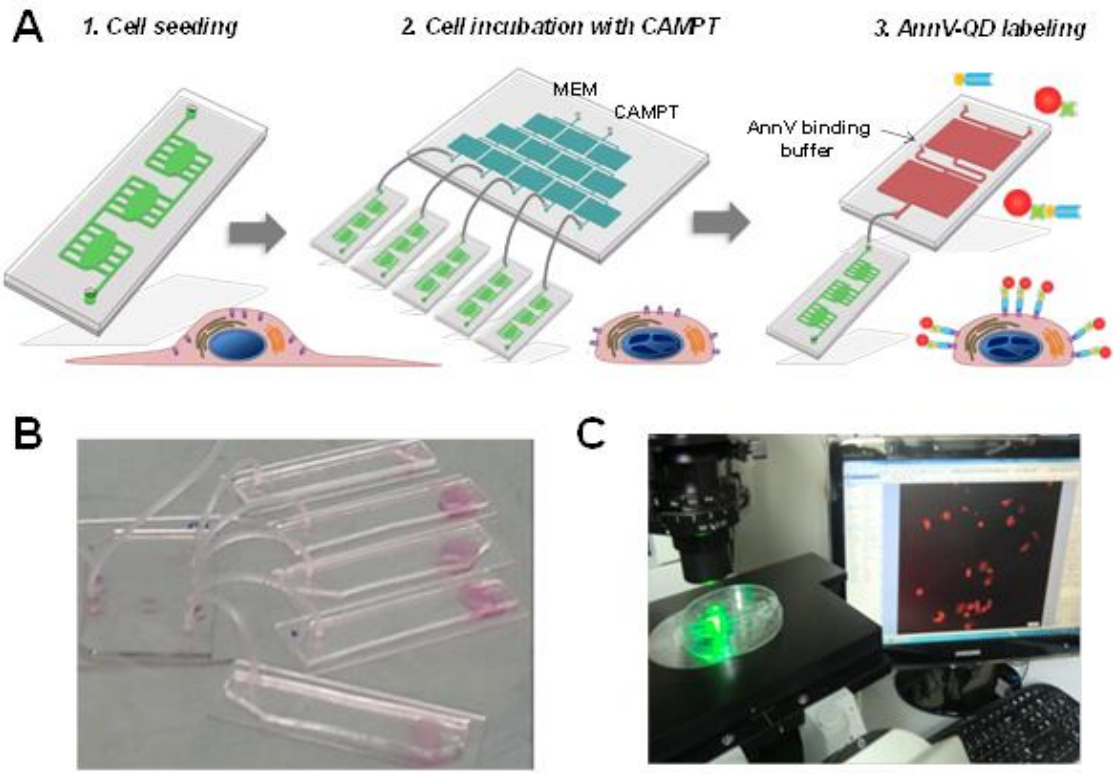

Figure S7. Sequential steps of the full assay. **(A)** Schematic representing what happens in each step of the assay. First, cells are seeded and adhered in the inner chambers of the CELL chips. Second, cells are incubated with different concentrations of CAMPT to induce the translocation of PS in the outer plasma membrane of apoptotic cells. Third, cells are incubated with AnnV-QD to label apoptotic cells, **(B)** Picture showing details of the connection between the CGG chip and CELL chips, and **(C).** Picture showing the fluorescence microscope image captions of the AnnV-QD labeled cells.

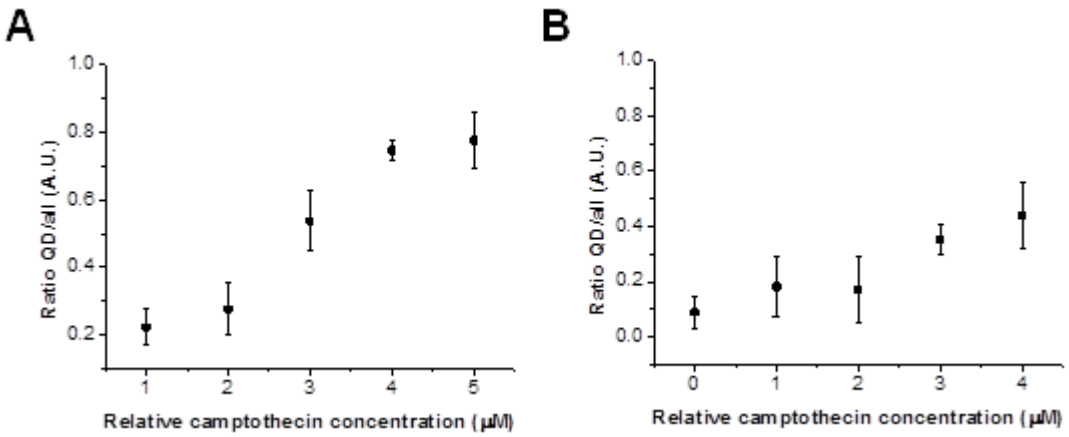

Figure S8. Full assay comparison carried out in different days. Full assays of cell apoptosis monitoring were carried out several times in order to evaluate the variability of the experiment. Incubations of 4h with CAMPT were carried out and the ratio of apoptotic cells (QD-labeled cells) from the total number of cells was established. Graphs obtained from data of a first assay **(A)** and a second assay, and **(B)** show the same trend although the number of apoptotic cells varies from one day to another. The error bars correspond to the standard deviations.

Annex II. Supporting information of Chapter 6

A. Image of the channel where APTES deposited at a concentration of 20% is removed after 3 minutes of continous flow of 2.5 µl/min. QDs were able to immobilize but after the first washing step the APTES film was scratched due to the flow and removed from the glass surface.

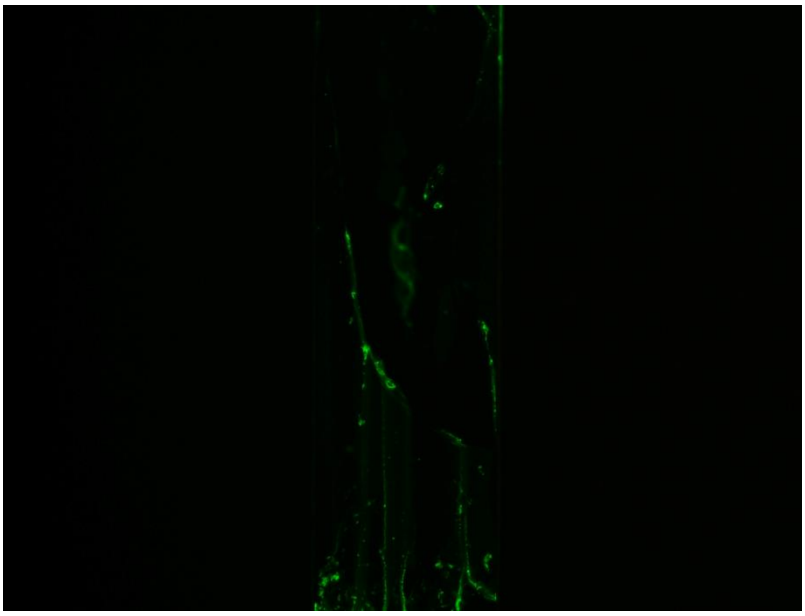

B. Fluorescence intensities from images acquired at different timepoints during hybridization were quantified for different chips. Normalized mean values for each image were displayed in graphs showing the trend of a typical binding curve and with minimal variation between experiments carried out in different platforms (depicted in the graph as error bars).

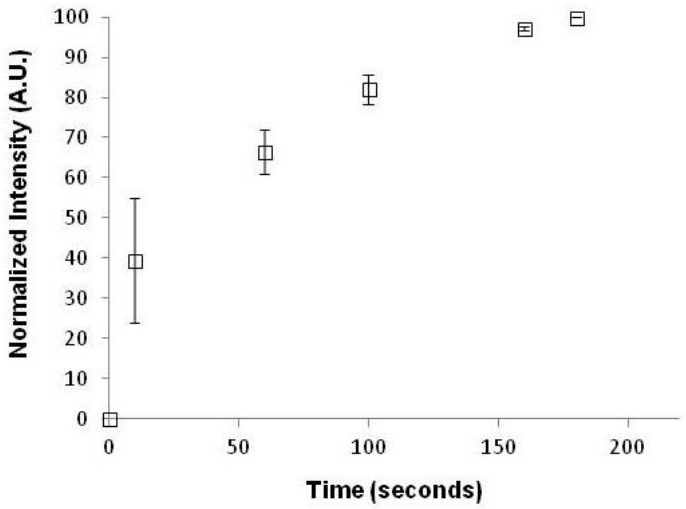

Annex III. Publications related with this thesis

Journal of Nanobiotechnology

BioMed Central

Research

Open Access

QDs versus Alexa: reality of promising tools for immunocytochemistry

Helena Montón[1], Carme Nogués[2], Emma Rossinyol[1], Onofre Castell[1] and Mònica Roldán*[1]

Address: [1]Servei de Microscòpia, Universitat Autònoma de Barcelona, Bellaterra Campus, 08193 Bellaterra, Barcelona, Spain and [2]Departament de Biologia Cellular, Fisiologia i Immunologia, Universitat Autònoma de Barcelona, Bellaterra Campus, 08193 Bellaterra, Barcelona, Spain

Email: Helena Montón - helena.monton@campus.uab.cat; Carme Nogués - carme.nogues@uab.cat; Emma Rossinyol - emma.rossinyol@uab.cat; Onofre Castell - onofre.castell@uab.cat; Mònica Roldán* - monica.roldan@uab.cat

* Corresponding author

Published: 27 May 2009

Journal of Nanobiotechnology 2009, **7**:4 doi:10.1186/1477-3155-7-4

Received: 5 March 2009
Accepted: 27 May 2009

This article is available from: http://www.jnanobiotechnology.com/content/7/1/4

Abstract

Background: The unique photonic properties of the recently developed fluorescent semiconductor nanocrystals (QDs) have made them a potential tool in biological research. However, QDs are not yet a part of routine laboratory techniques. Double and triple immunocytochemistries were performed in HeLa cell cultures with commercial CdSe QDs conjugated to antibodies. The optical characteristics, due to which QDs can be used as immunolabels, were evaluated in terms of emission spectra, photostability and specificity.

Results: QDs were used as secondary and tertiary antibodies to detect β-tubulin (microtubule network), GM130 (Golgi complex) and EEA1 (endosomal system). The data obtained were compared to homologous Alexa Fluor 594 organic dyes. It was found that QDs are excellent fluorochromes with higher intensity, narrower bandwidth values and higher photostability than Alexa dyes in an immunocytochemical process. In terms of specificity, QDs showed high specificity against GM130 and EEA1 primary antibodies, but poor specificity against β-tubulin. Alexa dyes showed good specificity for all the targets tested.

Conclusion: This study demonstrates the great potential of QDs, as they are shown to have superior properties to Alexa dyes. Although their specificity still needs to be improved in some cases, QDs conjugated to antibodies can be used instead of organic molecules in routine immunocytochemistry.

Background

Semiconductor nanocrystals called Quantum Dots (QDs) are fluorochromes with many advantages compared to the organic fluorescent dyes habitually used in immunocytochemistry procedures [1]. Their water solubility and capacity to be conjugated with different biomolecules have only recently been established [2]; therefore, their application in both the biological and medical research fields is still scarce.

Since the first microscope appeared up to the present day, different kinds of dyes (fluorescent proteins, small fluorescent molecules, etc.) have been used to detect or localize different biomolecules within an intracellular context.

In the last decade, when nanotechnology became relevant, QDs were introduced as a promising methodological tool due to their intrinsic brightness, high photostability, high molar extinction coefficient, narrow emission band, and excitability with several wavelengths [3]. These qualities opened the possibility to handle samples labeled with different colors, preventing fluorescent signal crossing-over, using a single laser line to excite different QDs at the same time [4].

QDs are aggregates of atoms -from hundreds to tens of thousands that behave as one- of semiconductor materials that produce a crystalline matrix (nanocrystal). Composition, size and shape of this matrix determine their physical characteristics. The properties of nanocrystals vary according to their size, which ranges generally from 1 to 10 nm in diameter [5]; whereas smaller QDs emit in shorter wavelengths, bigger QDs emit in longer wavelengths. The crystalline core of QDs is composed of cadmium selenide and covered with a zinc sulfide shell. Moreover, some QDs are coated with different kinds of polymers and molecules in order to make them water-soluble and to facilitate their conjugation to different biomolecules, providing a specific functionality [6-9].

QDs can be linked to many molecules, such as DNA, proteins and antibodies, and therefore they have a wide range of applications in the biosciences. To date, QDs have been used to localize proteins [10,11] and mRNA within the cell [12], to label cancer markers [13], to follow in vivo metastatic cells during extravasation [14] or to track embryonic stem cells in deep tissues [15].

The aim of this study was to use QDs as secondary and tertiary antibodies in a routine immunocytochemistry procedure in which organic dyes are currently used. Therefore, we characterized the shape, size and optical properties of QD 655 (IgG or streptavidin conjugated) in order to develop a standard protocol for protein immunodetection using QDs. We have made a comparative study of fluorescence intensity, bandwidth, photostability, specificity and the quality of QD 655 versus its homologous organic fluorophore, Alexa 594 (IgG or streptavidin conjugated), to evaluate the possibility of replacing Alexa with QDs in this protein detection procedure.

Results

QDs characterization by HRTEM

QD 655 showed a cone-like shape (Figure 1) with no differences in shape between QDs conjugated to streptavidin or to IgG. However, when comparing the size of the QDs conjugated to IgG with those conjugated to streptavidin, significant differences ($p < 0.05$) were found. QD 655-IgG is bigger ($15.4 \pm 0.2 \times 6.4 \pm 0.1$ nm) than QD 655-strep ($13.1 \pm 2.8 \times 6.3 \pm 0.9$ nm).

QDs characterization by CLSM

QDs have been reported to present several optical advantages in fluorescence detection regarding conventional organic fluorophores. QD 655 has been compared to Alexa 594 to evaluate differences in fluorescence intensity, bandwidth, photostability and specificity.

Spectra emission

First, the maximum fluorescence emission peak (λ_{em}) of both fluorophores was assessed using the lambdascan function of the CLSM. QD 655 presented its maximum at 651 nm, whereas Alexa 594 had its peak at 615 nm (Figure 2, Table 1). The λ_{em} value recorded was identical for the same fluorophore independently of its conjugation (IgG or strep).

Second, the fluorescence intensity (FI) level of QD 655 (Ig or Strep) and Alexa 594 (Ig or strep) was calculated. The FI level of QD 655 was higher than that of Alexa 594 (Table 1).

Differences in bandwidth, calculated from the emission profiles (Figure 2), were also found when both kinds of fluorophores were compared. QDs had narrower values of bandwidth than the homologous Alexas (Table 1).

Photostability

Photostability was assessed by exposing immunolabeled cultures for eight minutes at the maximum power laser line of 561 nm. For the first 90 seconds, the initial fluorescence intensity of β-tubulin labeled with QD 655s was reduced by about 5%. The same laser incidence produced an intensity reduction of 90% in cultures labeled with Alexa 594s. At the end of the irradiation period, no β-tubulin was detected in cultures labeled with Alexa 594s, whereas in cultures labeled with QD 655s, β-tubulin still kept up to 10%–40% of the initial fluorescence intensity (Figure 3 and 4).

Staining specificity

Staining specificity was analyzed on cell cultures labeled with primary antibody against the microtubule network (β-tubulin), Golgi complex (GM130) or endosomal system (EEA1). Brightness of both fluorophores conjugated to IgG was similar (Figure 5). Differences in specificity were detected when QD 655-IgG was used as a secondary antibody against β-tubulin. The network of microtubules was not well defined, with background and QD aggregates that had not selectively linked to β-tubulin. In contrast, Alexa 594-IgG was very specific and the microtubule network was definitely detectable. When QDs and Alexas were used as tertiary antibodies, the tubulin network was clearly detected by both fluorophores, but Alexa fluorochromes were more specific in pinpointing the tubulin filament structure. No differences in specificity were

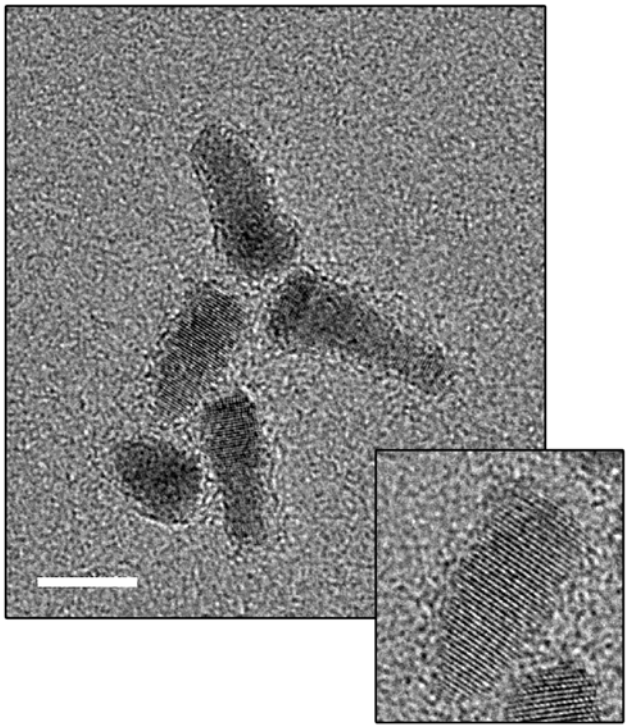

Figure 1
HRTEM QD characterization. The large image shows a general view of QD 655 dispersion. The small image shows a detail of a single QD 655 cone-like nanocrystal. Its crystalline structure core can be seen. Scale bar = 10 nm.

detected when QD 655 or Alexa 594 was used as a secondary or tertiary antibody against GM130 or EEA1. Both types of fluorophores showed similar specificity (Figure 6).

Discussion

In this work inorganic QDs were used to demonstrate their feasibility and advantages as a basic research technique in routine immunocytochemistry, as compared to Alexa organic dyes. To our knowledge, commercial QDs are not yet standardized; neither are they completely characterized to be used without further evaluation [16,17].

HRTEM characterization of QDs demonstrated differences in core size between the two types of QDs. In theory, these differences should be due to QD manufacturing, but the current methods used to produce QD allow particle size and particle size distribution to be controlled accurately [18]. Moreover, according to the Quantum Dot Corporation [2], there are only slight size differences in a given batch of QDs. However, other authors have found some variability in CdSe QDs size distribution [19].

One of the optical properties measured was the emission spectrum, which in QDs is related to their size. QD 655 conjugated to IgG or streptavidin displays a higher emission peak and a narrower bandwidth than its Alexa homologue. These advantageous characteristics have been well documented previously by different authors [4,13,20] and offer the possibility of using different QDs simultaneously without overlapping emission bands. The bandwidth of our batch of QD 655 (IgG and strep) was similar to that described in the literature [18,20].

Slight differences in size result in slight variations in the emission wavelength. As a consequence, the emission spectrum of a certain nanocrystal ensemble will be broader than an individual QD spectrum [21]. A variation in size distribution of 5% translates into a bandwidth of approximately 25–30 nm, a narrow value compared to the bandwidth of many fluorescent dyes [21]. Since the size distribution of each QD analyzed in this study was about 10%, it was expected that the bandwidth would be greater (ca. 35 nm).

Another optical characteristic analyzed was the intrinsic brightness of both fluorophores. The fluorescence intensity (FI) was higher in QDs than in Alexas. Most authors agree that QDs have superior brightness than organic fluorophores [1,13,20,22]. However, other studies have found that QDs are not as bright as expected [23]. Slight differences in FI (ca. 8%) were detected between both QDs, while in Alexas these differences were inappreciable. Other authors have found that the FI of QD 525-IgG was nearly one-third that of QD 525-streptavidin [24].

Photostability was the third optical property analyzed, and the entire scientific community agrees that this is the best advantage of QDs, as compared to other fluorescent dyes [3,5]. Our study confirms that QDs have the highest photostability. This characteristic is very important when in vivo analyses are carried out and long-term experiments are necessary and use multiple targets [25]. But photostability is also a determining factor in fixed samples in which some magnification is needed to find the best resolution to observe subcellular structures. Before QDs came out, Alexa dyes were considered to be the most photostable fluorophores [26]. Nowadays, this reality has changed: Alexa fluorophores lose almost all of their fluorescence in only 90 seconds of laser exposure, while we have demonstrated that QDs can be exposed to laser light for eight consecutive minutes and less than 40% of their initial fluorescence is lost.

All of these characteristics confirm that QDs have unique optical properties that make them powerful fluorescent dyes. In addition to the increasing interest in QDs in fluorescence techniques, their electron-dense core has poten-

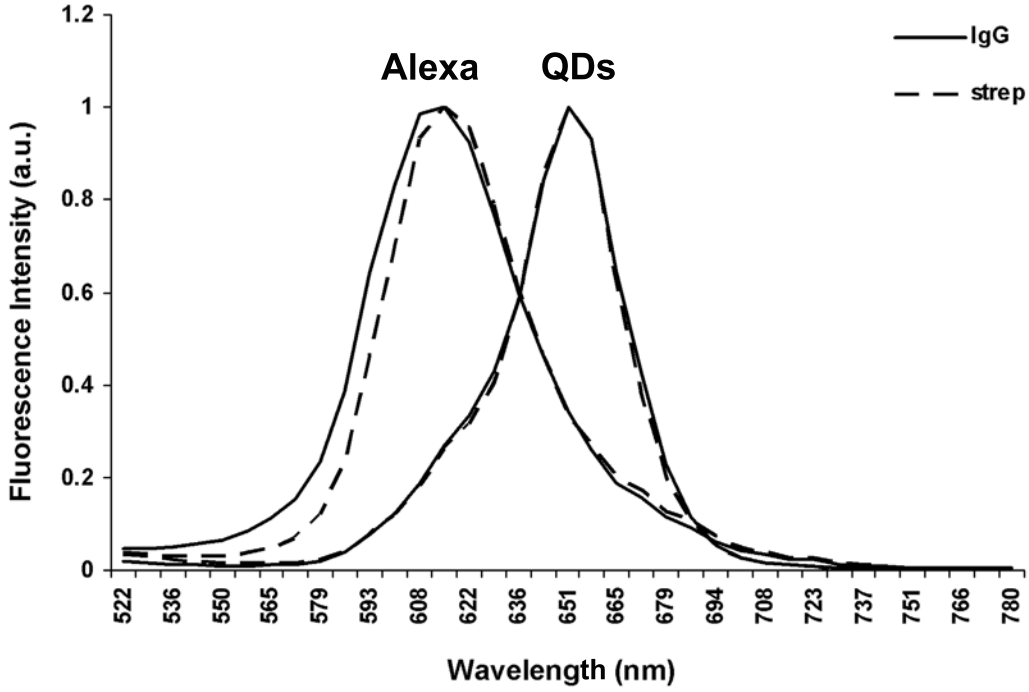

Figure 2
Fluorescence emission spectra. Spectral profile representing fluorescence intensity versus emission wavelength (500–780 nm) for QD 655-IgG, QD 655-Streptavidin and their Alexa homologues. Excitation wavelength = 488 nm.

tial to carry out correlated studies between CLSM and TEM, which would allow protein localization inside cells on a nanometric scale [11]. However, there is some controversy regarding the specificity of QDs as immunolabels. While some authors argue that QDs have comparable or even superior specificity in relation to organic fluorophores [27], others consider that QDs are appropriate fluorophores to be used as immunolabels, although without increasing sensitivity, and with higher, non-specific binding and aggregation than Alexa dyes [18,23]. Low specificity could be due to different reasons: i) a non-optimal concentration of QDs that could lead to a non-specific signal [1], or ii) a non-optimal surface chemistry of QDs that would affect their spectroscopic properties and colloidal stability as well as their biomolecular function or size, which could sterically hamper access to cellular targets [20]. Several authors have pointed out the importance of QD concentration for improving the sensitivity of detecting water pathogens [22], as well as improving specific immunostaining [1]. Before starting the QD characterization, we tested three different concentrations of QD 655 in order to use the most appropriate in which to perform this study (data not shown). The optimal concentration was 30 nM because there were scarce aggregates and the QD concentration was high enough to label the tubulin network.

Table 1: Spectral properties.

	Emission peak (nm)	FI[a]	Bandwidth (nm)[b]
Q655-IgG	651	200	35.5
Q655-strep	651	180	37
A594-IgG	615	75	48
A594-strep	615	75	53

Emission peak, fluorescence intensity (FI) and bandwidth for QD 655 and Alexa 594 analyzed at 488 nm excitation wavelength.
(a) Values in gray level (0–255).
(b) Calculated as the full width at 50% maximum of the emission spectrum (FWHM) in the FI profile.

On the other hand, specificity was higher when QDs were used as a tertiary antibody, but still lower compared to their Alexa homologue. Other authors have reported that QD sensibility is improved when they are used as tertiary antibodies [24]; this increase in sensibility is probably due to the high affinity between streptavidin and biotin, and to the signal amplification.

Finally, the specificity of QDs in detecting β-tubulin, GM130 and EEA1 proteins was tested. While specificity

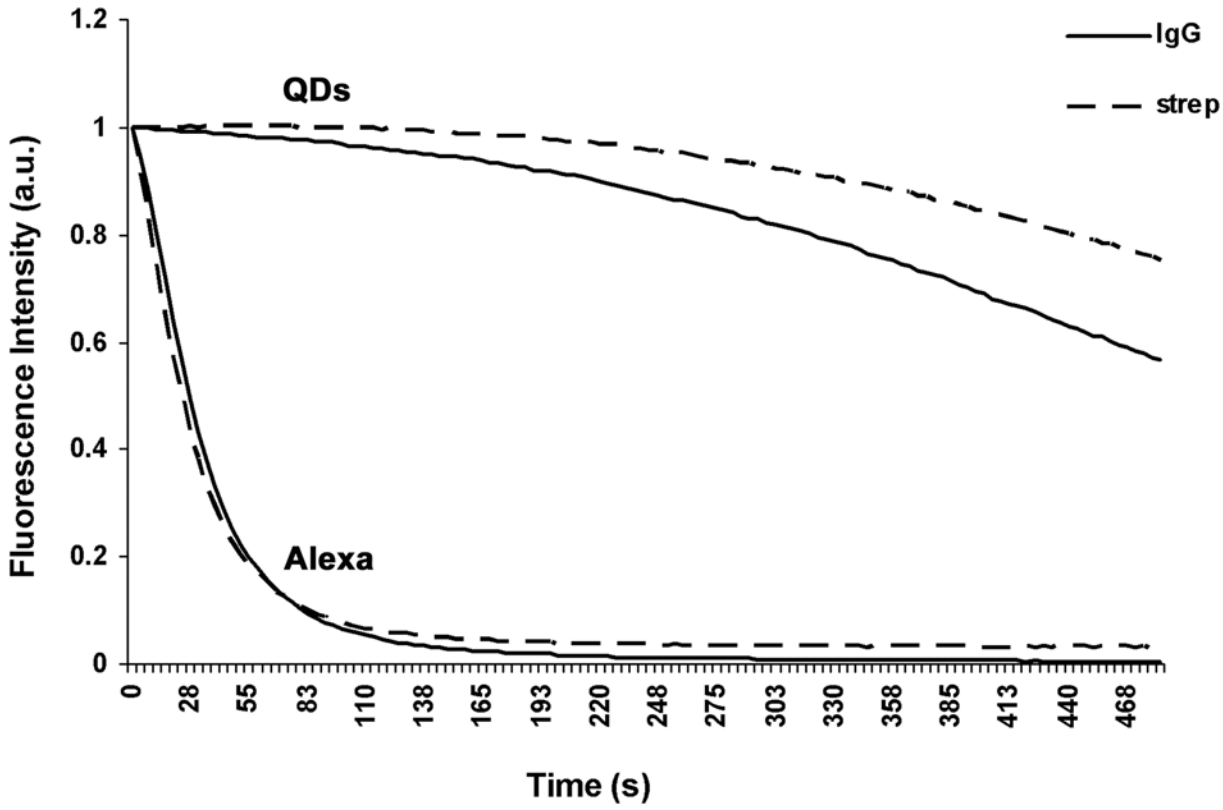

Figure 3
Photostability profile. Fluorescence intensity changes of QDs and Alexas during the irradiation period with the 561 nm laser line at maximum power.

against β-tubulin was lower than Alexa, no differences were observed when QDs were used to stain the Golgi complex (GM130 protein) or endosomes (EEA1). Specificity of QDs was higher for primary antibodies against proteins like GM130 and EEA1, which are scarce in the cell and are not involved in the composition of thin structures. Specificity was lower for proteins such as β-tubulin which is an abundant protein in the cell and that polymerizes producing an extremely well organized thin structure. QD 655 is one of the largest QDs commercialized, and it is possible that its size could sterically obstruct its access to its target [20].

Conclusion

QDs are excellent fluorophores for labeling cellular targets, as they display higher intensity, an enhanced signal to noise ratio, a narrower bandwidth and higher photostability than organic dyes. However, the specificity of QDs depends on the target they have to bind to. More studies are needed to improve the specificity of QDs so they can be used routinely, alone or in combination with organic fluorescent dyes, in all biological applications. In this study we were able to use QDs as secondary and tertiary antibodies to clearly detect discrete localized proteins. Therefore, in these cases, they can replace fluorescent organic molecules in routine immunocytochemistry procedures.

In the future, when better control of the synthesis and functionalization of QDs is possible, the range of biological applications of these fluorophores can be extended and they can become part of basic research techniques.

Materials and methods

Material

Two types of red emission spectra QDs were used as secondary and tertiary antibodies: QD 655 Goat $F(ab)_2$ anti-mouse IgG conjugate (QD 655-IgG) and QD 655 strepta-

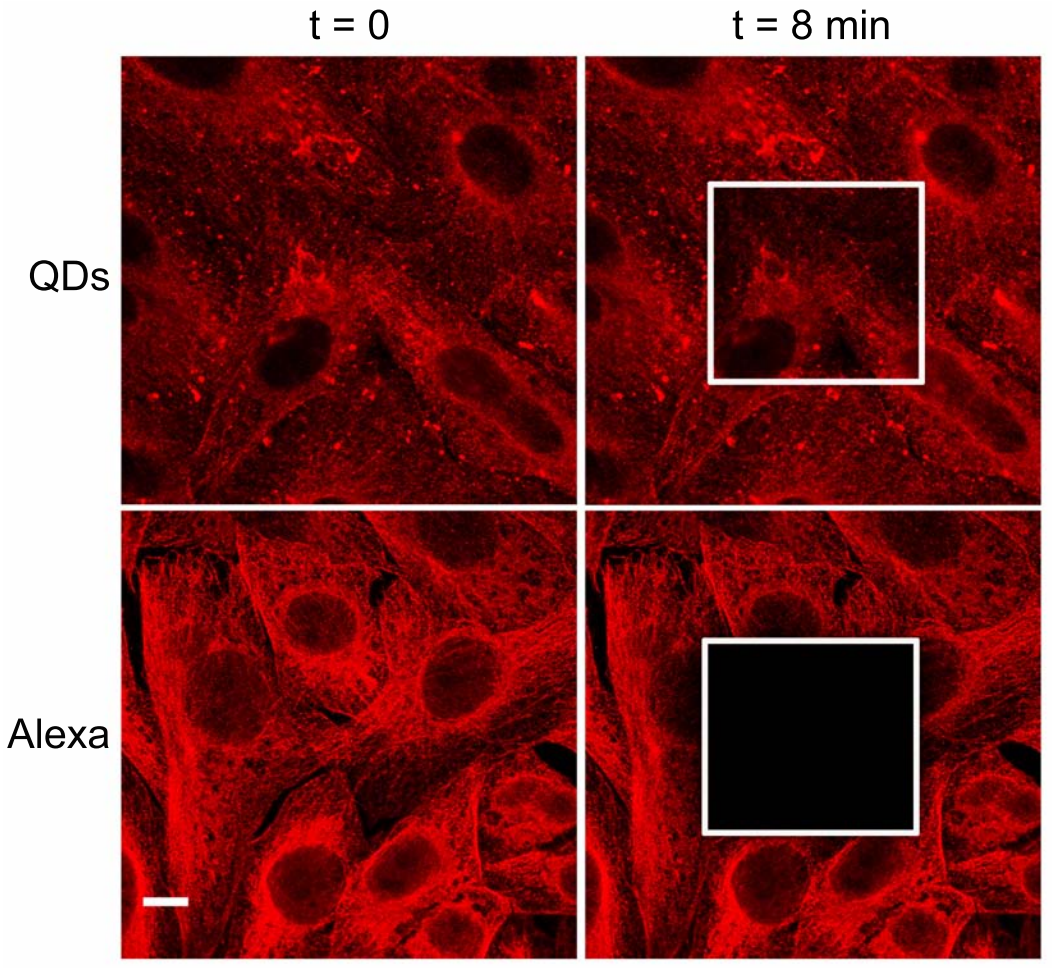

Figure 4
CLSM photostability images. Left-hand images correspond to the emission signal of QDs and Alexas conjugated to streptavidin before the irradiation period (t = 0 min) with the 561 nm laser line at its maximum power. Right-hand images show the emission signal of QDs and Alexas at the end of the irradiation period (t = 8 min). Note the loss of fluorescence intensity in the delimited area. Scale bar = 10 μm.

vidin conjugate (QD 655-strep). Two homologous red emission Alexa Fluor Dyes: Alexa 594 Goat F(ab)$_2$ anti-mouse IgG conjugate (Alexa 594-IgG) and Alexa 594 streptavidin conjugate (Alexa 594-strep) were used to compare to QD antibodies. Secondary antibodies QD 655-IgG and Alexa 594-IgG were purchased from Molecular Probes (Invitrogen Corp; Eugene, Oregon, USA), and Anti-Ms IgG biotin from Boheringer (Mannheim; Indianapolis, USA). Primary antibody monoclonal anti-β-tubulin was purchased from Sigma-Aldrich Chemie GmbH (Steinheim, Germany). GM130 and EEA1 primary antibodies were purchased from BD Biosciences (San Jose, California, USA).

High Resolution Transmission Electron Microscopy (HRTEM)

To carry out a HRTEM analysis, 0.5 μl of each QD was diluted in 500 μl of MilliQ water and centrifuged for 10 minutes at 6000 rpm to eliminate all organic precipitates. A drop of each diluted QD was deposited on a carbon layer copper grid and air-dried.

Images of each type of QD were obtained with a HRTEM, using a JEOL JEM 2011 transmission electron microscope (Jeol LTD; Tokyo, Japan) operating at 200 kV. The sizes of the QDs were determined with Digital Micrograph software (Gatan Inc; Warrendale, Pennsylvania, USA) and data obtained were processed with statistics software Origin-8 (OriginLab Corporation; Northampton, Massachusetts, USA).

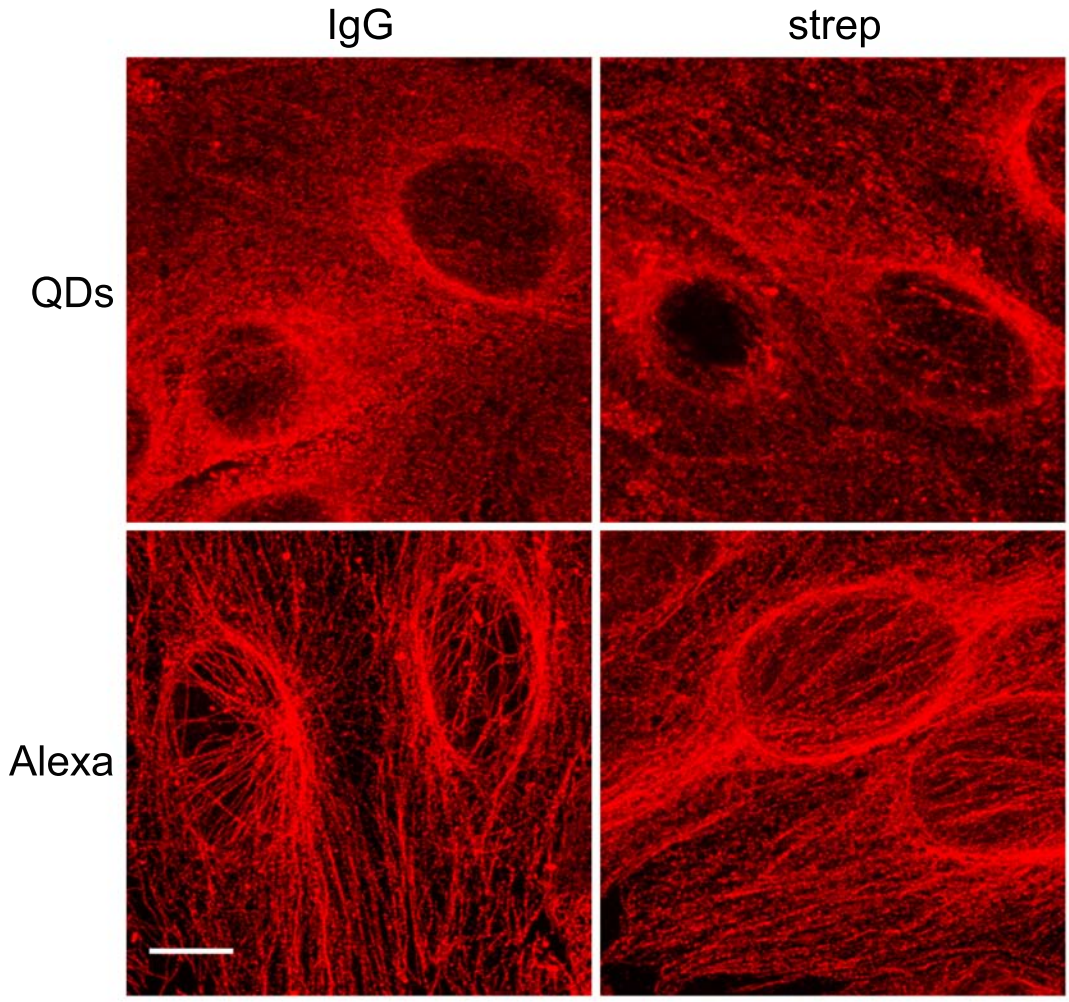

Figure 5
CLSM specificity analysis of β-tubulin labeling. Maximum intensity projections of the distribution of the tubulin network labeled with QDs (top images) show lower specificity than their organic Alexa homologue labeling (bottom images). Scale bar = 10 μm.

Cell cultures

Two different culture cell lines, Vero (ATCC-CCL-81) and HeLa (ATCC-CCL-2), were used. Cells were maintained in MEM (GIBCO, Rockville, Maryland, USA) supplemented with 10% Fetal Calf Serum (GIBCO) and incubated at 37°C and 5% CO_2 in a humidified atmosphere.

Immunocytochemistry

For immunocytochemistry analysis, cells were seeded onto glass coverslips and incubated at 37°C and 5% CO2, until confluence was reached. Cells were fixed in 4% paraformaldehyde (Electron Microscopy Sciences; Fort Washington, Pennsylvania, USA) in 0.01 M phosphate buffer saline (Sigma Aldrich Chemie GmbH; Steinheim, Germany) for 15 min, permeabilized in 0.25% Triton X-100 (Fluka Chemie AG; Buchs, Switzerland) for 15 min and blocked in 6% bovine serum albumin (Sigma Aldrich Chemie GmbH; Steinheim, Germany) for 40 min. Finally, cells were incubated with the anti-β-tubulin monoclonal antibody (4 μg/ml) to detect the microtubule network, with the GM130 antibody (10 μg/ml) to detect the Golgi complex or with the EEA1 antibody (2.5 μg/ml) to detect the endosomal system. In all cases the primary antibody was incubated for 1 h at 37°C.

To perform secondary immunodetection, anti-Ms IgG antibody conjugated to Alexa or QDs (4 μg/ml and 30 nM final concentration, respectively) was used. For tertiary immunodetection, cells were first incubated with Anti-Ms IgG Biotin (1 μg/ml) for 1 h at 37°C, and then with

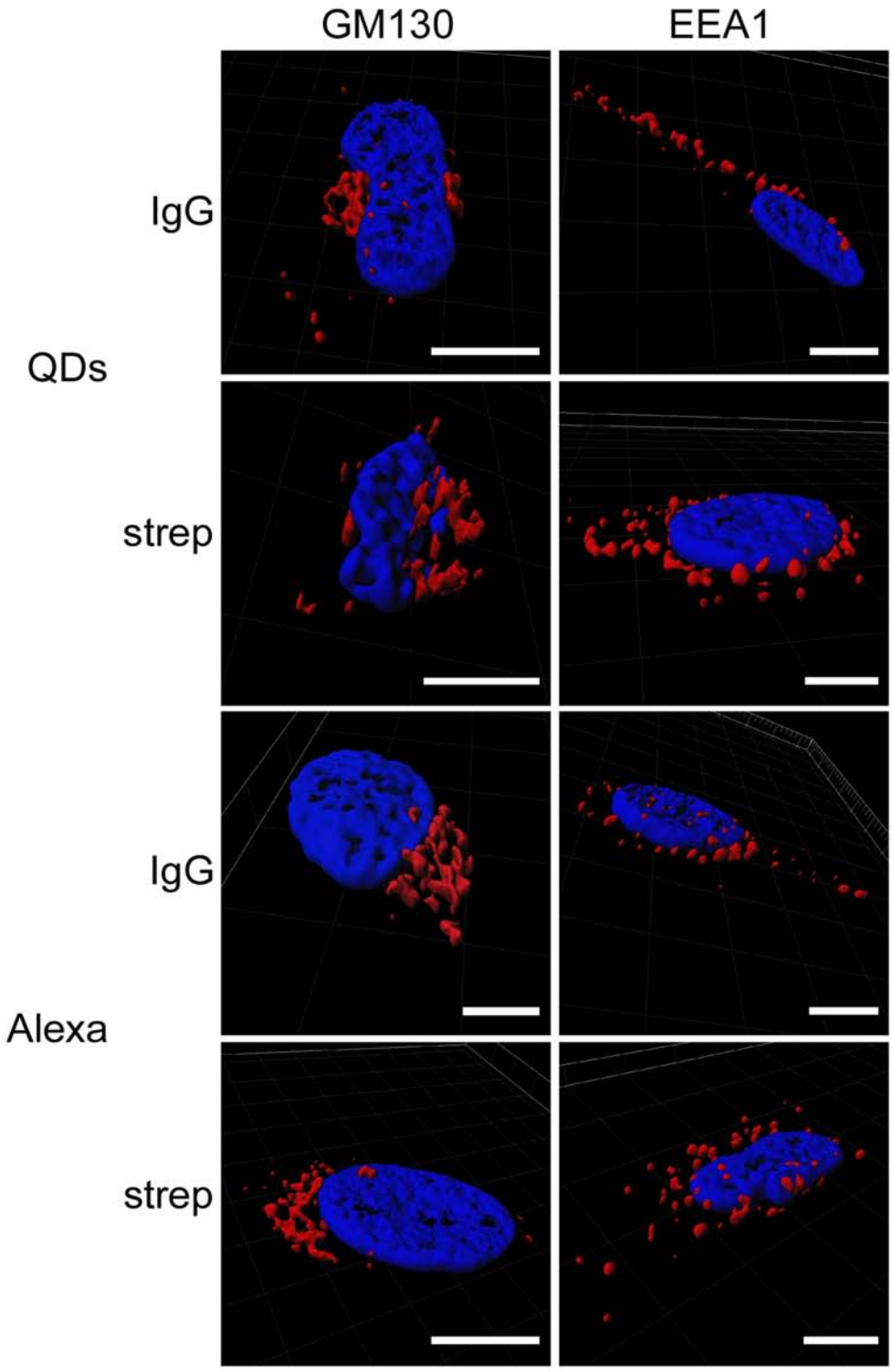

Figure 6
CLSM specificity analysis of GM130 and EEA1 labeling. Isosurface representation of the cell shows the nucleus (blue) labeled with Hoechst 33342, Golgi complex (GM130) and endosomal system (EEA1) (red) within a three-dimensional volumetric x-y-z data field. Scale bar = 10 μm.

streptavidin conjugated to Alexa or QDs (4 μg/ml and 30 nM final concentration, respectively). Coverslips were mounted onto glass slides using Fluoprep mounting media (bioMérieux® SA, Marcy l'Etoile, France) to preserve fluorescence.

Confocal Laser Scanning Microscopy (CLSM)

Images were captured with a CLSM Leica TCS-SP5 AOBS spectral (Leica Microsystems Heidelberg GmbH; Mannheim, Germany) using a Plan-Apochromatic 63× objective (NA 1.4, oil).

Series of images (xyλ), called lambdastacks, were taken to determine the spectra emission of QDs and Alexas and to establish their bandwidth. The excitation wavelength used was the 488 nm line of an Ar laser. The AOTF was set at 40% and 80% for QDs and Alexas, respectively.

The emission detection was set from 500 to 780 nm. The confocal pinhole for each lambdastack was fixed at 2 Airy units. For each xy focal plane, confocal microscopy measured the emission variation every 10 nm (lambda step size = 7 nm). The emission spectra analysis was processed using the CLSM software (Leica LAS AF). A Region of Interest (ROI) was delimited to determine the fluorescence intensity (FI) in the selected area in relation to the wavelength. To analyze immunolabeled cells, 45 ROIs of 2 μm^2 were selected near cell nuclei; FI and bandwidth were calculated in the selected ROIs.

Photostability experiments were performed using the Live Data Mode function of the CLSM, which permits monitoring long time-lapse experiments. Each type of fluorophore was illuminated with a 561 nm excitation laser line for 8 minutes (100% power, zoom = 6). Images were taken at 1 second intervals, in 512 × 512 pixels with 8 bits of dynamic range. In the area where the laser was at its maximum illumination power, 45 ROIs of 2 μm^2 were selected to show the FI in the region in relation to time.

Secondary or tertiary antibody specificity was evaluated using the xyz mode of the CLSM, which permits one to scan the xy plane along the z axis. Images were captured every 0.2 μm along 3 μm of thickness, with 1 Airy confocal pinhole. From the xyz series obtained by CLSM, maximum intensity projections were achieved with Leica LAS AF software, and three-dimensional models were generated using Imaris software (Bitplane; Zürich, Switzerland).

Statistical analysis

To determine if there were significant differences in size between QDs conjugated to IgG or to streptavidin, a two-sample T-Student's test (T-test) for comparison of means, with 95% confidence, was carried out. Previously, a F-Fisher test was performed and equal variances were assumed due to the returned p-value of 0.389. The equality of means hypothesis was rejected when the p-value was lower than 0.05 ($p < 0.05$).

Competing interests

The authors declare that they have no competing interests.

Authors' contributions

HM performed the majority of the experiments and wrote the manuscript with MR and CN. ER contributed with the characterization by HRTEM and helped with data analysis. MR, CN and OC designed the overall project, helped with interpretation of data and revised the manuscript. All authors read and approved the final manuscript.

Acknowledgements

The authors would like to extend special thanks to Núria Barba for her support in the laboratory, Maria Montón for her contributions to statistical calculations and Maria Dolors Baró for her general support. The English of this manuscript has been read and corrected by Mr. Chuck Simmons, a native, English-speaking University Instructor of English.

References

1. Ness JM, Akhtar RS, Latham CB, Roth KA: **Combined tyramide signal amplification and quantum dots for sensitive and photostable immunofluorescence detection.** *J Histochem Cytochem* 2003, **51:**981-987.
2. Watson A, Wu XY, Bruchez M: **Lighting up cells with quantum dots.** *Biotechniques.* 2003, **34(2):**296-300.
3. Alivisatos AP: **Semiconductor clusters, nanocrystals, and quantum dots.** *Science* 1996, **271:**933-937.
4. Chattopadhyay PK, Price DA, Harper TF, Betts MR, Yu J, Gostick E, Perfetto SP, Goepfert P, Koup RA, De Rosa SC, Bruchez MP, Roederer M: **Quantum dot semiconductor nanocrystals for immunophenotyping by polychromatic flow cytometry.** *Nat Med* 2006, **12:**972-977.
5. Murray CB, Kagan CR, Bawendi MG: **Synthesis and characterization of monodisperse nanocrystals and close-packed nanocrystal assemblies.** *Annu Rev Mater Sci* 2000, **30:**545-610.
6. Medintz IL, Uyeda HT, Goldman ER, Mattoussi H: **Quantum dot bioconjugates for imaging, labelling and sensing.** *Nat Mat* 2005, **4:**435-446.
7. Yu WW, Chang E, Drezek R, Colvin VL: **Water-soluble quantum dots for biomedical applications.** *Biochem Biophys Res Commun* 2006, **348:**781-786.
8. Jamieson T, Bakhshi R, Petrova D, Pocock R, Imani M, Seifalian AM: **Biological applications of quantum dots.** *Biomaterials* 2007, **28:**4717-4732.
9. Iga AM, Robertson JH, Winslet MC, Seifalian AM: **Clinical potential of quantum dots.** *J Biomed Biotechnol* 2007, **2007:**76087.
10. Nisman R, Dellaire G, Ren Y, Li R, Bazett-Jones DP: **Application of quantum dots as probes for correlative fluorescence, conventional, and energy-filtered transmission electron microscopy.** *J Histochem Cytochem* 2004, **52:**13-18.
11. Giepmans BNG, Deerinck TJ, Smarr BL, Jones YZ, Ellisman MH: **Correlated light and electron microscopic imaging of multiple endogenous proteins using Quantum dots.** *Nat Met* 2005, **2:**743-749.
12. Matsuno A, Itoh J, Takekoshi S, Nagashima T, Osamura RY: **Three-dimensional imaging of the intracellular localization of growth hormone and prolactin and their mRNA using nanocrystal (Quantum dot) and confocal laser scanning microscopy techniques.** *J Histochem Cytochem* 2005, **53:**833-838.
13. Wu XY, Liu HJ, Liu JQ, Haley KN, Treadway JA, Larson JP, Ge NF, Peale F, Bruchez MP: **Immunofluorescent labeling of cancer marker Her2 and other cellular targets with semiconductor quantum dots.** *Nat Biotechnol* 2003, **21:**41-46.

14. Voura EB, Jaiswal JK, Mattoussi H, Simon SM: **Tracking metastatic tumor cell extravasation with quantum dot nanocrystals and fluorescence emission-scanning microscopy.** *Nat Med* 2004, **10:**993-998.
15. Lin S, Xie XY, Patel MR, Yang YH, Li ZJ, Cao F, Gheysens O, Zhang Y, Gambhir SS, Rao JH, Wu JC: **Quantum dot imaging for embryonic stem cells.** *Bmc Biotechnol* 2007, **7:**67.
16. Tonti D, van Mourik F, Chergui M: **On the excitation wavelength dependence of the luminescence yield of colloidal CdSe quantum dots.** *Nano Lett* 2004, **4:**2483-2487.
17. Wu Y, Campos SK, Lopez GP, Ozbun MA, Sklar LA, Buranda T: **The development of quantum dot calibration beads and quantitative multicolor bioassays in flow cytometry and microscopy.** *Anal Biochem* 2007, **364:**180-192.
18. Bailey RE, Smith AM, Nie SM: **Quantum dots in biology and medicine.** *Physica E* 2004, **25:**1-12.
19. Li LS, Hu JT, Yang WD, Alivisatos AP: **Band gap variation of size- and shape-controlled colloidal CdSe quantum rods.** *Nano Lett* 2001, **1:**349-351.
20. Resch-Genger U, Grabolle M, Cavaliere-Jaricot S, Nitschke R, Nann T: **Quantum dots versus organic dyes as fluorescent labels.** *Nat Met* 2008, **5:**763-775.
21. Jorge PAS, Martins MA, Trindade T, Santos JL, Farahi F: **Optical fiber sensing using quantum dots.** *Sensors* 2007, **7:**3489-3534.
22. Lee LY, Ong SL, Hu JY, Ng WJ, Feng YY, Tan XL, Wong SW: **Use of semiconductor quantum dots for photostable immunofluorescence Labeling of Cryptosporidium parvum.** *Appl Environ Microbiol* 2004, **70:**5732-5736.
23. Ferrari BC, Bergquist PL: **Quantum dots as alternatives to organic fluorophores for Cryptosporidium detection using conventional flow cytometry and specific monoclonal antibodies: Lessons learned.** *Cytom Part a* 2007, **71A:**265-271.
24. Fountaine TJ, Wincovitch SM, Geho DH, Garfield SH, Pittaluga S: **Multispectral imaging of clinically relevant cellular targets in tonsil and lymphoid tissue using semiconductor quantum dots.** *Mod Pathol* 2006, **19:**1181-1191.
25. Fu AH, Gu WW, Larabell C, Alivisatos AP: **Semiconductor nanocrystals for biological imaging.** *Curr Opin Neurobiol* 2005, **15:**568-575.
26. Panchuk-Voloshina N, Haugland RP, Bishop-Stewart J, Bhalgat MK, Millard PJ, Mao F, Leung WY, Haugland RP: **Alexa dyes, a series of new fluorescent dyes that yield exceptionally bright, photostable conjugates.** *J Histochem Cytochem* 1999, **47:**1179-1188.
27. Hahn MA, Tabb JS, Krauss TD: **Detection of single bacterial pathogens with semiconductor quantum dots.** *Anal Chem* 2005, **77:**4861-4869.

Nanoscale

PAPER

Cite this: *Nanoscale*, 2015, **7**, 4097

Annexin-V/quantum dot probes for multimodal apoptosis monitoring in living cells: improving bioanalysis using electrochemistry†

Helena Montón,[a,b] Claudio Parolo,[b] Antonio Aranda-Ramos,[a] Arben Merkoçi*[b,c] and Carme Nogués*[a]

There is a great demand to develop novel techniques that allow useful and complete monitoring of apoptosis, which is a key factor of several diseases and a target for drug development. Here, we present the use of a novel dual electrochemical/optical label for the detection and study of apoptosis. We combined the specificity of Annexin-V for phosphatidylserine, a phospholipid expressed in the outer membrane of apoptotic cells, with the optical and electrochemical properties of quantum dots to create a more efficient label. Using this conjugate we addressed three important issues: (i) we made the labeling of apoptotic cells faster (30 min) and easier; (ii) we fully characterized the samples by common cell biological techniques (confocal laser scanning microscopy, scanning electron microscopy and flow cytometry); and (iii) we developed a fast, cheap and quantitative electrochemical detection method for apoptotic cells with results in full agreement with those obtained by flow cytometry.

Received 5th December 2014,
Accepted 27th January 2015

DOI: 10.1039/c4nr07191c

www.rsc.org/nanoscale

1 Introduction

The development of new techniques to detect and study apoptosis is crucial to fully understand how its deregulation leads to disorders such as cancer,[1,2] neurodegenerative diseases[3] and myocardial infarction,[4] among others. Nowadays, most techniques used to detect apoptotic cells aim to label phosphatidylserine (PS), a negatively charged aminophospholipid, whose translocation from the inner to the outer plasma membrane is a distinctive hallmark of early stages of apoptosis.[5–8] Methods based on PS recognition are useful clinical tools for early diagnosis, evaluation of disease progression, and monitoring the therapy efficacy, besides providing excellent quantitative analysis in living cells and new potential targets for drug discovery.[9,10] To date, Annexin-V (AnnV), a phospholipid-binding protein with high affinity for PS,[11] has been widely used as an imaging tool to monitor the apoptosis progression when conjugated to a fluorescent dye.[12–15] Nevertheless, its applicability is restrained by the properties of common fluorescent dyes, which have limited photostability and a tendency to photobleach.[16,17]

Considering this framework, CdSe/ZnS quantum dots (QDs) are excellent tools to overcome the inconvenience caused by organic dyes;[18] in fact, they exhibit size-dependent tunable narrow fluorescence emission spectra, a high-resistance threshold to chemical and photodegradation, high extinction coefficient and high quantum yield.[19,20] They are already widely used in fluorescence based technologies[21,22] such as fluorescence microscopy and confocal laser scanning microscopy (CLSM),[23–26] flow cytometry,[27] spectroscopy[28,29] and microarrays.[30–32] Another unique characteristic of QDs, over dyes and enzymes, is that their high electron density allows for their use also as electron microscopy labels. Although fluorescence-based and electron microscopy methods provide accurate detection of apoptosis, most of them are time-consuming, troublesome, expensive and require qualified staff to analyze the results. A complementary and quantitative electrochemical detection of apoptosis would overcome these drawbacks. Several studies have reported the use of voltammetry to detect QDs as electrochemical labels, taking advantage of their redox properties.[33–36]

Herein, we describe the use of AnnV–QD conjugates as dual optical/electrochemical labels for complete monitoring of apoptosis in living leukemia-derived THP-1 cells (Fig. 1). Using this label, we were able to: (i) make the labeling process easier and faster (30 min) than most commercially available kits,

[a]*Departament de Biologia Cel·lular, Fisiologia i Immunologia, Universitat Autònoma de Barcelona, Campus UAB-Facultat de Biociències, 08193 Bellaterra, Barcelona, Spain. E-mail: carme.nogues@uab.cat*

[b]*Nanobioelectronics & Biosensors Group, Institut Català de Nanociència i Nanotecnologia ICN2, Campus UAB, 08193 Bellaterra, Barcelona, Spain. E-mail: arben.merkoci@icn.cat*

[c]*ICREA - Institució Catalana de Recerca i Estudis Avançats, 08010 Barcelona, Spain*

†Electronic supplementary information (ESI) available: Optical microscopy images of apoptotic induced cell cultures at different times and negative control of flow cytometry. See DOI: 10.1039/c4nr07191c

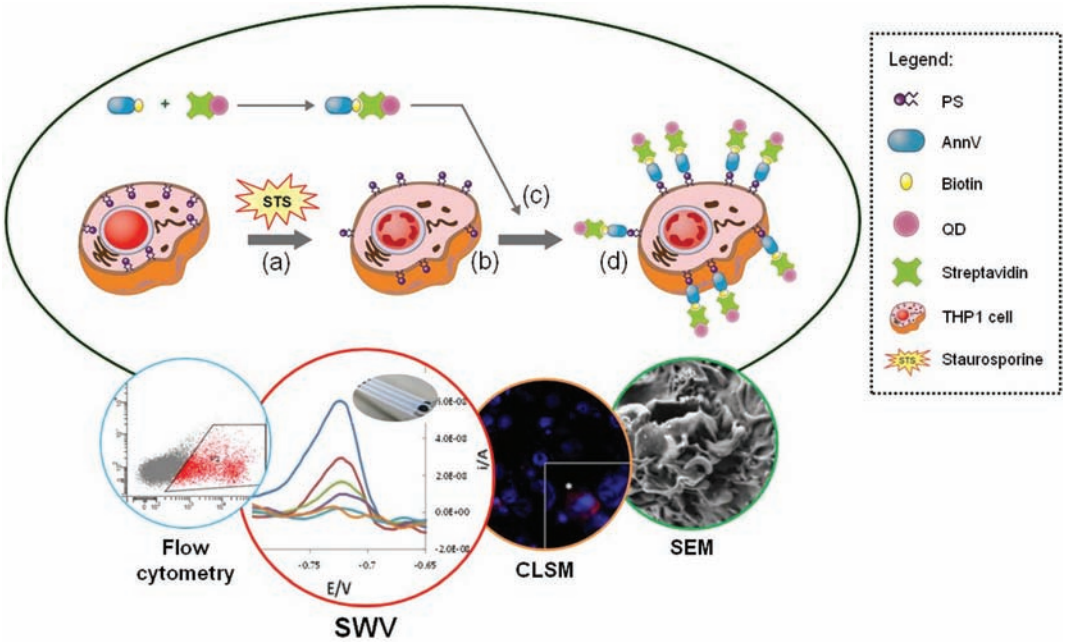

Fig. 1 Use of Annexin-V/quantum dot probes for optical and electrochemical detection of apoptotic cells. THP-1 cell cultures are incubated with staurosporine (STS) (a), a pro-apoptotic drug, and as a consequence phosphatidylserine (PS) is externalized (b). AnnV–QD conjugates previously prepared are added to the cell cultures (c) and bound to PS expressed in the outer membrane of apoptosis induced THP-1 cells (d). Due to the properties of QDs (they are fluorescent, electroactive and electron dense) diverse analyses can be performed.

(ii) study the same sample with classical cell biology techniques (CLSM, scanning electron microscopy (SEM) and flow cytometry) obtaining a deep overview of the cell status, and (iii) develop a cheap, easy-to-use, fast and quantitative electrochemical technique, with results in full agreement with those obtained by flow cytometry.

2. Experimental

2.1 Reagents and instruments

RPMI-1640 (Gibco), foetal bovine serum (FBS) (Gibco) and L-glutamine (Gibco), for cell cultures, and Qdot® 655 Streptavidin Conjugates (Invitrogen), dimer EthD (Invitrogen) and Hoechst 33342 (Invitrogen), for labeling the cells, were purchased from Life Technologies S.A. (Spain). T-25 and T-75 flasks (Nunc) were purchased from Thermo Scientific and a hemocytometer with a Bürker grid was purchased from Brand Gmbh + Co KG (Germany). A HERAcell 150 incubator (Heraeus, Spain) and an Eppendorf Centrifuge 5804 R (Eppendorf Ibérica S.L. Spain) were used for cell culture maintenance and in some steps of the experimental procedure.

Staurosporine (STS) and dimethyl sulfoxide (DMSO) for the apoptosis induction step were purchased from Sigma (Spain) and Annexin-V biotin (Biovision Inc.) was purchased from Deltaclon S.L. (Spain). The sample shaker used for preparation of the conjugate was a TS-100 Thermo shaker (Spain).

Reagents for PBS and Annexin-V binding buffer preparation were purchased from Sigma, Aldrich or Fluka. All the solutions were prepared using mQ water, produced using a Milli-Q system (>18.2 MΩ cm^{-1}) purchased from Millipore (Sweden).

2.2 Cell culture and induction of apoptosis

The human monocytic THP-1 cell line (ATCC® TIB-202TM) was maintained at a density of 5–8 × 10^5 cells mL^{-1} in 75 cm^2 flasks in RPMI-1640 medium supplemented with 2 mM L-glutamine and 10% FBS under standard conditions (5% CO_2 at 37 °C).

For apoptosis induction, 2 mL of cell suspension at a concentration of 5 × 10^5 cells mL^{-1} were transferred to 25 cm^2 flasks where 3 μL of 0.5 mg mL^{-1} of STS diluted in DMSO were added (induced cultures). An equivalent volume of DMSO was added into the control flasks (control cultures). Cultures were kept under standard conditions for 6 h. Two washing cycles with PBS were performed in order to remove any presence of STS in the cell cultures transferring cell suspensions to centrifuge tubes and spinning at 300*g* for 5 min. The final pellets were resuspended in 200 μL PBS.

During incubation with STS, THP-1 cell cultures were checked using an inverted microscope with a phase-contrast objective. We took images of the control and apoptosis-induced cell cultures in order to observe changes occurring in the cells due to the effect of STS such as cell shrinkage and membrane blebbing (Fig. SI 1†).

2.3 Annexin-V–QD conjugate preparation

AnnV–QD conjugates were prepared according to the manufacturer's protocol. Briefly, 3 μL of 2 μM streptavidin–QD solution

were incubated with 187 μL of QD conjugation buffer and 10 μL of biotinylated Annexin-V for 45 min in a thermo-shaker at 500 rpm at 25 °C and stored at 4 °C until use.

2.4 Simple labelling protocol for apoptosis

A simple labeling procedure was carried out by the addition of 200 μL of AnnV–QD conjugate and 200 μL of Ca^{2+} containing binding buffer to the cell suspensions (prepared in 200 μL PBS). It was then incubated at room temperature (RT) in a rocker shaker for 30 min. Thereafter, in order to eliminate the unbound AnnV–QD conjugates two washing cycles with PBS were performed.

2.5 Confocal laser scanning microscopy

A 10 μL drop of the labeled cell suspension was placed in a bottom glass petri dish for confocal imaging. Images were captured with a CLSM Leica TCS-SP5 AOBS spectral (Leica Microsystems Heidelberg GmbH; Mannheim, Germany) using Plan-Apochromatic 20× and 40× objectives (NA 0.9 and NA 1.2, respectively).

Simultaneous excitation of the PS-expressing cells (labeled with AnnV–QD) and their nuclei (Hoechst staining) was performed using a 405 nm blue laser diode and simultaneous detection was done using two different photomultipliers (PMTs), one per each corresponding spectral range. CLSM software (Leica LAS AF) was used to obtain the overlapped images of nuclei and AnnV–QD labeling. Stacks of *XY* images at different *Z* planes were processed using ImageJ (NIH, Maryland, USA) and Imaris 3D rendering software (Bitplane AG, Switzerland). In order to perform semiquantitative analyses, fluorescence intensity data from the images were obtained using ImageJ extracting the sum of intensities of all pixels for the nuclei (FIN) and the QD (FIQD) labeling, separately for each given image. Average intensities of 3 pairs of images, from different areas, were calculated and the average ratio FIQD/FIN was used to quantify cell death.

Further projections and 3-D views of apoptotic cells were performed using Imaris software.

2.6 Sample preparation for SEM analysis

Labeled-cell suspensions were washed with 0.1 M cacodylate buffer for 1 min and then fixed with 2.5% glutaraldehyde in 0.1 M cacodylate buffer, for 1 h at RT. Cells were incubated again with 0.1 M cacodylate buffer for 1 min and then dehydrated sequentially in increasing concentrations of cold ethanol (50, 70, and 90% for 8 min each). To complete the dehydration process samples were incubated two times in 100% ethanol (8 min each, 25 °C) and finally resuspended in hexamethyldisilazane solution (Sigma-Aldrich) for 15 min at RT. A 50 μL of each sample was placed on separate glass coverslips and let dry for 15 min at RT. SEM samples were kept in a desiccator at 25 °C until analysis.

The volume of all reagents used in the sample preparation was 1 mL and after each of the above-mentioned step cells were recovered by centrifugation (300*g*, 5 min).

Prior to SEM analysis (Magellan®FE-SEM, FEI), glass coverslips were placed over a typical SEM sample holder and the edges of the coverslips were painted with silver ink in order to increase their conductivity and facilitate the analysis of the samples.

This protocol avoids the use of metallization steps keeping intact the cellular structure and allows a direct visualization of small metallic nanoparticles such as QDs on the cell surface.

2.7 Flow cytometry

AnnV–QD labeled cells (20 000 cells) were analyzed to quantify the number of apoptotic cells in both induced and control cultures using a FACSCanto II flow cytometer (BD Biosciences, Franklin Lakes, NJ) equipped with the BD Biosciences FACSDiva™ software.

2.8 Electrochemical detection of apoptotic cells

The electrochemical detection of apoptotic cells was done using mercury-modified screen printed electrodes (from ItalSens, acquired through PalmSens) by placing 30 μL of the AnnV–QD labeled cells onto the working electrode. Apoptotic cells were detected electrochemically through the presence of Cd ions (as defects at the Cd QD surface) contained in the QD structure by direct voltammetric detection. This methodology has been previously reported by our group[33] and applied now with some minimal modifications. Briefly, the Cd(II) contained in the QDs was reduced to Cd(0) applying a potential of −1.1 V for 5 min. After that, a square wave voltammetry (SWV) was performed by scanning the potential from −1.1 to −0.4 V (step potential 10 mV, modulation amplitude 30 mV, frequency 15 Hz) and measuring the current value (analytical signal) due to the oxidation of Cd(0) to Cd(II). The oxidation process generates a peak of current at −0.8 V which intensity is related to the quantity of QDs in contact with the working electrode surface. The electrochemical detection in the samples was directly performed in PBS at pH 7.4.

Different concentrations of cells ranging from 20 000 to 1250 were measured and three measures using three different electrodes (represented as error bars in the graphs) were performed per sample.

3. Results and discussion

3.1 Optimization of apoptosis induction and labelling with AnnV–QD probes

In this study, we used a human monocytic leukemia cell line, THP-1, as a target of Staurosporine (STS), a commonly used drug to induce apoptosis in cell-based assays.[37,38] Although several studies report the apoptotic effect of STS, concentrations and incubation times change depending on the cell line and specific assay requirements.[39,40] We observed that 5 μg mL^{-1} of STS for 6 hours provoke the expected effect in THP-1 cell cultures by exhibiting early apoptotic symptoms such as cell shrinkage or membrane blebbing (Fig. S-1 in the ESI†). We also optimized the labeling steps in order to make

the method faster and easier than the use of Annexin-V-biotin kits in conjunction with conventional streptavidin or avidin-dye reagents. In fact in these procedures, cells are first incubated with Annexin-V-biotin followed by a second incubation with a fluorescently labeled streptavidin; besides, after each incubation step several washing steps are necessary, making the overall labeling process at least longer than 1 h. In the proposed method the Annexin-V-biotin is pre-incubated with streptavidin–QDs and the resulting conjugates can be stored at 4 °C, protected from light, until use. In this way we minimized the number of steps, decreasing the overall assay time to 30 min.

3.2 *In vitro* CLSM monitoring of apoptosis in THP-1 cell cultures

In order to study the efficiency and specificity of AnnV–QD conjugates to detect apoptotic cells, we analyzed the sample using both CLSM and SEM. In particular, taking advantage of the fluorescence emission of QDs, we used CLSM to obtain qualitative information on the assay by comparing images of the control and apoptosis-induced samples (Fig. 2a). Images in Fig. 2a show the differences in the amount of AnnV–QD labeled-cells (in red) between the two samples. Nuclear staining (in blue; using Hoechst 33342 dye) confirms the apoptotic status of cells in the induced cultures, where DNA condensation and nuclear fragmentation are evident (inset box in Fig. 2a). We used ImageJ software to analyze three random areas in both samples (control and induced) to attain the integrated fluorescence intensity of nuclear (FIN) and QD (FIQD) staining. The histogram in Fig. 2b displays the FIQD/FIN ratio of control and induced samples, respectively 0.022 ± 0.001 and 0.06 ± 0.001 A.U. The higher ratio observed in the induced sample indicates a prevalence of apoptotic cells in the culture incubated with STS. Furthermore, by scanning the sample along the *Z* axis, we obtained information on the whole-cell labeling. A cross section of a selected stack of an apoptotic cell is shown in Fig. 2c. *XZ* and *YZ* plane projections show the relative localization of AnnV–QD labeling, which is restricted to the periphery of the cells, as expected, and also the fragmentation of the nucleus. Finally, this peripheral localization can also be seen in a surface-rendered 3-D reconstruction of an apoptotic cell, which gives a more complete volumetric view of the same labeling information (Fig. 2d).

3.3 SEM analysis of apoptotic THP-1 cells and AnnV–QD labeling at the plasma membrane

We performed SEM analysis to see in detail the external morphology of the cells, and to evaluate the presence or absence of QDs in the plasma membrane surface (CdSe/ZnS QDs can be visualized by SEM thanks to their electron dense

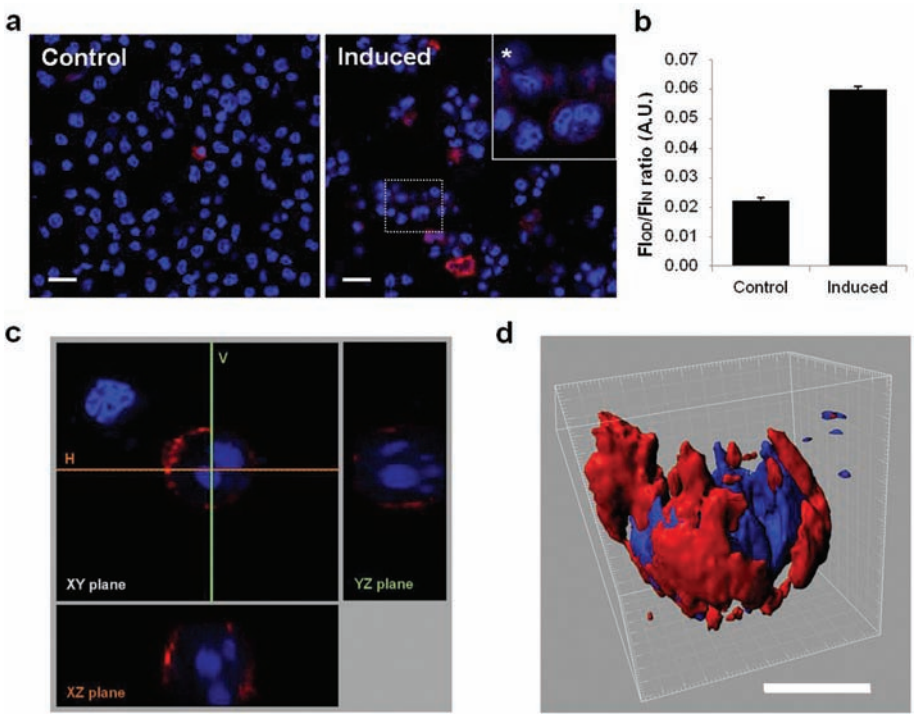

Fig. 2 CLSM analysis. (a) Images of THP-1 cells after AnnV–QD labeling (red) show few apoptotic cells in control cultures and many in induced ones. Nuclei were counterstained with Hoechst (blue). A zoom in a selected region (dashed line) is displayed in a box for more detail (*). Scale bar 20 μm. (b) Apoptosis in control and induced cultures was established from the images acquired. Fluorescence intensities of nuclei (FI_N, Hoechst stain) and of AnnV–QD (FI_{QD}, QDs) bound to cells were quantified and the ratio FI_{QD}/FI_N was calculated. This ratio was twice in induced cultures compared to control ones. (c) A cross section projection allows the visualization of a *XZ* plane (horizontal (H) section) and a *YZ* plane (vertical (V) section), where DNA condensation and nuclear fragmentation can be clearly observed. (d) 3-D rendered projection shows the peripheral localization of the AnnV–QDs in a volumetric view. Scale bar 5 μm.

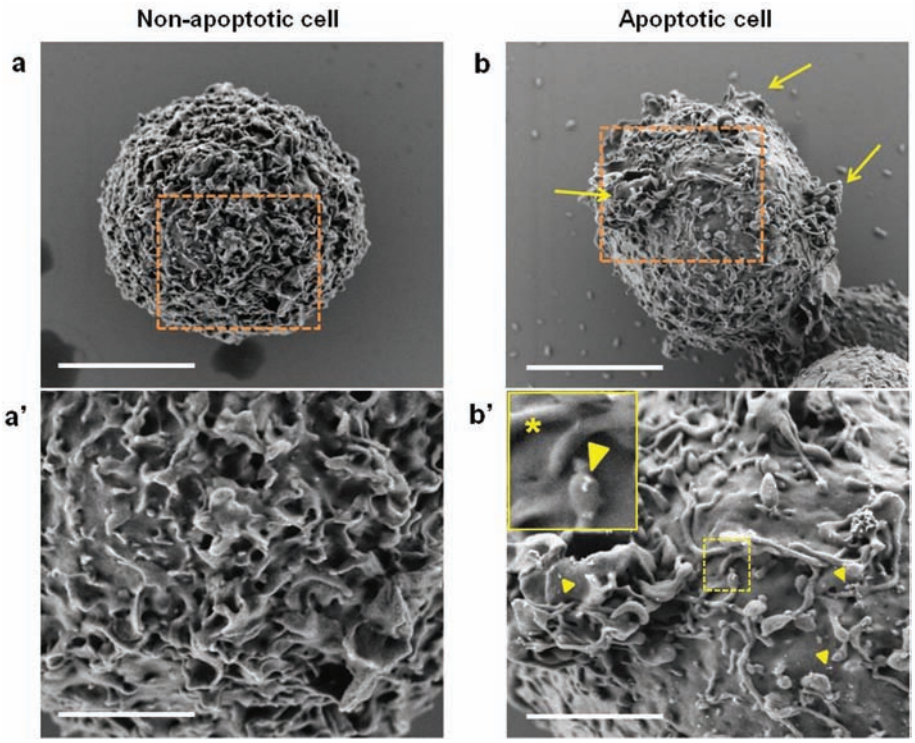

Fig. 3 SEM analysis. The morphology of control and apoptotic cells and the presence of QDs in the outer membrane of cells were evaluated by SEM imaging. Images a and b were taken at 20 000× to check the size and morphology of cells, scale bar 5 μm. Apoptotic cells (b) shown to be smaller in size (shrinkage) and also presented big evaginations or blebbing (indicated by arrows), typical of apoptotic processes. Images a′ and b′ were taken at 50 000× in a selected area (dashed square in top images) in order to evaluate the presence of QDs in the membrane (bright dots indicated by arrowheads), scale bar 2 μm. No QDs were present in non-apoptotic cells (a′) whereas in apoptotic cells (b′) dispersed or groups of QDs were observed. In the inset (*) a detail of a selected area (dashed square) is displayed and two QDs in the membrane of the cell can be clearly observed.

composition). Fig. 3a and 3b show non-apoptotic and apoptotic cells at 20 000× magnification respectively: whereas non-apoptotic cells (Fig. 3a) had usual morphologies, apoptotic cells (Fig. 3b) decreased in size (shrinkage) and presented membrane blebbing (pointed out in the picture by yellow arrows), which are typical of apoptotic processes. Moreover at 50 000× magnification, the presence of QDs was evaluated: no QDs were observed in non-apoptotic cells (Fig. 3a′). However, in apoptotic cells, QDs (displayed as bright dots in the image) were present in their membranes (yellow arrowheads in Fig. 3b′), corresponding to what was expected, due to the interaction of AnnV–QD with the externalized PS.

3.4 Quantification of AnnV–QD labeled apoptotic THP-1 cells by flow cytometry

We also used flow cytometry to analyze the same samples used for CLSM and SEM; in this way we could prove both the versatility of AnnV–QD labels using a different technique and the acquisition of quantitative data to be used for evaluating the performance of the new electrochemical detection. In particular, for each culture, 20 000 cells were analyzed and representative plots were obtained for each sample. Fig. 4 shows the distribution of the total cell culture population. The red colored area corresponds to the apoptotic cell population

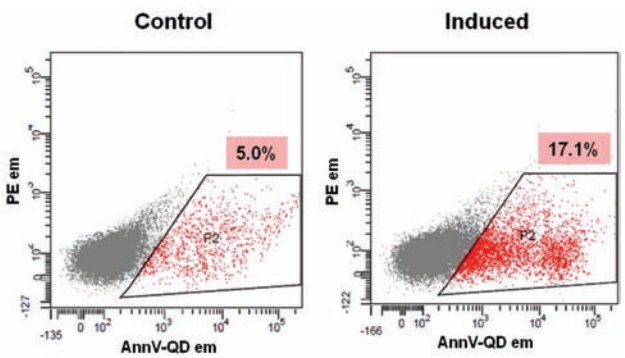

Fig. 4 Flow cytometry analysis. A total of 20 000 cells from control and induced cultures were analyzed and the number of cells emitting fluorescence (AnnV–QD labelled cells) were quantified (P2 area; red dots). The population of AnnV–QD labeled cells (P2) increased substantially in induced cell cultures (17.1% in front of 5.0% of the control). AnnV–QD em = fluorescence intensity emitted at 655 nm. PE em = fluorescence intensity emitted at 585 nm (used as control).

labeled with AnnV–QD, which was determined according to the negative control analyzed under the same conditions (Fig. S-2 in the ESI†). Comparing both plots, a more condensed red area is observed in the apoptosis induced culture than in the control one, as expected. We extracted numerical data from

the plots and calculated the percentage of apoptosis for each sample. Apoptotic cells constituted 5% of the control sample, as usual in normal healthy or untreated cell cultures,[37] whereas for induced cultures it was 17.1%. These results indicate that apoptosis was successfully induced by STS and that the AnnV–QD labeling method allowed the specific detection of apoptotic cells *via* flow cytometry.

3.5 Electrochemical stripping detection of apoptotic THP-1 cells through QDs

Finally, we developed an electrochemical method, based on stripping voltammetry of QDs (Fig. 5a), to detect apoptotic cells. It is based on the redox properties of the CdSe/ZnS QDs, which produced a characteristic oxidative peak at −0.720 V. The peak intensity can be used to estimate the amount of QDs in the sample that in turn can be related to the quantity of apoptotic cells present. Stripping voltammetry was performed in PBS using disposable screen printed electrodes and a potentiostat, as shown in Fig. 5b. In this way, an entire population of cells can be screened, checking the effect of the drug on their viability. In Fig. 5c, the histogram displays the peak values obtained by electrochemical detection of serial dilutions of control and apoptotic-induced cells. Considering the same number of cells, the apoptotic-induced cells generated higher peaks compared to control samples, due to the higher amount of QDs present in their plasma membrane, indicating the specific binding of AnnV–QDs to the externalized PS. The difference is observable in a range from 20 000 to 1250 cells (inset of Fig. 5c shows a classical read-out of the electrochemical stripping detection of different dilutions of apoptotic cells). Control cell cultures, as observed by CLSM and flow cytometry, also gave low intensity signals due to the basal apoptotic activity of a normal cell culture. This electrochemical method allows quantitative comparison of the effect of a drug on an induced sample and a control one, and, when used in correlation with flow cytometry data, allows us to estimate the number of apoptotic cells in the sample. In the present case, the flow cytometry results indicate that 17% of cells analyzed in the induced sample are apoptotic cells, thus, we can assume that in the smallest concentration used in the electrochemical detection, consisting of 1250 cells, about 212 were apoptotic cells.

3.6 Correlation between electrochemistry and other quantitative techniques

We compared the results obtained from analyzing 20 000 cells by flow cytometry and electrochemistry, as well as with those from CLSM (Table 1). Data collected showed an excellent correlation (~97.7%) between flow cytometry and electrochemistry, with almost the same value of fold-increase between the control and the apoptosis induced sample, 3.42 and 3.50 respectively. The 2.72 fold increase obtained from CLSM is also in good agreement with the previous ones (~78%) (although it cannot be used as a quantitative result, due to the lack of statistical significance of the technique). This new electrochemical method can be considered as a faster (readout

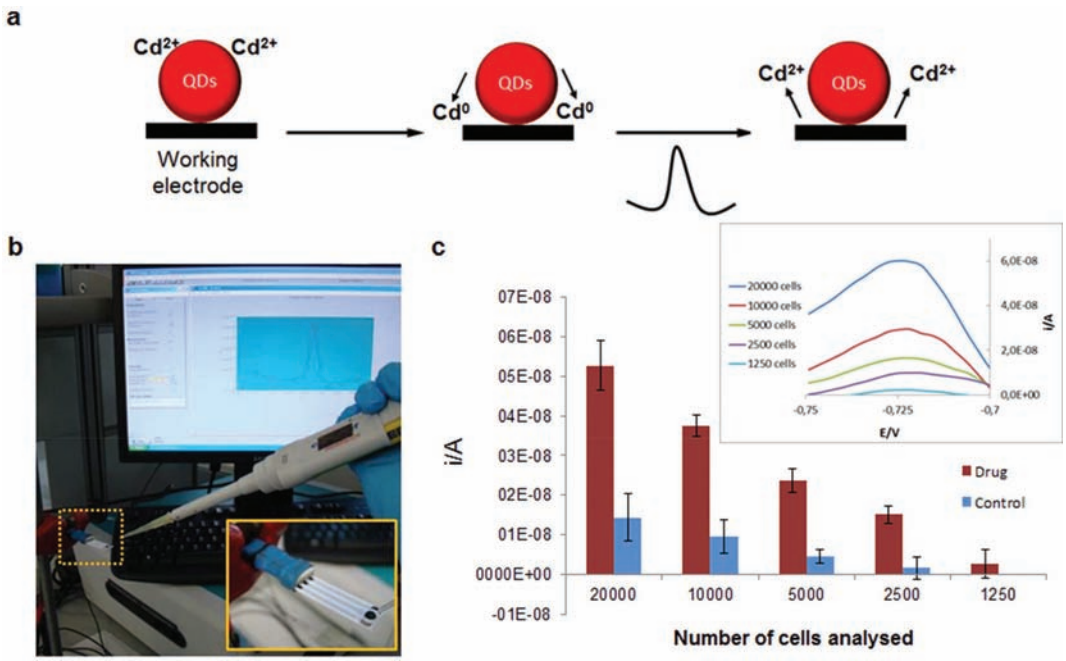

Fig. 5 Electrochemical detection. (a) Schematic of electrochemical detection by SWV of QDs. First Cd ions (as defects at the CdSe QD surface) are reduced to Cd^0 and the subsequent oxidation to Cd^{2+} generates a peak, the intensity of which corresponds to the amount of QDs present on the electrode surface. (b) Photo of the set-up for the electrochemical detection. (c) Electrochemical stripping peak currents obtained measuring different amounts of induced-apoptotic cells (red columns) and control cells (blue columns). In the inset typical electrochemical stripping curves obtained for the apoptotic cells are shown.

Table 1 Apoptosis analysis. Correlation between electrochemistry, flow cytometry and confocal laser scanning microscopy (CLSM) measures

Technique	Control cells	Induced cells	Fold increase
Electrochemistry (nA)	15.0	52.50	3.50
Flow cytometry (%)	5.0	17.10	3.42
CLSM (A.U.)	0.022	0.06	2.72

obtained in less than 5 minutes), cheaper and easier-to-use alternative or complementary method to flow cytometry. Unlike other electrochemical methods for heavy metal detection (such as those incorporating QDs) all measurements are carried out in a cell-friendly saline solution instead of using strong acidic conditions. Other advantages of this method include the fact that it can be used by untrained personnel, that it is easily miniaturizable and that does not limit the user to working with samples containing high number of cells.

4. Conclusions

We have explored the use of AnnV–QD probes as optical and electrochemical labels to easily carry out correlative studies of the same sample using different techniques such as voltammetry, flow cytometry, CLSM and SEM. The complementary information obtained from the different methods provides greater insight into the apoptotic process, compared to data obtained from single techniques using other dyes or enzymes. The proposed quantitative, electrochemical-based method is faster, cheaper and more versatile than most of those currently in use and can be easily miniaturized into a point-of-care, microfluidic device, making it useful for both research and industrial settings. We expect this technique to be extended not only to other cell toxicity studies with interest for clinical industries, but also to the detection of any disease-biomarker expressed in the plasma membrane, with clear relevance for diagnostic applications.

Acknowledgements

The authors thank MICINN (project MAT2011-25870 and TEC2011-29140-C03-03), SMS (EU FP7 project) and the Generalitat de Catalunya (project 2014SGR-524) for supporting this project. We also would like to thank Paula Llergo-Noel (Cell Biology Unit, UAB, Barcelona) for the maintenance of cell cultures, Manuela Costa (Service of Cell cultures, Antibody production and Cytometry, UAB, Barcelona) for the advice in Flow Cytometry analysis, Marcos Rosado (Electron Microscopy Division, ICN2, Barcelona) for the help with SEM imaging, Dámaso Torres (Webmaster and Graphic Designer, ICN2, Barcelona) for the help in drawing schematics and Dr Eleanor Gray (London Centre for Nanotechnology, UCL, London) for helping during the revision of the manuscript.

Notes and references

1 J. F. Kerr, C. M. Winterford and B. V. Harmon, *Cancer*, 1994, **73**(12), 3018.
2 S. MacEwan and A. Chilkoti, *Nano Lett.*, 2014, **14**, 2058–2064.
3 M. P. Mattson, *Nat. Rev. Mol. Cell Biol.*, 2000, **1**, 120–129.
4 G. Takemura and H. Fujiwara, *J. Cell. Mol. Med.*, 2006, **10**, 56–75.
5 S. J. Martin, C. P. Reutelingsperger, A. J. McGahon, J. A. Rader, R. C. van Schie, D. M. LaFace and D. R. Green, *J. Exp. Med.*, 1995, **182**, 1545–1556.
6 G. Rimon, C. E. Bazenet, K. L. Philpott and L. L. Rubin, *J. Neurosci. Res.*, 1997, **48**, 563–570.
7 S. M. Van den Eijnde, L. Boshart, C. P. Reutelingsperger, C. I. De Zeeuw and C. Vermeij-Keers, *Cell Death Differ.*, 1997, **4**, 311–316.
8 P. A. Leventis and S. Grinstein, *Annu. Rev. Biophys.*, 2010, **39**, 407–427.
9 K. Schutters and C. Reutelingsperger, *Apoptosis*, 2010, **15**, 1072–1082.
10 H. Shi, R. T. K. Kwok, J. Liu, B. Xing, B. Z. Tang and B. Liu, *J. Am. Chem. Soc.*, 2012, **134**, 17972–17981.
11 H. A. Andree, C. P. Reutelingsperger, R. Hauptmann, H. C. Hemker, W. T. Hermens and G. M. Willems, *J. Biol. Chem.*, 1990, **265**, 4923–4928.
12 I. Vermes, C. Haanen, H. Steffens-Nakken and C. Reutelingsperger, *J. Immunol. Methods*, 1995, **184**, 39–51.
13 H. van Genderen, H. Kenis, P. Lux, L. Ungeth, C. Maassen, N. Deckers, J. Narula, L. Hofstra and C. Reutelingsperger, *Nat. Protoc.*, 2006, **1**, 363–367.
14 D. M. Monsalve, T. Merced, I. F. Fernández, S. Blanco, M. Vázquez-Cedeira and P. Lazo, *Cell Death Dis.*, 2013, **4**, e513.
15 L. Quinti, R. Weissleder and C.-H. Tung, *Nano Lett.*, 2006, **6**, 488–490.
16 U. Resch-Genger, M. Grabolle, S. Cavaliere-Jaricot, R. Nitschke and T. Nann, *Nat. Methods*, 2008, **5**, 763–775.
17 H. Montón, C. Nogués, E. Rossinyol, O. Castell and M. Roldán, *J. Nanobiotechnol.*, 2009, **7**, 4.
18 O. Kovtun, X. Arzeta-Ferrer and S. J. Rosenthal, *Nanoscale*, 2013, **5**, 12072–12081.
19 A. P. Alivisatos, W. Gu and C. Larabell, *Annu. Rev. Biomed. Eng.*, 2005, **7**, 55–76.
20 R. Gill, M. Zayats and I. Willner, *Angew. Chem., Int. Ed.*, 2008, **47**, 7602–7625.
21 R. Freeman, J. Girsh and I. Willner, *ACS Appl. Mater. Interfaces*, 2013, **5**, 2815–2834.
22 S. Jiang, K. Y. Win, S. Liu, C. P. Teng, Y. Zheng and M.-Y. Han, *Nanoscale*, 2013, **5**, 3127–3148.
23 S. Le Gac, I. Vermes and A. van den Berg, *Nano Lett.*, 2006, **6**, 1863–1869.
24 Y. Wang and L. Chen, *Nanomedicine*, 2011, **7**, 385–402.
25 X. Wu, H. Liu, J. Liu, K. N. Haley, J. A. Treadway, J. P. Larson, N. Ge, F. Peale and M. P. Bruchez, *Nat. Biotechnol.*, 2003, **21**, 41–46.

26 J. Dimitrijevic, L. Krapf, C. Wolter, C. Schmidtke, J.-P. Merkl, T. Jochum, A. Kornowski, A. Schüth, A. Gebert, G. Hüttmann, T. Vossmeyer and H. Weller, *Nanoscale*, 2014, **6**, 10413–10422.

27 P. K. Chattopadhyay, S. P. Perfetto, J. Yu and M. Roederer, *Wiley Interdiscip. Rev.: Nanomed. Nanobiotechnol.*, 2010, **2**, 334–348.

28 E. Petryayeva, W. R. Algar and I. L. Medintz, *Appl. Spectrosc.*, 2013, **67**, 215–252.

29 Y. Luo, C. Wang, T. Jiang, B. Zhang, J. Huang, P. Liao and W. Fu, *Biosens. Bioelectron.*, 2014, **51**, 136–142.

30 G. Rousserie, A. Sukhanova, K. Even-Desrumeaux, F. Fleury, P. Chames, D. Baty, V. Oleinikov, M. Pluot, J. H. M. Cohen and I. Nabiev, *Crit. Rev. Oncol. Hematol.*, 2010, **74**, 1–15.

31 E. Morales-Narváez, H. Montón, A. Fomicheva and A. Merkoçi, *Anal. Chem.*, 2012, **84**, 6821–6827.

32 E. Morales-Narváez, A. R. Hassan and A. Merkoçi, *Angew. Chem., Int. Ed.*, 2013, **52**, 13779–13783.

33 S. Marin and A. Merkoçi, *Nanotechnology*, 2009, **20**, 055101.

34 M. Medina-Sánchez, S. Miserere, S. Marín, G. Aragay and A. Merkoçi, *Lab Chip*, 2012, **12**, 2000–2005.

35 M. Amelia, T. Avellini, S. Monaco, S. Impellizzeri, I. Yildiz, F. M. Raymo and A. Credi, *Pure Appl. Chem.*, 2011, **83**, 1–8.

36 J. Wang, G. Liu and A. Merkoçi, *J. Am. Chem. Soc.*, 2003, **125**, 3214–3215.

37 Y. Wu, D. Connors, L. Barber, S. Jayachandra, U. M. Hanumegowda and S. P. Adams, *Toxicol. In Vitro*, 2009, **23**, 1170–1178.

38 W.-T. Li, H.-W. Tsao, Y.-Y. Chen, S.-W. Cheng and Y.-C. Hsu, *Photochem. Photobiol. Sci.*, 2007, **6**, 1341–1348.

39 A. H. Heussner and D. R. Dietrich, *Open J. Apoptosis*, 2013, **02**, 25–30.

40 N.-S. Chang, *BMC Cell Biol.*, 2002, **3**, 8.

Electronic Supplementary Information (ESI)

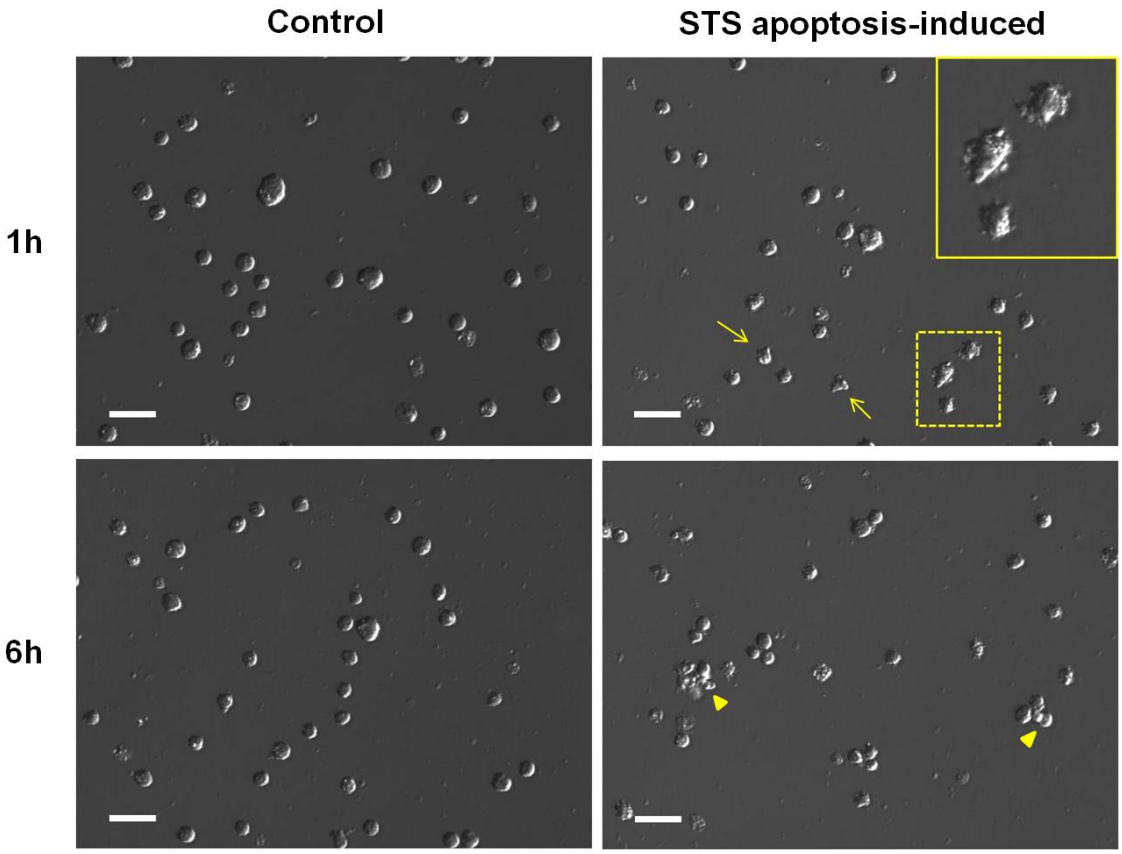

Fig. S-1. Check of cell cultures during pro-apoptotic drug (STS) incubation. Phase contrast images at 1 and 6 h show that some cells begin to change its homogenous round shape after 1 h in apoptosis-induced cell cultures exhibiting cell shrinkage and membrane blebbing (arrows and magnified squared area). After 6 h, the number of cells presenting shrinkage and membrane blebbing increases, and also a tendency to group in small lumps (arrow heads) can be observed in apoptosis-induced cell cultures whereas control cells preserve their healthy round shape and keep their single cell organization within the medium. Scale bars 20 µm.

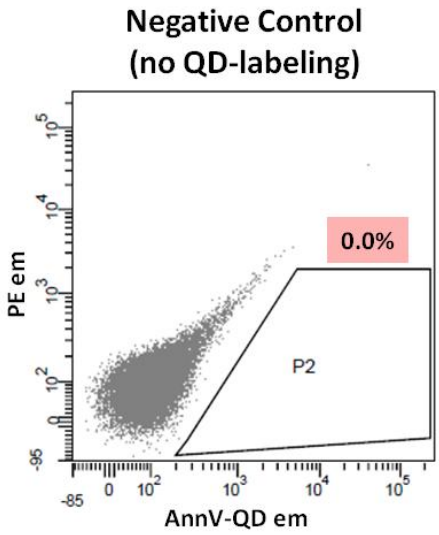

Fig. S-2. Negative control of flow cytometry analysis. A negative control without AnnV-QD labeling was analyzed in order to establish the parameters of QD labeling detection. P2 area was selected out of the cloud of control cells and in the region where QD were supposed to be detected according to their spectral characteristics (maximum emission at 655 nm). These settings were kept for the analysis of control and induced cultures. AnnV-QD em = fluorescence intensity emitted at 655 nm. PE em = fluorescence intensity emitted at 585 nm (used as control).